University of Strathclyde

Department of Electronic and Electrical Engineering

On the Protection of Compact DC Power Systems with High-Power Energy Storage

by

Puran Rakhra

A thesis presented in fulfilment of the
requirements for the degree of

Doctor of Philosophy

2017

Abstract

High-power energy storage systems (ESS) are being considered for future aerospace platforms and other compact DC power system applications to improve the overall transient performance of electrical power distribution systems. These sources are being integrated with advanced bidirectional power electronic converter interfaces with high bandwidth control systems and current limiting functionality. To date, the literature has primarily focused on the control and behaviour of high-power ESS during normal operating conditions with an emphasis on the systems level benefits they offer. Little consideration has been given to their response during network fault conditions.

Through simulation and hardware experimentation, this thesis demonstrates that an ESS, by design, can contribute significant levels of current to a fault as it attempts to sustain the network voltage. This behaviour inadvertently reduces the fault current contribution from the primary source of power on the network, reducing the effectiveness of associated protection devices (protection blinding).

The impact of several key DC power system design and operation parameters on the ESS fault response is quantified and a new critical fault impedance term, beyond which protection blinding can be expected to occur, is introduced. Building upon this new knowledge, enhancements to typical compact DC power system protection schemes which more effectively account for the presence of ESS are proposed and evaluated.

Differential protection schemes are shown to eliminate protection blinding whilst offering the greatest flexibility in increasing protection speed and fault discrimination, and maximising ESS availability. Adaptive protection schemes are shown to be a reliable backup option where a consistent protection system response can be obtained despite the potentially intermittent nature of the ESS fault current contribution. A novel control strategy that actively modifies the fault response of the ESS to facilitate the use of conventional overcurrent schemes is also proposed and demonstrated for applications where communications-based protection is unfavourable.

The thesis concludes by proposing a framework to guide protection engineers in the selection of appropriate protection and control strategies when considering the integration of high-power ESS within compact DC power systems.

Acknowledgements

I would like to express my deepest gratitude to Dr Stuart Galloway and Professor Graeme Burt for giving me the opportunity to work with the amazing team of people that they have built at Strathclyde.

I would especially like to thank Dr Patrick Norman and Dr Steven Fletcher for their technical guidance and professional mentorship throughout my career so far.

Thank you also to colleagues at Rolls-Royce for providing expert technical direction, training and financial support throughout my PhD.

A special thanks to my Brother who is responsible for my love of science and engineering.

To Ariana - your patience, encouragement and unfaltering support is the reason this thesis is complete. I cannot express in words the appreciation that I have for you.

And lastly to my parents - Gurdev and Jasbir - your journey through life and your words of wisdom have always remained a constant source of inspiration. This thesis is dedicated to you.

Contents

List of Figures

List of Tables

Glossary of Abbreviations

AAIB	Air Accidents Investigation Branch
AC	Alternating Current
ADC	Analogue to Digital Conversion
AEA	All-Electric Aircraft
AFCI	Arc-Fault Circuit Interrupter
AIE	Active Impedance Estimation
APU	Auxiliary Power Unit
ATRU	Autotransformer Rectifier Unit
BTC	Bus Tie Contactor
CAES	Compressed Air Energy Storage
CB	Circuit Breaker
COTS	Commercial off the Shelf
DAB	Dual Active Bridge
DC	Direct Current
DDC	Data Device Corporation
DOD	Depth of Discharge
DP	Differential Protection
ECS	Environmental Control System
ELCU	Electrical Load Contactor Unit
EMCB	Electro-Mechanical Circuit Breaker
EMI	Electromagnetic Interference
ESS	Energy Storage System
EV	Electric Vehicle
FMC	Fault Mode Control
GCU	Generator Control Unit
GLC	Generator Load Contactor
HCB	Hybrid Circuit Breaker
IDMT	Inverse Definitive Mean Time
IFEP	Integrated Full-Electric Propulsion
Li-ion	Lithium-ion

MEA	More-Electric Aircraft
MEE	More-Electric Engine
NaS	Sodium-Sulphur
NiCd	Nickel-Cadmium
PE	Power Electronic
PI	Proportional Integral
PWM	Pulse Width Modulation
RCCB	Remote Control Circuit Breaker
RCD	Residual Current Device
SOC	State of Charge
SMES	Superconducting Magnetic Energy Storage
SSCB	Solid-State Circuit Breaker
SSPC	Solid-State Power Controller
T&D	Transmission and Distribution
TES	Thermal Energy Storage
UAV	Unmanned Aerial Vehicle
UPS	Uninterruptable Power Supply
VRB	Vanadium Redox Battery
WIPS	Wing Ice Protection System
ZnBr	Zinc-Bromine

Chapter 1

Introduction

1.1 Introduction to the Research

Advanced power systems in future aerospace platforms are projected to consume more electrical energy [1], [2], incorporate greater levels of power electronic conversion [3]–[10] and integrate subsystems with increasingly dynamic load profiles [1], [11]–[16]. This growing complexity is being driven by the electrification of loads conventionally supplied by hydraulic and pneumatic power [1], [17], [18] owing to the fuel consumption savings and overall efficiency gains that can be made by incorporating a globally optimised electrical power off-take system from the engines [19]–[23]. This is being enabled by recent advances in the efficiency, the control and the power density of advanced power electronic converter interfaces. These changes are also putting significant strain on electrical generation systems that must be sufficiently rated to meet the increasing demand of these advanced subsystems, whilst being designed within strict physical and economic constraints. More pressingly, the rising operating cost of these platforms owing to the increasing price of fuel, together with strict government regulations to reduce emissions is incentivizing the adoption of technologies that will improve the efficiency and reliability of electrical power distribution.

DC power distribution is one such radical technological shift that is beginning to emerge throughout the power industry [24]. This is an enabling technology for the paralleling and power sharing of multiple non-synchronous converter interfaced generators and alternative power sources that can offer system wide benefits to the operation of future aircraft. Thus, DC power systems are underpinning the growing interest in the integration of advanced energy storage systems (ESS). This interest has been largely driven by the benefits that energy storage can offer to the

operational capability, flexibility and the efficiency of the power system. Applications range from large scale interconnected grid systems to more physically compact networks primarily considered within this thesis. Whilst particular focus is placed on future aircraft electrical power systems in both the commercial and the defence sector, it is anticipated that similar benefits of ESS integration are expected within marine vessel power systems and standalone micro-grids.

Conventional energy-dense storage mediums have been widely used throughout the industry to provide backup power in the event of loss of primary generation. More recently, advanced power-dense storage technologies are becoming more economically attractive and are now being proposed to play a number of complex roles at a systems level. Coupled with advanced power electronic converter interfaces and high-bandwidth control systems, ESSs can offer a number of benefits to the operation of the network. This includes capitalizing on the rapid response time to meet peak load demand, and maintaining power quality within regulated limits during variable load conditions or large switching events. These functions can improve the overall transient performance of the system, reduce the required primary generation capacity and increase the security of supply to loads [25].

However, the integration of an ESS into a compact and converter-dense power system adds further diversity to the systems dynamics, and thereby complicates the systems protection and control. Indeed, it is anticipated that power-dense ESSs may contribute a significant level of fault current during network disturbances, causing protection blinding of slower responding sources [26], [27]. The resulting impact on the safe operation of the system is uncertain and requires rigorous investigation before power-dense ESS can be widely adopted on safety critical systems. This thesis thereby answers the following research question:

How does the response of a high-power, high-bandwidth ESS integrated within a current limited compact DC power system environment impact the performance of the network-wide protection system under fault conditions?

Key characteristics of ESSs that define its response to electrical faults are identified. The decreased sensitivity of slower acting sources to various fault impedances owing to the rapid response of the ESS is demonstrated in simulation and the resulting protection blinding effects are quantified. The performance degradation of conventional overcurrent based protection approaches is experimentally validated and alternative protection schemes that address these limitations are proposed. A novel method of actively tailoring the fault response of the ESS to mitigate the effects of protection blinding whilst improving the overall protection performance for downstream faults is also proposed. Finally, a comprehensive protection framework that enables a power system designer to select the most suitable protection system solution when considering the integration of a high-bandwidth ESS in a compact power system is presented.

1.2 Research Motivation

There is a persistent financial and environmental incentive within the aerospace industry to reduce operating costs of aircraft in the form of fuel burn reduction. Engine manufacturers, airframers and system integrators are exploring a wide range of system design changes driven by advances in numerous technological areas that will enable future aircraft to be more fuel efficient. The most promising research objectives that are currently being pursued by the industry can be categorised into four broad areas:

1. Reducing the overall weight of the aircraft through the use of lighter-weight, composite materials in the manufacturing of fuselage, wings and engine nacelle components [28], [29]
2. Minimising aerodynamic drag through radical airframe and wing designs [30]–[33]
3. Optimisation of flight paths and air / ground traffic scheduling [34]–[38]
4. Increasing the efficiency of all on-board systems and reducing the overall fuel burn of the aircraft [1], [2], [12], [21], [39] through the integration of advanced power off-take and power distribution systems across the engine and airframe.

This thesis is written within the context of the fourth category. Reducing hydraulic, pneumatic and mechanical infrastructure and power off-take from the engines has been shown to improve fuel consumption as a result of a more fuel efficient engine operation [13], [17]. More efficient power extraction, power transfer, and energy consumption can be facilitated instead through a lightweight and interconnected electrical power distribution system. Air-framers and systems integrators commonly refer to developments in this area as evolutions of the 'more-electric aircraft' (MEA) or 'more-electric engine' (MEE) concept. These concepts broadly reflect the industry's long term vision to capitalise on the wide range of benefits that an advanced and interconnected electrical power system can offer to the operational

flexibility and efficiency of the overall system [40]. This vision has provided the impetus for academic and industrial research to focus on optimising the electrical system in terms of weight, volume, capacity, efficiency and reliability.

Conflictingly, the increased electrification of subsystems will significantly contribute to the rising demand of electrical power on modern commercial, defence and UAV platforms [1], [11], [13], [20]. Recent 'more-electric aircraft' such as the Airbus A380 and Boeing 787 incorporate 600kVA and 1.45MVA of electrical generation capacity respectively [17], [41], [42]. Electrical demand on future aircraft is projected to increase even further [12], [19]. Therefore, the additional weight and complexity of the electrical power system required to meet the projected demand, if poorly implemented, has the potential to outweigh the benefits of the more-electric design [12]. This trade-off has led to:

- Development of more power-dense electrical generation [43]-[45], [47], [49] and conversion systems [3], [20], [46], [48], [50]–[54]
- Research of lighter-weight and more reliable electrical power distribution technologies and architectures [9], [12], [19], [48], [49], [55], [56], [71]
- Exploration of the use of advanced energy storage systems to increase system flexibility and support demand [1], [7], [14], [57]–[65].

Looking forward, there are several technological trends, advancements and challenges associated with the design of compact electrical power systems for aerospace applications that are shaping the projected outcome of this vision. These are described in the following subsections.

1.2.1 Increased penetration of power electronic conversion

Advanced power electronic (PE) converter interfaces, drives and motors are rapidly becoming lighter, cheaper, more efficient, and more power-dense [66]–[69]. PE-driven loads offer significant performance improvements over their hydraulic/pneumatic counterparts owing to the increased efficiency and precision that electronically actuated systems can achieve [20], [43], [50], [70]. Examples include: on-engine fuel and oil pumps, environmental control systems (ECS), anti-icing systems and flight control surfaces [1], [10], [12], [13], [17], [47], [53]. Electronically driven active front end converter units are also being considered to replace conventional transformer based primary conversion units, owing to the considerable weight and volume reductions that can be achieved [3], [48], [52], [53]. These developments will lead to electrical systems on future aircraft incorporating a significantly greater density of power electronic converter units than on current platforms. For example, the electrical power distribution system on the most recent commercial MEA platform, the Boeing 787, includes four passive autotransformer rectifier units to supply +/-270V DC bus and two passive transformer rectifier units that supply 28V DC power, as well as four active inverters used for electrical engine start and driving the ECS compressor fans [221]. These passive conversion stages are expected to be replaced with active PE conversion technologies in future iterations of MEA systems that are more power-dense than current converters, and that offer additional functionality such as bi-directional power flow capability [53].

1.2.2 DC power distribution

The use of DC for primary power distribution has been shown to bring significant design, cost and efficiency benefits to a number of power system applications, including aircraft, shipboard and ground-based distribution systems [9], [24], [71]–[75]. Such systems may be referred to as 'compact DC systems' given the physically

compact nature of their power distribution architectures, where cable runs and bus bars are typically less than 50m and resistance of the distribution system is less than 1mΩ/m [24]. DC distribution can enable a significant reduction in the number of conversion stages in converter-dense power systems [72], [75]. Power can be distributed across DC electrical systems at higher operating voltages more closely aligned to cable ratings, enabling greater power transfer than equivalently rated cables employing AC distribution [76]. Finally, DC distribution enables sources to be paralleled with relative ease in comparison to AC sources that require synchronization [77], [78]. Paralleled generation through a DC network can offer unprecedented system flexibility enabling power sharing between multi-shaft or multi-engine electrical power off-takes at wider and more efficient engine speeds [45], [79]–[82]. However, DC electrical systems pose exceptionally demanding protection requirements that represent a significant barrier to more widespread adoption [24], [71], [83], [84]. Advanced communications based protection solutions using solid-state switchgear have been demonstrated to meet the performance criteria required to fully capitalise on the advantages that DC networks offer [85]. However, considerable research and development is still required certify these technologies for aerospace applications.

1.2.3 Power-dense ESS integration

The role of energy storage in aircraft electrical systems is diversifying. Conventionally, energy-dense storage mediums in the form of electrochemical batteries are used to supply emergency backup power to flight critical loads in the event of primary generation failure and no-break power transfer [6]. More recently, they are being considered to perform additional complex system functions. For example, the batteries installed on the Boeing 787 also provide power to start the Auxiliary Power Unit (APU) - which can power generators to start the main engines if needed - and navigation lights. The main batteries also support certain ground

operations such as refuelling when the engines/APU is offline [17], [86], [87]. Interest in the integration of advanced, power-dense energy storage technologies such as supercapacitors is also growing. These ESSs may be rated to deliver high-power, similarly matched to the rating of the primary generation system, but over a short period of time and can therefore offer a wide range of benefits to the operation of the electrical power system. For example, they are being considered to mitigate electrical transients caused by large load switching events to maintain power quality within regulated boundaries [25], [57], [88]–[92]. They are also being considered to supply pulse power loads to minimise any undesirable torque pulsations on the engine prime movers, decoupling any electromechanical interactions [1], [10], [25], [27], [54], [57]–[59], [61], [62], [88]–[90], [92]–[104]. In certain applications, they may even enable a reduction in the maximum rating of the primary generation system [43]. While the additional flexibility that these types of ESS bring to the overall system is beneficial, the impact that ESS have on the performance of the network wide protection system during faults is not well understood and has received little attention in the literature. In particular, it is uncertain whether the fault detection time of protection devices that apply time-based discrimination is impacted by the additional (and potentially significant) contribution of fault current from a secondary source when integrated in a converter-fed, current-limited, DC power distribution system.

This is therefore the motivation for this research. It is anticipated that this body of work will aid power system designers considering the integration of fast acting and power-dense energy storage systems in evaluating the impact that the ESS will have on the performance of the network wide protection system. Note that the complexity and maturity of the individual ESS types is not the focus of this research. As such, device level challenges and developments associated with specific storage mediums will not be discussed in detail. Instead, energy storage integration will be explored at a systems level, where the impact of the ESS control and behaviour on the protection system performance will be evaluated in response to abnormal network conditions. Finally, a framework is developed that enables the systems

integrator to select the most suitable protection system to ensure safe operation of the power system under a variety of fault conditions. This is anticipated to be a valuable power system design tool for the industry.

1.3 Principle Contributions

This thesis provides the following contributions to knowledge:

- Identification and experimental validation of the protection blinding risk resulting from the integration of power-dense ESS into compact DC power systems.
- Quantification of the degrading of protection system performance resulting from the ESS induced protection blinding. Evaluation of the sensitivity of its extent to key ESS and wider system design parameters.
- Proposal, derivation and validation of a new "critical fault impedance" term which defines the conditions when protection blinding will occur on a given system, enabling a rapid assessment of protection risk.
- Identification, application and quantitative evaluation of most effective protection solutions to mitigate protection performance degradation.
- Design, demonstration and analysis of a novel ESS fault mode control that mitigates the blinding of conventional protection approaches but does not limit normal functionality of the ESS.
- Proposal of optimised integrated network protection and ESS fault mode control setup for future aircraft applications.

1.4 Publications

The following publications have been completed during the course of this PhD:

1.4.1 Journal Articles

P. Rakhra, P. J. Norman, S. D. A. Fletcher, S. J. Galloway, and G. M. Burt, "Evaluation of the Impact of High-Bandwidth Energy-Storage Systems on DC Protection," *IEEE Transactions on Power Delivery*, vol. 31, no. 2, pp. 586–595, 2016.

P. Rakhra, P. Norman, S. Fletcher, S. Galloway, and G. Burt, "A Holistic Approach towards Optimizing Energy Storage Response during Network Faulted Conditions within an Aircraft Electrical Power System," *SAE International Journal of Aerospace*, vol. 5, no. 2, pp. 548–556, 2012.

S. D. A. Fletcher, P. Norman, S. Galloway, P. Rakhra, G. Burt, and V. Lowe, "Modelling and Simulation Enabled UAV Electrical Power System Design," *SAE International Journal of Aerospace*, vol. 4, no. 2, pp. 1074–1083, 2011.

1.4.2 Conference Papers

P. Rakhra, P. J. Norman, S. J. Galloway, and G. M. Burt, "Experimental Validation of Protection Blinding on DC Aircraft Electrical Power Systems with Power-Dense Energy Storage," *IET Proceedings of Power Electronics Machines and Drives Conference*, p. 1-6, 2016.

P. Rakhra, P. J. Norman, S. D. A. Fletcher, S. J. Galloway, and G. M. Burt, "Toward Optimising Energy Storage Response during Network Faulted Conditions within an Aircraft Electrical Power System," *Electrical Systems for Aircraft, Railway and Ship Propulsion*, pp. 1–7, 2012.

P. Rakhra, P. Norman, S. Fletcher, S. Galloway, and G. Burt, "A Holistic Approach towards Optimizing Energy Storage Response during Network Faulted Conditions within an Aircraft Electrical Power System," *SAE Power Systems Conference*, 2012.

P. Rakhra, P. J. Norman, S. J. Galloway, and G. M. Burt, "Modelling and Simulation of a MEA Twin Generator UAV Electrical Power System," *University Power Engineering Conference*, no. 1, pp. 1–5, 2011.

1.5 Thesis Overview

Chapter 2 reviews the relevant background material. The chapter introduces the principles of storing energy and defines the measurands by which energy storage systems are quantified. It then presents relevant trends associated with certain energy storage technologies that are valuable to power system designers. A review of the state-of-the-art in various energy storage mediums and associated energy conversion technologies suitable for a wide range of power system applications is also presented. A discussion on the most viable storage technologies for aerospace applications and their projected use cases concludes the chapter.

Chapter 3 presents the technical challenges associated with the integration of power-dense energy storage systems into aircraft electrical power systems. This includes a review of the state-of-the-art in DC protection systems. Assumptions associated with ESS's bidirectional functionality, current limiting capability and control operations are also discussed.

The primary contributions to knowledge are presented in Chapters 4, 5 and 6. Chapter 4 outlines the method by which the impact of the ESS fault response on the performance of the network protection system is quantified. Through modelling, simulation and hardware experimentation, it is demonstrated that an ESS, by design, can cause protection blinding whereby the effectiveness of network protection devices is reduced. A new critical fault impedance term beyond which protection blinding can be expected to occur is introduced in this chapter. The mathematical derivation by which it can be determined using key DC power system design and operation parameters is also defined. Alternative protection approaches

that minimise the adverse impact of ESS integration and enhance the overall performance of the system, enabling the ESS to be used more effectively under fault conditions are evaluated in Chapter 5. A novel control mode that adapts the ESS behaviour as a function of fault location to enhance protection system response is proposed and evaluated in Chapter 6. Chapter 7 concludes the thesis by discussing the selection of the optimal protection system solution when considering the integration of a high-power ESS for new build or retrofit power systems.

Chapter 2

Energy Storage: Technologies, Trends and Applications

This chapter introduces the background material that is relevant to the contributions of this thesis. First, the mechanisms and constituent elements of energy storage systems (ESS) that enable useful quantities of energy to be stored within the context of electrical power systems are defined. ESS variants are categorised by energy type, and the measurands by which they are compared and quantified are described. Relevant trends associated with the most viable storage technologies for aerospace applications and their projected use cases are then presented. Finally, a comprehensive literature review of the functions and roles that state-of-the-art high-power, high-bandwidth ESS play in a broad range of compact DC power system applications is conducted.

2.1 Energy Storage Systems and Technologies

The objective of storing energy within a system is to perform work at a later moment in time from when that energy is first generated. Energy can be stored using a wide range of mediums and devices that may be suitable for a specific application depending on a number of economic, physical and functional factors. Naturally, capital cost of installing energy storage is a limiting factor in all power system applications, particularly for large-scale solutions that require significant technology and infrastructure investment, such as pumped hydro stations and compressed air storage facilities [25], [90], [105], [106]. Indeed, the economic viability of integrating energy storage within any power system application must be

justified by the economic return generated by the service that it provides [25], [107]–[109].

Similarly, the physical constraints of a specific power system application will dictate the viability of a particular energy storage solution. For example, weight and volume constraints on future transportation applications such as full-electric ships [61], [92], electric vehicles [90], [94], [97] and more electric aircraft [1], [58], [60], [110], [111] are particularly demanding when considering the integration of energy storage.

In addition to these factors, the constraints associated with the behavioural characteristics of an energy storage system will limit its ability to meet the requirements of a particular application. Behavioural constraints include: the total quantity of energy that the medium has the capacity to store; the maximum rate that energy can be accumulated by or extracted from the storage medium (i.e. its power rating); and the overall bandwidth (or time constant) of the energy storage system [25], [95], [106].

These factors are limited by a number of physical characteristics of the medium itself and the bi-directional energy conversion mechanisms that enable one form of energy to be converted into the corresponding form of energy that is being stored. For example, a pumped hydro system will store energy in the form of a gravitational potential whereby a mass of water is retained at altitude via a dam or reservoir. This stored potential is converted into electrical energy via a turbine and electrical generator when this water is released to a lower altitude at a regulated flow rate. Energy is then re-accumulated via the use of a hydro-pump system that replenishes the reservoir [25], [107], [109], [112]–[114]. In a similar manner, electrochemical batteries retain energy in the form of a chemical potential whereby voltaic cells are connected in series by a conductive electrolyte containing electro-active ions. Batteries convert this stored chemical energy directly into electrical energy via reduction-oxidation reactions at the cell electrodes when connected to an external circuit, permitting the simultaneous movement of electrons through the circuit, and

ions through the electrolyte. A reversal of this process enables the ions to be replenished and the battery to be recharged [94], [95], [114], [115].

Energy storage devices or mediums that retain energy in a form that is different from the principle form of energy performing work within that system, or devices that require regulation, must employ active mechanisms of energy conversion to function effectively. Accordingly, integration of energy storage into an electrical power system is normally achieved via a conversion interface (such as a power electronic converter or charge controller) that may be commanded via a control system to actively regulate the charging and discharging process of the storage medium. However, the functions of charging and discharging the energy storage medium do not necessarily need to be performed by a single bidirectional conversion interface. For example, a heat storage system for wind power application may be implemented using a large resistive load to 'charge' the heat storage facility, whilst an independently controlled heat exchanger, steam turbine and generator interface may be used to discharge the device [113]. Alternatively, devices such as capacitors or electrochemical batteries that store energy in the form of electrical potential may be passively connected to the network in applications where active regulation of the stored energy is not required [114].

The energy storage medium (including its internal energy conversion mechanisms), its power electronic converter interface and its governing control system are collectively referred to as the energy storage system (ESS). ESS variants can be classified by the type of energy that is stored. These are: mechanical, thermal, chemical, electrical and electrochemical storage types [107], as shown in Figure 2.1.
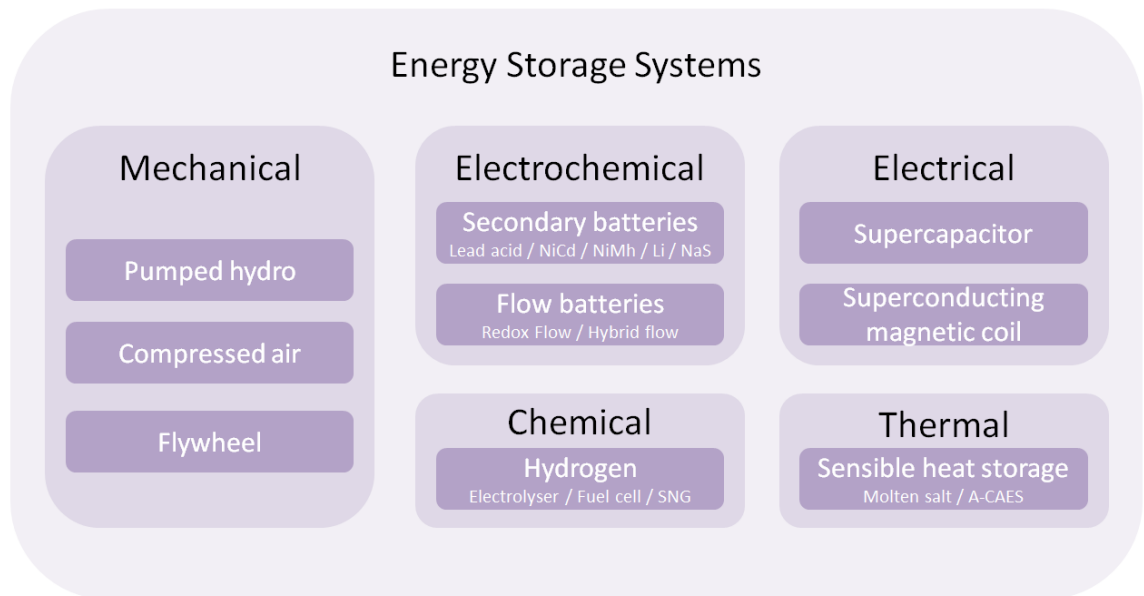
Figure 2.1: Classification of energy storage system technologies [107]

The extensive range of ESS technologies that are categorised in Figure 2.1 may be employed in a variety of different power system applications. In order to determine the viability of a particular ESS for a specific power system application, the physical and functional characteristics of that ESS, in addition to its limitations, must be quantified for comparison and technical evaluation. The measurands by which ESSs are quantified are discussed in the following subsections.

2.2 Quantification of energy storage systems

2.2.1 Storage capacity and state-of-charge

Storage capacity is a measure of the maximum quantity of energy, in Joules (J) or kilowatt-hours (kWh), that an ESS can store. Similarly, the state-of-charge (SOC) [222] of an ESS is the quantity of energy remaining within the ESS as a percentage of its maximum capacity. Whilst this term is more accurately used to quantify the remaining energy in an electrical or electrochemical ESS, such as a supercapacitor or

electrochemical battery, the same terminology is applied to mechanical, thermal or chemical mediums [108].

In a similar manner, the depth-of-discharge (DOD) is the quantity of energy extracted from the ESS as a percentage of maximum capacity. Many ESSs impose a fixed DOD threshold that limits the quantity of energy that can be extracted to perform useful work. A DOD threshold may be intentionally applied to maximise the cycle life of the medium, for example in the active prevention of deep discharge of electrochemical batteries in photovoltaic systems [108], or may be a physical limitation of the device such as the minimum operating speed of a flywheel ESS [112], [116], [117]. Certain storage mediums such as flow batteries allow for 100% discharge capability with minimal to no impact on the cycle life performance [112], [113]. Thus it is often beneficial to quantify the useable capacity of an ESS, determined by the difference between the maximum capacity and the allowable DOD threshold.

2.2.2 Power rating and bandwidth

The maximum rate that energy can be extracted from or accumulated by an ESS is defined by its overall power rating [113]. The physical constraints that restrict the charge/discharge rate of an ESS are dependent on a number of device specific limitations and internal conversion mechanisms. For example, the maximum rate-of-change of angular velocity that a flywheel ESS can achieve may be limited by: the maximum current rating of its power electronic drive system; the maximum torque that can be generated by its electrical motor; and the torsional stress constraints of its drive shaft [95], [118]. A passive electrical storage medium such as a supercapacitor or electrochemical battery will have a maximum charge/discharge current that is restricted by the maximum rate at which electroactive components may be supplied to or extracted from its active electrode surfaces [94], [119]–[121]. Similarly, the physical limitations of internal processes within chemical storage devices, such as the maximum rate of electrode reactions in fuel cells [94] and flow

batteries [113] will constrain the overall power rating of the ESS. These limitations may be represented by the storage medium's equivalent internal impedance [122]. This internal impedance may change as a function of time depending on a number of factors including the ESS type, its internal chemical properties, its age and its operating temperature.

In a similar manner, the response time of an ESS (assuming a first order approximation) is the measure of the time it takes for an ESS to respond to a step change in demand. The term bandwidth may alternatively be used to describe this characteristic of an ESS given the inverse relationship with the time constant. The overall bandwidth of an ESS may again be limited by the time constants associated with internal conversion mechanisms of a specific ESS technology [57].

Alternatively, the bandwidth of an ESS may be intentionally restricted to limit its dynamic performance via the adjustment of the closed-loop controller gains or feedback system associated with its power electronic converter interface [59], [123]. For example, this may be implemented on a fuel cell system to prevent fuel starvation problems and to improve the lifetime of the ESS [100].

2.2.3 Energy density and power density

The gravimetric energy density of an ESS is a measure of the maximum quantity of energy per unit mass, in Wh/kg, that the device can store. Similarly, the gravimetric power density, measured in W/kg, is the maximum power per unit mass that the ESS can deliver. These measurands, in addition to their volumetric equivalent, are particularly useful quantification metrics for power system integrators to assess and compare weight and volume footprints of various ESS technologies for a particular application. A Ragone chart [113], which displays energy density vs. power density on a logarithmic scale as shown in Figure 2.2, is widely used for this purpose. This chart compares the approximate energy densities and power densities of a broad range of energy storage mediums including electrolytic capacitors, supercapacitors, superconducting magnetic energy storage (SMES) systems, thermal energy storage

(TES) systems, flywheels and fuel cells, in addition to a number of electrochemical battery technologies. These include vanadium redox (VRB) or flow batteries, lead-acid, zinc-bromine (ZnBr), nickel-cadmium (NiCd), sodium-sulphur (NaS) and lithium-ion (Li-ion) battery variants. As evident from the chart, supercapacitors and electrolytic capacitors are the most power-dense energy storage medium, whilst fuel cells offer the greatest energy density. Interestingly, Li-ion batteries have relatively high energy density and power density, making them useful for a diverse range of applications. Each storage medium, within their approximate range and discharge time, can be rapidly traded off and may be selected given reasonable assumptions associated with the scalability of a particular ESS technology.
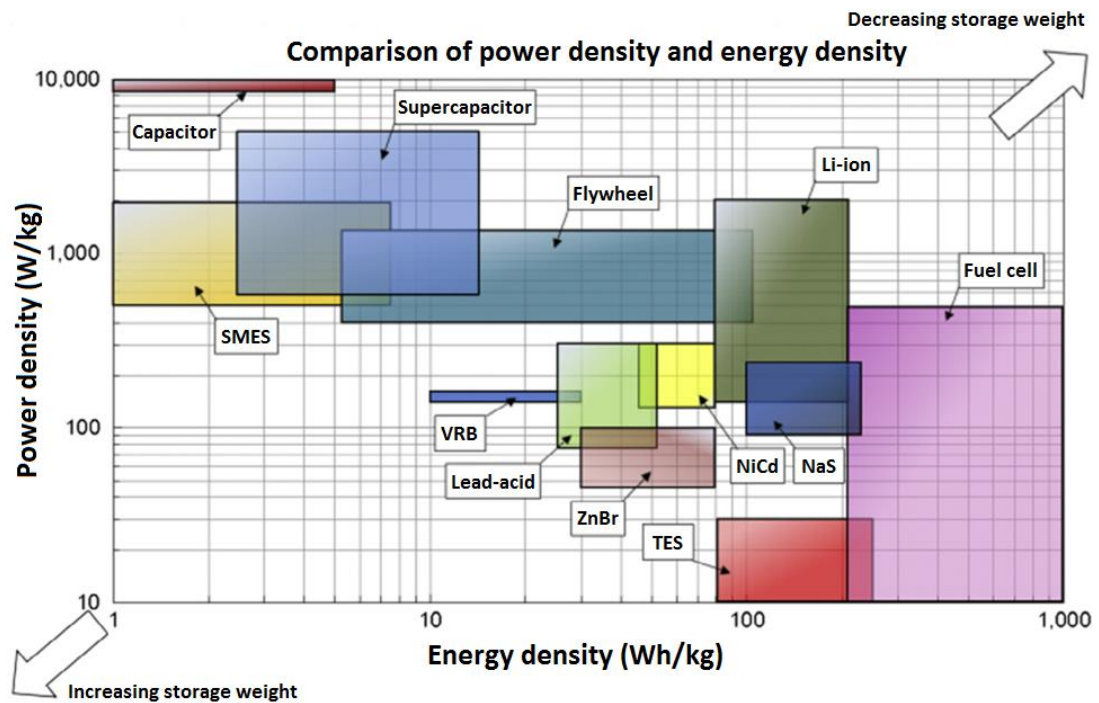
Figure 2.2: Ragone chart of energy storage mediums [113]

2.2.3 Life Cycle

The life cycle of an ESS is the number of full charge-discharge cycles that an ESS can withstand without significant degradation to its performance throughout its operational lifetime. This measurand is particularly useful in determining the

operational lifetime of a medium within a power system, and provides the system integrator with a reasonable estimation of its replacement or maintenance cycle.

2.3 Historical and current use of energy storage on aircraft electrical systems

Electrochemical batteries are conventionally the only form of electrical energy storage employed on aircraft power systems. They are predominantly used to provide back-up power for flight critical loads in the event of primary generation failure and have been in use since the era of twin channel 28V DC power distribution systems on aircraft of the 1940s and 1950s [41]. To this day, defence and commercial aerospace platforms still integrate battery ESSs directly to the 28V DC bus with sufficient capacity to deliver power to essential loads for up to 30 minutes under emergency power conditions [60]. In modern defence platforms, the batteries are also required to provide power independently for the re-ignition of jet engines in the event of engine flameout.

In more recent years, advanced electrical systems on commercial MEA such as the Boeing 787 integrate battery systems that utilise more energy-dense chemistries such as Li-ion or Ni-Cd [17], [86]. These ESSs also benefit from greater life cycle performance with deep-discharge capability and can therefore service more demanding network roles. For example, they are being used at the beginning of the flight cycle to supply power to the auxiliary starter motor drives in order to start-up the auxiliary power unit (APU) [10], [124]. Moreover, the batteries may require having the sufficient capacity to provide multiple start-up attempts. The APU generator is then used to bring the main engines online through the appropriate power electronic drives, essentially eliminating the need for a ground supply to energise the aircraft for take-off [17], [86]. Airbus Group is also investigating the integration of a hydrogen fuel cell ESS to replace conventional APUs on certain platforms [60], [125]. This early stage research aims to evaluate the feasibility of such system modifications and to determine the fuel and weight savings that may be achieved as a result. However, considerable research is still required to quantify

the benefits and to evaluate the reliability of fuel cells under the extreme conditions that they are likely to be subjected to within this application [19], [125]. Boeing have similarly demonstrated a hydrogen fuel-cell powered aircraft concept [126].

2.4 State-of-the-art and future trends of ESS use on aircraft electrical systems

2.4.1 Energy-dense storage systems

Looking forward, energy-dense electrochemical ESSs will play a more central role on future all-electric aircraft (AEA) platforms. For example, the electrical system on the Solar Impulse II concept demonstrator incorporates four Li-ion batteries with a capacity of 38.5kWh each [127]. This concept aircraft is designed to stay in flight over a period of several days using its photovoltaic generation system to charge its battery bank during sunlight hours. The batteries then supply power to all critical loads, avionics, environmental control systems and electrical propulsion drives during non-sunlight hours. Airbus Group's E-Fan concept demonstrator is another all-electric aircraft that employs a large bank of Li-ion batteries to supply the aircraft's fan-based propulsion system [128]. The first hardware iteration of this aircraft was recently demonstrated with a flight time of approximately 45 minutes. The second iteration is intended to be in flight for longer than 1.5 hours as a more energy-dense battery technology is developed [128]. A similar short duration 'inter-city' all-electric concept aircraft was demonstrated by a European consortium led program, ENFICA-FC [129]. This light-aircraft was powered by a combination of Li-ion batteries and a hydrogen fuel cell ESS to drive its electrical propulsion system and power its various avionic subsystems. Flight duration of 39 minutes was achieved by this demonstrator, establishing the viability of a 'zero CO_2 emission' hydrogen powered platform.

These small, single/dual passenger, all-electric aircraft concept demonstrators are evidently forming the test beds for evaluating the durability and performance of

advanced, energy-dense storage technologies in real-world flight conditions. However, the pace of adoption of state-of-the-art ESSs within commercial and defence aircraft is comparatively slower given the safety critical nature of the industry and the rigorous certification processes associated with deploying new technologies. The predominant energy storage medium that will continue to be deployed within these systems is likely to be Li-ion battery modules owing to their sufficiently high energy-density, simplicity of design and ease of integration [1], [2], [12], [19], [20], [57]. Nevertheless, research is still being undertaken to investigate alternative energy storage solutions that may offer other system wide benefits to the efficiency and functionality of advanced power systems on future aerospace platforms. One such area of recent interest is the integration of more power-dense ESSs. The following section provides a discussion on the benefits that power-dense ESSs can bring to the operational flexibility of aircraft electrical systems and other compact DC power system applications.

2.4.2 Power-dense storage systems

Power-dense ESSs with highly dynamic charge/discharge characteristics are being considered to perform a number of demanding roles and complex network functions within aircraft electrical power systems and other compact DC power system applications. These include meeting peak load demand, providing short term backup power and maintaining power quality during variable load conditions or switching events. They are also being considered to decouple the interactions between the electrical power system and the aircraft engine [57]. Such functionality can increase overall system efficiency, provide better transient performance, potentially reduce primary generation capacity and increase security of supply [58], [90], [95], [97], [98], [105], [112], [117]. Other applications include DC microgrids [88]–[90], integrated full-electric propulsion (IFEP) systems on marine platforms [61], [91], [92] and electric vehicle drivetrains [10], [94], [101], [124]. Figure 2.3 shows a chart of a broad range of ESS technologies, categorized by their discharge time characteristics and available power rating, enabling storage mediums to be

rapidly evaluated in terms of their suitability to meet the specific power and discharge time requirements of a particular application [25]. The storage technologies are grouped into short-term power quality and uninterruptable power supply (UPS) applications, medium-term transmission and distribution (T&D) grid support and load shifting applications, and long-term bulk power management applications. The data shown in Table 2.1 collated by Lou et al. in [113] provides a more detailed breakdown of the ESS technology characteristics including the overall efficiency, storage durability, self-discharge, lifetime and life cycle of each. From Figure 2.3 and Table 2.1, it is clear that the specific ESS technologies that can meet the rapid discharge time and power rating requirements to perform these functions include supercapacitor, SMES and flywheel energy storage systems [58], [113]. However, given the strict weight and volume restrictions on aerospace applications [1], supercapacitors are considered the most viable technology due to their achievable power density [57], [59]. This is also underpinned by their high life cycle rate, peak power output and fast discharge capability, as shown in Table 2.1.
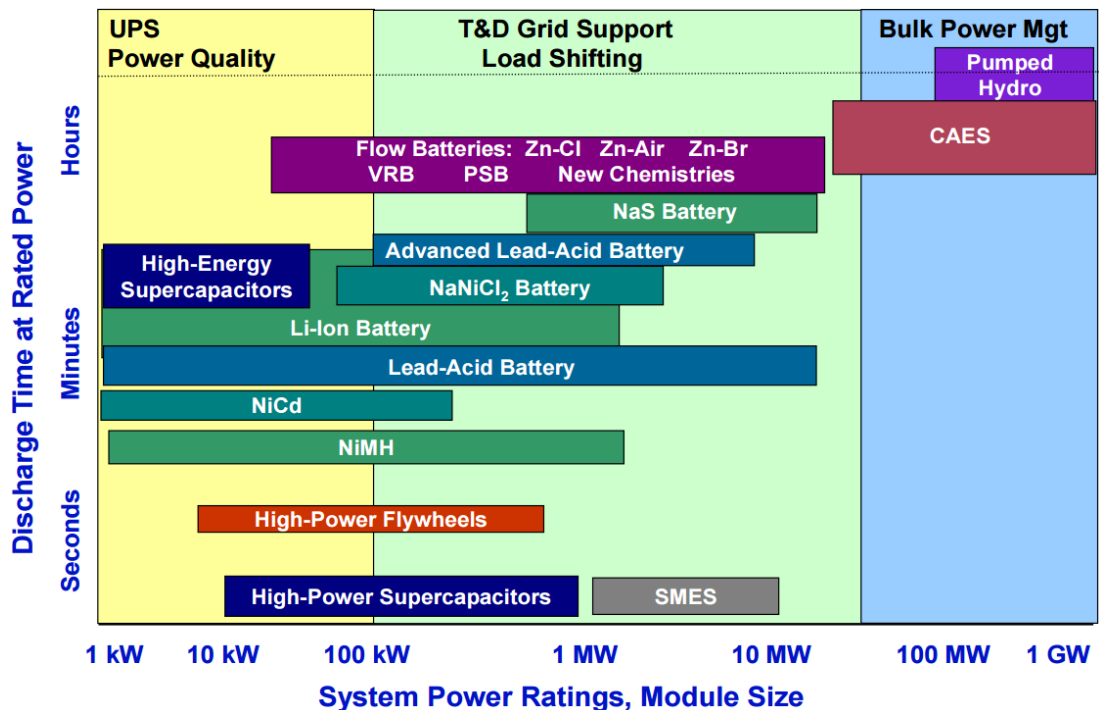
Figure 2.3: Discharge time characteristics of energy storage technologies [25]

Table 2.1: Data associated with various energy storage system technologies [113]

EES technology	Power range (MW)	Discharge time (ms–h)	Overall efficiency	Power density (W/kg)	Energy density (Wh/kg)	Storage durability	Self-discharge (per day)	Lifetime (years)	Life cycles (cycles)
Pumped Hydro	10–5000	1–24 h	0.70–0.82	-	0.5–1.5	h–months	Negligible	50–60	20000–50000
CAES (underground)	5–400	1–24 h	0.7–0.89	-	30–60	h–months	Small	20–40	>13,000
CAES (aboveground)	3–15	2–4 h	0.70–0.90	-	-	h–days	Small	20–40	>13,000
Flywheel	Up to 0.25	ms–15 m	0.93–0.95	1000	5–100	s–min	100%	15–20	20,000–100,000
Lead–acid	Up to 20	s–h	0.70–0.90	75–300	30–50	min–days	0.1–0.3%	5–15	2000–4500
NaS	0.05–8	s–h	0.75–0.90	150–230	150–250	s–h	20%	10–15	2500–4500
NaNiCl2 (ZEBRA)	50	2–5 h	0.86–0.88	150–200	100–140	s–h	15%	15	2500–3000
Ni–Cd	Up to 40	s–h	0.60–0.73	50–1000	15–300	min–days	0.2–0.6%	10–20	2000–2500
Li-ion	up to 0.01	m–h	0.85–0.95	50–2000	150–350	min–days	0.1–0.3%	5–15	1500–4500
VRB	0.03–3	s–10 h	0.65–0.85	166	10–35	h–months	Small	5–10	10,000–13,000
Zn–Br	0.05–2	s–10 h	0.60–0.70	45	30–85	h–months	Small	5–10	5000–10,000
Fe–Cr	1–100	4–8 h	0.72–0.75	-	-	-	-	10–15	>10,000
PSB	15	s–10 h	0.65–0.85	-	-	h–months	Small	10–15	2000–2500
SMES	0.1–10	ms–8 s	0.95–0.98	500-2000	0.5–5	min–h	10–15%	15–20	>100,000
Capacitors	Up to 0.05	ms–60 m	0.60–0.65	100,000	0.05–5	s–h	40%	5–8	50,000
Supercapacitor	Up to 0.3	ms–60 m	0.85–0.95	800–5000	2.5–50	s–h	20–40%	10–20	>100,000
Hydrogen (fuel cell)	0.3–50	s–24 h	0.33–0.42	500	100–10,000	h–months	Negligible	15–20	20,000

Commercial supercapacitor systems supplied by various manufacturers that are available on the market today exhibit a power density of up to approximately 5000kW/kg [113]. However, this is projected to significantly increase with the introduction of state-of-the-art systems exploiting recent breakthroughs in carbon nanotube and grapheme technology enabling a significant increase in electrode surface areas [130]–[133]. These devices are often subject to comparison with their energy-dense counterparts such as battery systems, however, their dynamic performances are notably distinct [112], [114]. Whereas batteries are a very useful solution for applications that require a significant quantity of energy over a relatively long period of time, super-capacitors can deliver a particularly high quantity of power over a much shorter period of time. In addition, supercapacitors offer a charge/discharge life cycle considerably greater than that of battery systems. Their limit, however, lies in the energy density that can be up to two orders of magnitude smaller than that of high capacity batteries [113]. Thus, employment of both devices in aircraft electrical networks may provide useful solutions to unique challenges. Interestingly, developments in the electrode design of advanced lithium based battery technology are enabling significant improvements to the power density of such mediums that may be comparable to supercapacitor performance [134]. Thus, the potential to use these ESSs for both bulk storage (long-term power) and power quality purposes (short-term power) could be significantly advantageous, and may provide a more competitive solution in comparison to separate energy storage devices for tailored network roles.

The following section provides a comprehensive literature review of the roles, functions and applications of advanced high-power, high-bandwidth ESSs within a broad range of DC power system applications. The applicability of these functions within the context of aircraft electrical power systems are discussed and analysed.

2.5 Review of applications and challenges of high-power ESS integration within compact DC power systems applications

This section provides a literature review of the functional-level applications and systems-level benefits of integrating a high-power ESS within a variety of DC power system applications throughout the power industry.

The functions that high-power ESS's perform are categorised into three broad areas. These are:

- Maintaining power quality and mitigating voltage transients
- Meeting peak load demand
- Offering short term backup power and voltage support

Integration of high-power ESS's have been proposed for a number of power system applications including telecommunications platforms [106], [135], [136], DC microgrids [62], [65], [88], [89], future aircraft [1], [57], [58], [63], [93], [104], electric vehicle powertrains [94], [97], [124], and power distribution systems for the all-electric ship [58], [61], [69], [73], [92].

The ESS, in each of these applications, offers systems-level benefits to the functional capability, transient performance and physical design of the electrical system. This section categorises the particular network conditions and scenarios for which power-dense ESSs can offer systemic benefits. The operational requirements of the power-dense energy storage system to perform these particular functions are established, and the applicability of these functions within the context of an aircraft electrical power system is analysed.

2.5.1 Power quality / voltage transient mitigation

Voltage transients normally occur within electrical power systems due to large step changes in electrical demand from loads connected to the network [24], [78], [83].

Voltage transients can be classified as either undervoltages or overvoltages [24]. Sustained undervoltage conditions have the potential to interrupt continuity of supply to loads, potentially causing electronically driven loads to shut down [71]. Overvoltages can be particularly hazardous, potentially damaging sensitive loads and increasing the likelihood of insulation breakdown within cables [71]. To minimise the disruptive propagation of electrical transients, strict regulations that specify the transient envelopes for electrical power distribution buses are adhered to in order to standardise the requirements of electrical sources and subsystems integrated to the network. The most commonly referenced power quality standards that define the upper and lower limits, and duration of voltage transients for aerospace applications is MIL-STD-704F [137]. The normal transient envelope for the 28V DC and 270V DC bus is shown in Figures 2.4 and 2.5.
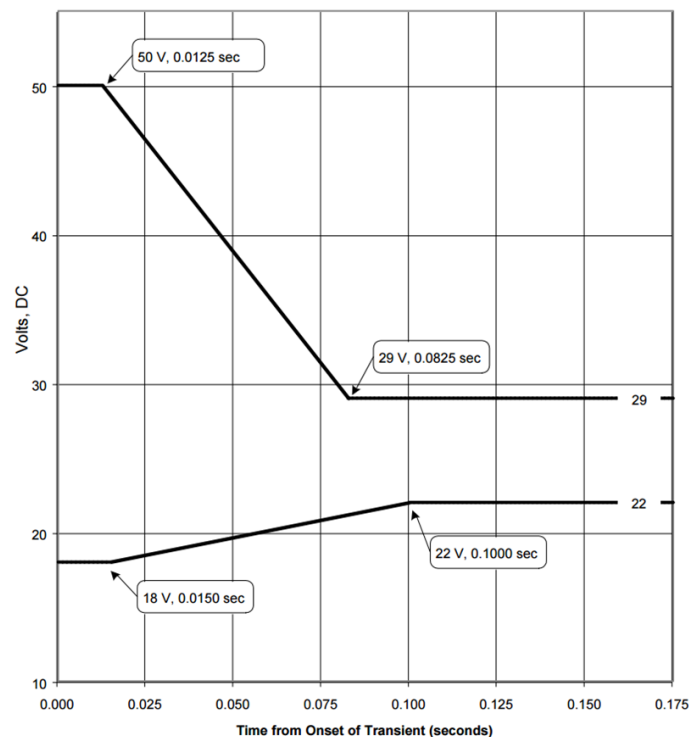
Figure 2.4: MIL-704F voltage transient envelope for 28V DC bus for load transitions [137]
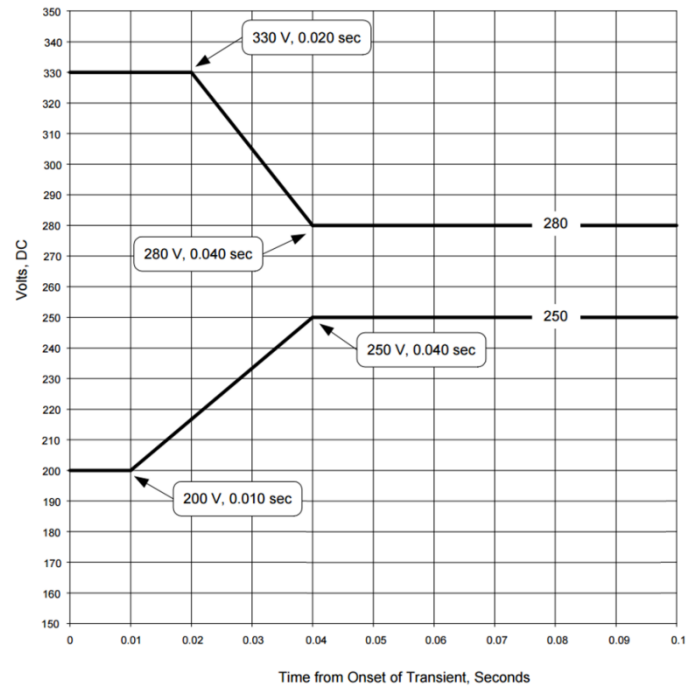
Figure 2.5: MIL-704F voltage transient envelope for 270V DC bus for load transitions [137]

These standards are also being embraced by commercial airframers and system integrators with growing interest in the wider use of 270V DC distribution on future commercial platforms [9], [57], [84], [104], [138], [139]. When integrating power system components, the systems integrator must ensure that the primary source of power and associated power electronic conversion that regulate the DC bus are sufficiently rated such that normal voltage transients produced by any load steps do not exceed the thresholds depicted in Figure 2.5. To meet this criterion, the primary generation system must also have a sufficiently rapid response time. All loads and subsystems connected to the DC network must also be designed to withstand all transients that lie within the defined transient envelope.

However, electrical systems on future aircraft that incorporate greater levels of high-power electrical loading may experience significant voltage transients that exceed these thresholds if regulation of the bus voltage is poorly managed [82]. High-power loads may be abruptly switched into the network via contactors or

29

electromechanical breakers causing a sudden increase in demand, if no soft-start functionality is provided. Similarly, immediate disconnection of these higher power loads may result in significant overvoltages if voltage regulation is not appropriately designed. Example high-power electrical subsystems on future MEA aircraft include environmental control systems (ECS) and electrical wing ice protection systems (WIPS) [1], [11]–[13], [17], [19]. Electromechanical actuators for wing ailerons and flaps may also exhibit more dynamic load profiles that may regenerate energy back to the DC bus, causing undesirable overvoltages. Furthermore, loads driven by power electronic converters with large input filter capacitance, when switched into the network, may cause sever undervoltages and large current overshoots as the capacitors energise. Controlled turn-on of such subsystems using soft-start pre-charge circuits [51], [53], [140] or advanced SSPCs to limit inrush may alleviate the depth of undervoltage produced [84], [141]. However, the only commercially available SSPCs installed on existing platforms with this functionality are 28V DC devices.

One approach to reduce the severity of voltage transients is to improve the response time of the primary generation system to meet the initial demand of higher power loads on the network. If the DC bus is supplied via an uncontrolled passive front end such as an autotransformer rectifier unit (ATRU), then the DC voltage dynamics will be governed by the regulation of the AC side voltage via the generator control unit (GCU). Reducing the overall time constant of the overall closed loop control may improve the DC transient response. Indeed, greater DC side capacitance and incorporation of an outer DC voltage control loop as part of the GCU controller may also improve DC transient behaviour if passive rectification is used. Alternatively, an active rectifier employing high frequency switching may be integrated to improve DC side voltage regulation through the use of high bandwidth controller designs allowing the DC side voltage regulation to be decoupled from the GCU/AC side control. This may enable higher power loading transitions without violating power quality standards on either side of the converter.

However, both of these solutions, although technologically feasible, may have significant complexity, cost and reliability implications for the primary generation design. Additionally, the burden of meeting the electrical demand of these high-power loads is placed entirely on electrical engine off-take. Evaluation of the impact on the engine off-take components and the subsequent transient performance of the engine itself is an area of ongoing research within academia and industry. For example, Todd et al. have shown in [142] that large electrical transients can produce undesirable torque transients on engine mounted gearboxes that drive the primary generators on commercial and defence aircraft. These transients may increase maintenance costs over the lifetime of the engine as mechanical gear box components are exposed to greater wear. However, implementation of torque slew rate limitation control [59] may minimise the propagation of such large electrical transients through to mechanical systems.

Integration of a power-dense ESS has therefore been proposed to improve the overall transient performance of the electrical power system by absorbing or exporting power to stabilise the DC voltage during load transitions and thereby minimise the propagation torque pulsations. Initial feasibility studies have been performed by Wu et al [59] and others [14], [57], [58] for more electric aircraft applications and are currently being explored by various industrial systems integrators.

Precedent has been taken from application areas such as state-of-the-art electric vehicle power trains where the use of supercapacitor based ESSs have been proposed to improve performance of electrochemical batteries and fuel cell systems [90], [94], [97], [124], [134], [143]. Similar functionality has been demonstrated in more conventional grid level distributed generation sources to minimise impact on gear boxes in wind turbines driven generators [89], [144].

2.5.2 Meeting peak demand

Power systems must be designed to ensure that the total installed generation capacity on the network matches the aggregated demand from connected loads. Incorporation of additional loads on a system that have highly dynamic or transient load profiles can have significant implications on the required rating of primary generation and may compromise the viability of a particular system design. For example, within a MEA application, installation of additional generation capacity can result in significant weight penalties that can substantially increase the operating costs of an aircraft by means of increased fuel burn. Similar implications for electric vehicle applications and marine power systems can also be incurred. Integration of power-dense energy storage to meet the demand of peak power loads may prove to alleviate the need for increasing primary generation capacity, and in certain applications, may even serve to reduce it [62], [99], [113], [117], [134]. For example, Figure 2.6 shows a high-level diagram of an electric vehicle with an integrated supercapacitor ESS, coupled to the primary drivetrain.
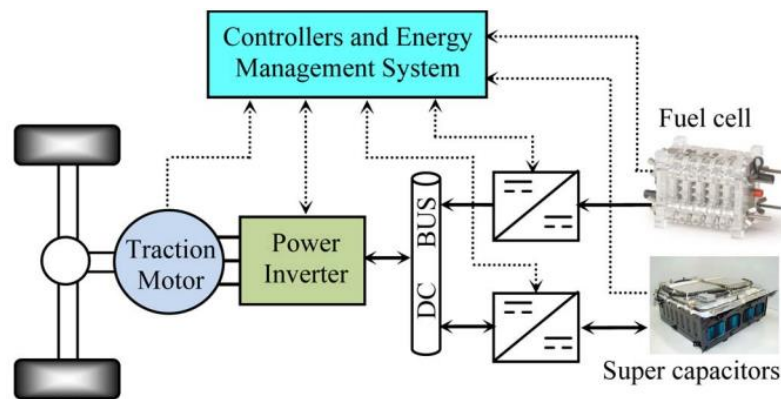
Figure 2.6: Typical EV drivetrain with integrated supercapacitor based ESS

Within this application, the supercapacitor ESS is used to provide power during moments of peak demand, for example when the car is accelerating. This can

decrease the demand placed on the primary energy source (fuel cell system or electrochemical batteries) and can enable a reduction of the power rating of its primary converter interface [134]. This in turn has the potential to reduce this particular component's weight, volume and cooling system requirements.

On marine platforms such as aircraft carriers, flywheel energy storage devices are being proposed to supply the significant quantity of power required to launch military jets using its electrically actuated slingshot mechanism [145]. They have also been proposed to support large peak power motoring loads on IFEP systems [61], [91], [92]. Other applications include supporting the supply of peak power to electrical weapons systems and high-power radar loads that exhibit cyclic demand profiles [61], [73], [99]. Power-dense energy storage, in all these application areas, may alleviate the need to increase the overall rating of the primary generation to match demand.

Given the benefits demonstrated within other compact DC power system applications, there has been considerable interest in the integration of power-dense ESSs on future MEA platforms to meet the peak load demand of various electrical subsystems. In particular, they are being considered to meet the demand of high torque motoring systems for electrically actuated flaps, slats, ailerons and rudders etc [7], [10], [14], [111], [146], [147]. Similarly, they are also being proposed for high-power cyclic loads such as radar systems [9], [62].

2.5.3 Short term backup power / voltage support

A typical use of an ESS in many application areas is to provide immediate short term backup power in the event of a loss of primary power. This mode of operation can be described as 'voltage support mode' and can be provided by both power-dense and energy dense ESSs. In the event of a sustained reduction in network voltage, the ESS is used to continuously supply power to maintain the system voltage at its nominal operating level. This is a primary function of ESSs in applications that require an uninterruptable power supply (UPS) including telecommunications equipment and datacentres where even a short term undervoltage condition can be extremely disruptive [148]–[150]. Common storage technologies that are used for UPS systems include flywheel energy storage systems, electrochemical batteries and supercapacitors [107], [113], [149], [150]. Such systems ensure a continuous supply of power to sensitive loads for a period of time that is sufficient to allow longer-term backup generation to be activated. Other examples include microgrid systems and shipboard electrical systems that incorporate medium to large scale energy storage systems. Within these applications, the ESS is kept at 100% SOC during normal operating conditions to enable voltage support for the maximum possible duration. Detection of undervoltage conditions from a centralised power management system, or in certain cases from the measurement of voltage from the terminals of the ESS can be used to trigger the activation of voltage support functionality [61], [91], [92].

Within the context of an aircraft electrical system, this function is automatically provided by the backup battery system. However, only flight critical loads such as those required to safely operate the aircraft under emergency conditions are supported by this function. On future aerospace platforms that may incorporate power-dense ESSs on the high voltage DC bus, this voltage support function may also be provided for a short period assuming sufficient capacity is available. This may be particularly useful during periods of network reconfiguration. For example, in the event of a generator fault or loss of on engine, the electrical network

reconfigures to enable the connection of the APU generator or until load shedding takes place. During this transition, all loads may be supplied by a single generator for a short period of time as the APU initiates. As an alternative, the energy storage device may be used to provide this short term power, or at least support the primary generation in order to reduce the significant demand placed on the single generator [12], [125], [151]. This functionality may enable a reduction in generator overcurrent rating and may also reduce the engine transient response during these conditions.

2.6 Conclusions

The quantity and complexity of roles that ESSs are being proposed to play in modern aircraft is increasing owing to the systemic performance improvements that may be made. The most viable storage technologies for aerospace applications and their projected use cases were presented in this chapter together with a review of the functions that state-of-the-art in high-bandwidth, high-power energy storage play within a broad range of compact DC power system applications. The following chapter explores the challenges associated with integrating such energy storage systems.

Chapter 3

State-of-the-art in DC protection and a review of power-dense ESS fault behaviour

This chapter presents the state-of-the-art in the intersection of two seemingly disparate areas of research: the protection of compact DC power systems, and the integration of high-power, high-bandwidth energy storage systems within compact DC power systems. The system-level interaction of these integrated subsystems underpins the following research question answered in this thesis:

How does the response of a high-power, high-bandwidth ESS integrated within a current limited compact DC power system environment impact the performance of the network-wide protection system under fault conditions?

The chapter begins by introducing the topic of power system protection, and hence establishes the motivation for preventing the destructive and potentially fatal effects of faults within aircraft electrical power systems. A review of the state-of-the-art in DC fault detection techniques, protection switchgear and protection systems for future MEA and other compact DC power systems applications is then conducted.

The following subsection reviews the enabling technologies for the effective integration of high-power ESSs within electrical power systems. Functional requirements of the ESS power electronic converter interface are derived, taking into account the physical constraints and limitations associated with its operation. Functional-level control strategies that enable different modes of ESS operation are analysed and assumptions associated with overall ESS behaviour under normal and abnormal conditions (i.e. during network faults) are then defined.

Finally, the shortcomings in the literature that fail to address the challenges associated with ESS behaviour during network faults are analysed. In particular, the seemingly limited research and discussion on the performance of protection systems (within existing or new build applications) as a result of the fault response of network integrated energy storage is investigated.

3.1 Aircraft electrical power system faults

Electrical faults are a source of significant fire risk on aerospace platforms. A recent example reported by the UK Air Accidents Investigation Branch (AAIB) involved a Boeing 777 that experienced an electrical failure on the main distribution bus after a second generator was brought online [152]. This failure resulted in severe internal arcing events and short circuits within the two main power contactors of the main bus, compromising the contactor casing and igniting nearby insulation blankets with fire and heat causing damage to the structure, cooling ducts and wiring. In 2012, electrical arcing between a main feeder wire and a titanium hydraulic line of an F-22 Raptor military aircraft was sufficient to breach the material, causing the hydraulic fluid to ignite and thus resulting in the catastrophic failure of the aircraft [153]. Faults can occur within sections of an aircraft electrical power system due to a variety of causes, including:

- Abrasion of cable insulation due to chafing, repeated flexing, or contact with high temperature surfaces leading to exposure of energised conductors.
- Internal faults within generators, transformers, power electronic converters, distribution units and any corresponding connectors due to aging, continuous environmental exposure or vibration.
- Breakdown of insulation caused by excess overloading or by overvoltages due to electrical switching transients.
- Secondary damage from accidental mechanical failures.

Faults can occur within both the AC and DC sections of an electrical network and may cause considerable physical damage at the point of fault. Damage may also be incurred by system components through which fault current is carried.

AC side faults on three-phase systems can be classified as one of the following: phase-to-phase or three-phase 'balanced' faults; or single-phase-, phase-to-phase- or three-phase-to-earth faults. DC side faults can be classified as: rail-to-rail or rail-to-rail-to-earth for two-wire systems, and/or rail-to earth (positive or negative) in the case of three-level mid-point earthed DC distribution systems. Note that the metal fuselage (or structural airframe on modern composite body platforms) is used for earthing the aircraft electrical system [154].

A fault with negligible fault impedance is referred to as a short circuit. If the path of fault current flows through some external impedance, such as through the composite material of the fuselage, then this impedance is known as the fault impedance. Equally as hazardous is an open-circuit fault condition which may be caused by a loose connection or a break in a conductor where series arcing can occur as the break develops. This can cause significant localised increases in temperature with potentially detrimental consequences to equipment in close proximity [152], [153].

Faults may also be classified as being sustained (e.g. a solidly clamped short-circuit or a complete break in a conductor), semi-sustained (e.g. the conduction path of the fault 'burns-out' after sufficient energy has been dissipated through it), or intermittent (e.g. a loose connection or exposed conductor causing recurring faults due to vibration). It is also possible for one type of fault to develop into another type over time. For example, series or parallel arc faults may evolve into a short circuit fault if the exposed conductor forms a conduction path to earth.

It is the role of the protection system to prevent any systemic damage that may lead to catastrophic failures caused by electrical faults. This is achieved by rapidly and discriminatively isolating faulted sections of the network via dedicated

protection switchgear. These switchgear devices may be distributed across the network and may be designed to operate in isolation or in coordination with other such devices. Similarly, coordination with internal protection functions of electrical sources or power converters may be achieved in accordance with the specific requirements of the application. The following section outlines the key design and performance criteria for the operation of electrical protection systems.

3.2 Protection system design criteria

The function of an electrical protection system is to promptly and automatically disconnect any element or section of a network which starts to operate in an abnormal manner that may cause damage to the rest of the system. Reference [155] outlines the key design criteria of an electrical protection system for any power system application. These criteria are:

- Selectivity – In the event of a fault on a network, the protection system should trip only those switchgear devices whose operation is required to isolate the fault. This is also known as `discrimination'.

- Speed – The protection system should aim to isolate faults on a network as rapidly as possible to reduce fault related damage and prevent cascading faults through the collapse of the network voltage.

- Stability – The protection system should remain unaffected by conditions external to the protected zone (usually associated with unit protection).

- Sensitivity – The protection system should be sensitive to a minimum operating level.

- Reliability – Protection equipment and protection system performance should be highly reliable. Reference [156] outlines the following criteria by which operational reliability of a protection system is measured:
  - Dependability – The measure of the degree of certainty that a protection system will operate correctly when required, and at the

designed speed. Dependability is a concern when a fault occurs within a defined zone of protection.

- o Security – The measure of the degree of certainty that a protection system will not operate incorrectly or faster than designed. Security is a concern for operation of the system under normal (un-faulted) operating conditions and for faults external to the protected zone.

- Backup functionality – The protection system must have a means of isolating a given fault in the event of a failure-to-detect or failure-to-isolate condition. Backup functionality may be enabled by the provision of redundant protection system elements, graded co-ordination of devices, or secondary or tertiary systems.

As with the system design objectives, the importance of each of these factors varies with the requirements of a particular application area. For the purposes of the protection systems investigated within this thesis, particular emphasis is given to the selectivity and speed criteria (and the subsequent impact on protection system operational reliability). The following subsection outlines principles of operation of an electrical protection system and describes the functions of its constituent elements.

3.2.1 Operational principles of protection systems

All protection systems operate using the same underlying principles. Protection systems and devices require a means of acquiring measurements associated with the electrical system (either directly or indirectly); a means of determining whether a fault has occurred; and a means of isolating sections of the network. Figure 3.1 shows a flowchart of the constituent elements of a protection system.
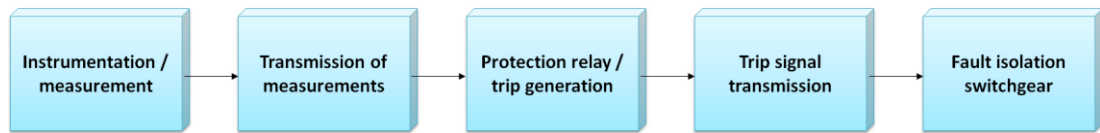
Figure 3.1: Constituent elements of a protection system

Power system measurands, i.e. voltage, current and/or temperature, are acquired using appropriate instrumentation or sensing technology suitable for the application. For example, temperature measurement may be used to detect internal overheating of power system components such as converters, triggering isolation to prevent thermal damage. These measurands are then transmitted either electrically (i.e. analogue transmission) or communicated (i.e. digital transmission) via an appropriate communications protocol to a protection relay. Fault detection is performed by the protection relay component which generates a trip signal after an appropriate delay (where necessary) in the event of a positive determination of a fault condition. Fault isolation is then performed by a corresponding switchgear device (such as a breaker, contactor or solid-state switch) that is triggered by the transmitted protection relay trip signal.

Passive protection devices for relatively low voltage/current applications such as circuit breakers (CBs), residual current devices (RCDs) and fuses all employ electro-mechanical or electro-thermal trip mechanisms, normally relying on a direct means of measuring current and/or voltage to function [157], [158]. In higher voltage/current applications, an indirect means of obtaining these measurements is used, such as voltage/current transformers [159], Hall Effect devices [160], optical sensing technology exploiting the Faraday Effect [161] or equivalent instrumentation [162]. Conventionally, the electrical outputs from these instruments are fed directly to an electromechanical protection relay via a pilot wire mechanism. Depending on the application and deployed technology, the relays themselves may be motor operated, utilise a magnetic induction disk mechanism or may function using an electromagnetic solenoid [155], [163].

Modern protection relays are electronic in nature and operate using power system measurands that are digitally sampled prior to being computationally processed through software implemented protection algorithms. The protection algorithms executed by these devices may be tailored to perform specific protection functions, enabling more configurable protection schemes with greater operational reliability, accuracy and flexibility. Typical examples of fault detection algorithms include instantaneous overcurrent and undervoltage protection, or more complex time-dependant algorithms including fault energy evaluation (i^2t), inverse definitive minimum time (IDMT) relaying and arc fault detection. Functions that rely on the computation of measurements from multiple remote sections of the network such as differential unit protection are also widely employed within many power system applications [155].

Irrespective of the power system application and protection system type, the constituent elements of advanced electronic protection relays are fundamentally similar. Figure 3.2 shows a representative diagram of these constituent elements.
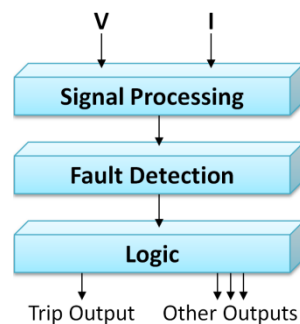
Figure 3.2: Constituent elements of a protection relay

Measurements of voltage/current obtained by the power system instrumentation systems are normally sampled at a relatively high frequency using an analogue-to-digital conversion system (ADC) and acquired via the signal processing unit, as shown in Figure 3.2. Signal conditioning such as filtering functions to remove certain frequency components may also be performed by the signal processing unit. In addition, transformations such as Fourier transforms and further processing such as

the derivation of the rate-of-change of acquired measurands may be performed to extract the necessary information required by the fault detection element of the relay. The fault detection element processes this information through a relevant software implemented fault detection algorithm.

The computed output from the fault detection algorithm is then compared to predetermined thresholds/trip-curves using logic functions or circuitry that determine the trip status of the device when these trip-thresholds are exceeded. A gate driver circuit (or equivalent for an electromechanical breaker) receives this trip signal prompting the opening of the relevant switch device. Other outputs and data may be made available by protection relays, for example overload and undervoltage detection and the number of historical trips that may not necessarily be used for triggering isolation devices. Both fault detection and isolation functions may be performed on the individual protection device itself, or separately in the case of centralised, communications based protection solutions that are expanded upon in later sections of this thesis.

3.3 State-of-the-art in aircraft electrical protection systems

The growing necessity for the incorporation of advanced, electronically controlled protection devices for MEA platforms is being driven by the increase in complexity, power density and interconnectivity of future aircraft electrical systems. These systems are incorporating greater quantities of power electronic conversion, higher-voltage DC distribution architectures, increasingly dynamic loads and advanced energy storage systems. Advanced protection devices can perform complex relaying functions offering improved trip accuracy over conventional protection devices that may lead to significant improvements to the safe operation of electrical distribution systems on future aircraft. This subsection provides a literature review of conventional and state-of-the-art electrical protection devices and schemes applicable to aircraft power systems.

3.3.1 Conventional overcurrent protection

Electrical protection devices are critical to the safe and secure operation of aircraft power distribution systems and associated subsystems. Conventional circuit breaker (CB) devices are still widely utilised on current platforms to protect loads and distribution cables from damage caused by short-circuit electrical faults. These protection devices are typically rated to protect 28V DC and 115V$_{rms}$ AC distribution systems offering trip-times of 0.36 – 1.4 seconds for overcurrent thresholds that are 10 times the rated current of the device [164]. Approximate i^2t trip-time curves for commercial-off-the-shelf (COTS) CB devices are shown in Figure 3.3. These curves indicate the trip-times associated with the CB device when the fault current, given as a percentage of the rated load current, exceeds the set current rating of the device. Trip settings of a relay can often be user configurable, allowing the trip-curve to be shifted along the % Rated Current axis, to allow for optimising the trip thresholds as represented by the 160% rate current trip-time curve.

Remote control circuit breaker (RCCB) devices offer similar protection functionality to conventional CBs, but with the added flexibility to operate the device manually from a remote location via appropriate circuitry [84]. A diagram of a COTS CB and RCCB is shown in Figure 3.4.
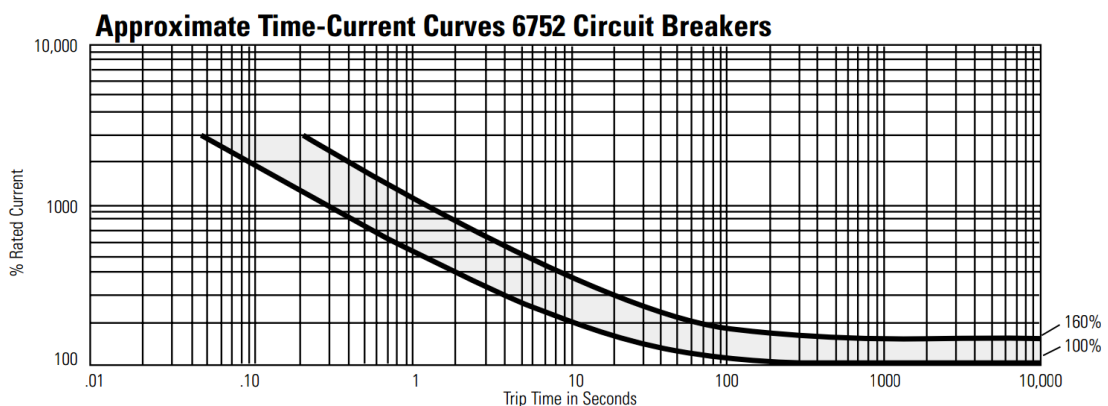
Figure 3.3: Approximate time-current curves of COTS aircraft CBs [164]
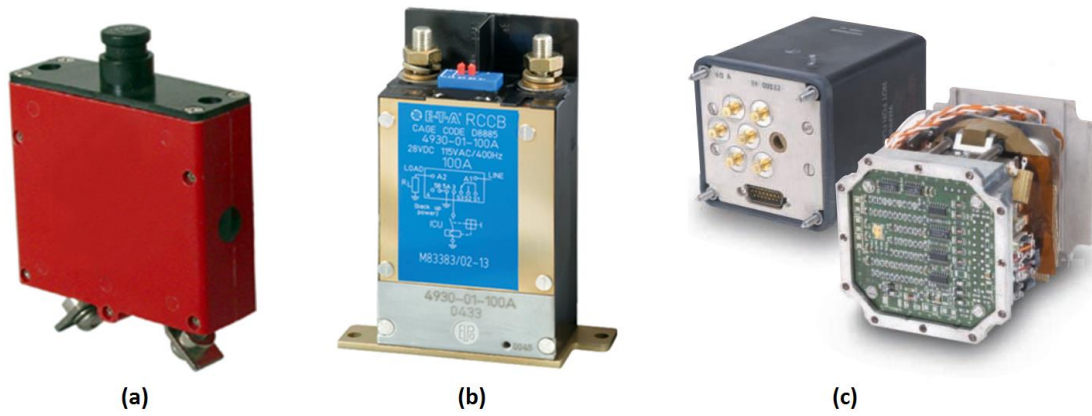
Figure 3.4: (a) Sensata single-phase AC circuit breaker [164], (b) E-T-A RCCB [165] and (c) Esterline high-power electrical load contactor unit [166]

Higher-power AC loads and network sections are typically connected to the power system via electronic load contactor units (ELCUs) (COTS ELCU shown in Figure 3.4 (c)). These devices also offer per-phase overcurrent and phase-imbalance protection functionality via on-board electronics [41], [166]. A representative diagram of the constituent components of ELCU is illustrated in Figure 3.5.
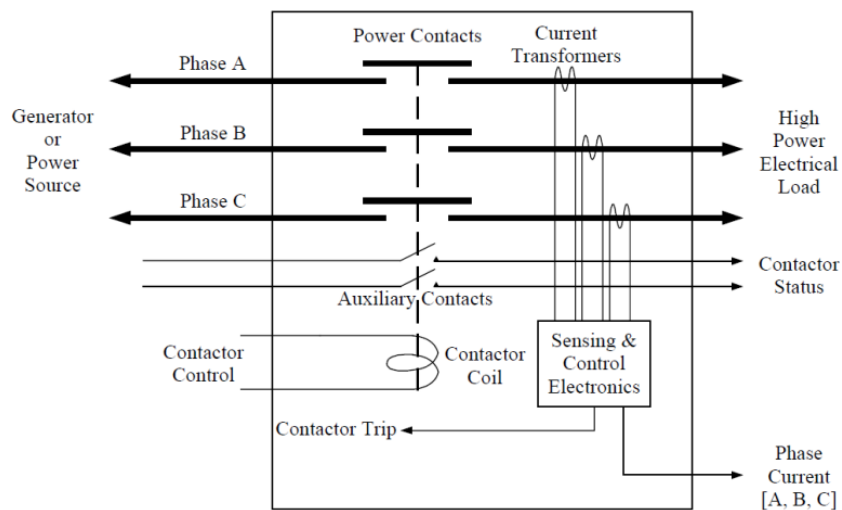
Figure 3.5: Representative diagram of an ELCU AC protection device [41]

These switch/protection devices incorporate appropriate instrumentation to enable individual phase currents to be measured and processed by internal control electronics to compute a trip signal in the event of a fault, actuating the corresponding electrical contacts. These devices are also configurable to allow the device trip characteristics to be closely aligned with the connected load or network section. The typical overcurrent protection algorithm employed on ELCUs is a modified form of i^2t to emulate the performance of mechanical devices such conventional circuit breakers or thermal fuses. However, they can also be configured to receive external trip signals that enable them to be used for more complex protection schemes. For example, this external trip functionality may be utilised by a differential protection scheme for protecting safety critical sections of the network, as discussed in the following section.

3.3.2 Differential protection

Differential protection (DP) is an established and widely adopted method used throughout the power industry to detect short-circuit faults by exploiting Kirchhoff's current laws [155], [167]. It is a rapid and highly selective method of detecting faults within a specified location on a network or within power system equipment such as motors, generators or transformers [167]. Within an aircraft power system, the electrical off-take system from the engine mounted generators to the main AC distribution bus is protected using DP. This primary protection function is normally performed by the generator control unit (GCU) and enables the rapid detection, discrimination and isolation of faults located within predefined zones of the AC network that the GCU monitors. A simplified diagram illustrating the GCU DP for the Airbus A319 aircraft is shown in Figure 3.6 [168].
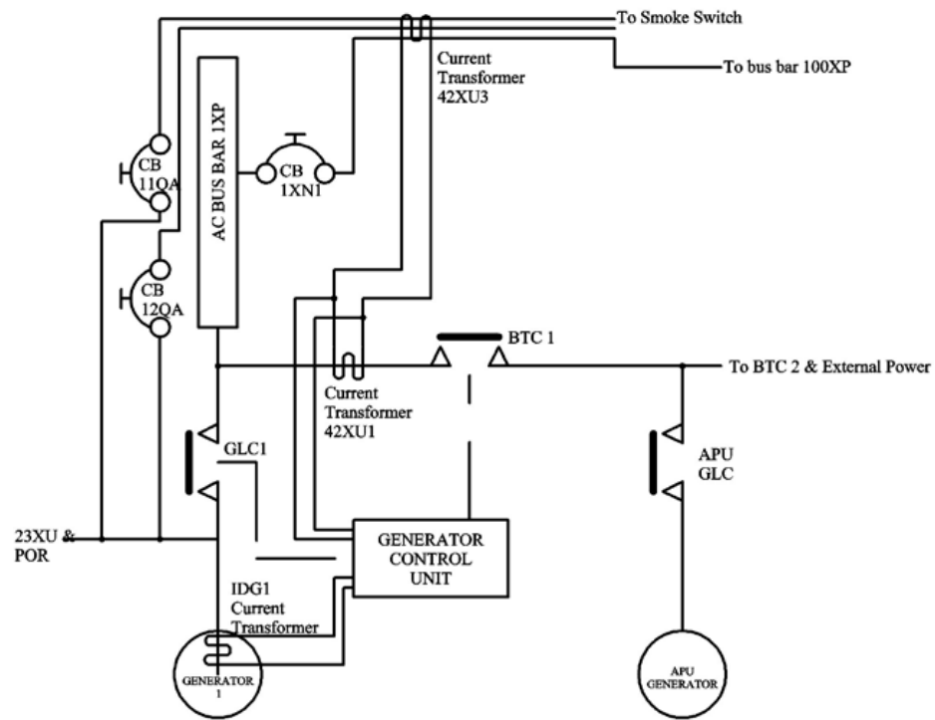
Figure 3.6: Simplified schematic of the primary conversion, CTs and GCU DP [168]

The differential protection functionality provided by the GCU uses current transformers (CTs) located at strategic points on the primary feeder network that continually measure current at these locations [41]. There is one CT within the generator, one downstream of the bus tie contactor (BTC) and one downstream of the primary AC Bus. Under normal operating conditions, the generator load contactor (GLC) is closed, the BTC is open, and power flows from the primary generator to all loads via the AC bus bar. Alternatively, if the primary generation is offline, the GLC will be open whilst the BTC and APU GLC will be closed, allowing power to flow from the APU to the loads.

Two differential zones are provided by the GCU on this particular system [168]. The GCU continually monitors the difference in current measured at these CTs. In the event that a difference in current greater than a predetermined trip threshold is reached for greater than 40ms, then the DP is triggered and both the BTC and GLC are opened, de-energising the AC bus bar.

After a further period of time (approx. 100ms), a second differential measurement is taken. If the difference in current no longer exists then the fault is assumed to have been located within the section of network between the GLC and the BTC or on the AC busbar, as the isolation of electrical power to the network has removed the fault. Under this fault condition, the BTC and GLC remain open and the generator is de-excited.

However, if the difference in current at the CTs is still detected at the second time of measurement, then the fault is assumed to have been located upstream from the GLC – i.e. a generator fault or fault located on the generator feeder. Under this fault condition, the GCU ensures that the GLC remains open but the BTC is allowed to close to enable the connection of the affected electrical network to another source of AC power (e.g. alternative engine generator or an APU generator).

3.3.3 Arc fault detection

Whereas conventional electro-thermal CBs are designed to protect wiring from thermal damage during excessive overcurrent scenarios, detection and discrimination of arcing events on aircraft electrical systems requires the use of computational electronics to determine if an arc fault is present on the system [169]. For example, commercial arc fault protection devices such as Labinal Power Systems' Arc-Fault Circuit Interrupters (AFCI) [170] measure and analyse the current waveform to recognise unique signatures of arcing events.

In the literature, a number of different current signature analysis algorithms have been proposed in recent years for detecting arc faults. Some reflectometry based methods use a time domain approach [171], [172], while others rely on a frequency domain [173] or a wavelet analysis [174], [175]. More recent developments to detect intermittent arc faults using a transmission matrix approach to model sections of the network, and locate them using a genetic algorithm have been implemented by Yaramasu et al [176].

3.3.4 Fault location using harmonic analysis

Accurately determining the location of a fault within an aircraft electrical power system is valuable for the reliable operation of both online protection systems and offline systems used for post-fault maintenance. Harmonic analysis methods using current and voltage waveforms to locate faults have been demonstrated within the literature for a wide range of power system applications. These methods can be broadly categorised as being based on either impedance estimation techniques [223] or travelling wave analysis methods (high-speed propagation of current and voltage fault transient waveforms) [224]. Travelling wave analysis methods are not commonly considered for estimating fault location within physically compact power system applications with relatively short cable lengths such as aircraft electrical systems due to the significantly high bandwidth data acquisition and computational requirements.

However, various impedance estimation methods applicable to aircraft power systems have been proposed in the literature. For example, a passive harmonic impedance estimation technique has been proposed by Zhou et al in [177] and mathematically validated in [178] that uses the third harmonic frequency of the AC current and voltage profiles to identify the impedance and location of a fault within a few fundamental cycles. Although initially demonstrated as an offline method, it has been proposed that it may be developed into an online tool to predict the location of network faults for use as a backup protection mechanism.

A similar technique called active impedance estimation (AIE) has been demonstrated in a zonal DC marine power system that uses a power converter connected to the bus to inject a short-duration spread frequency current to measure the bus impedance [179]. Through processing of the voltage and current responses, the system impedance is estimated as observed from a strategic point of measurement. A portable unit that also uses this technique has been demonstrated by Jia et al in [180] that may be suitable for post-fault maintenance processes.

These methods may be applicable to DC electrical power systems on future aircraft platforms.

3.3.5 Fault current limited DC systems

Faults in DC networks can pose exceptionally demanding protection challenges in terms of speed of propagation and fault current magnitude in comparison to faults within AC systems [83], [181]. Safe network operation during fault conditions is especially challenging in compact, power-dense systems with minimal fault path impedance. In particular, interconnected DC distribution systems have been shown to experience significantly high fault current levels that require rapid protection system performance [24], [55], [182]. These issues are strongly driven by the behavioural characteristics of standard voltage source converters, used for rectification in DC networks, under fault conditions. These are namely: the inability to limit fault current and the relatively low fault tolerance of the converters [83], [181]. Increasingly popular solutions to overcome these limitations include the redesign of the converter to be more fault-tolerant and the use of converter based current limiting to suppress fault current [85], [183], [184]. Advanced topologies of certain power electronic converters also enable galvanic isolation between the input and output stages of conversion, preventing passive uncontrolled conduction of fault current through the converter in the event of a fault. One such topology applicable for aircraft applications is the dual-active bridge (DAB) DC-DC converter and is being considered for use as the interface between the +/-270V DC and the 28V DC buses [7].

The use of converter current limiting potentially reduces the speed requirements of the protection system enabling the continued use of standard AC side circuit breakers or electromechanical DC switchgear for fault clearance [183], [185]–[190]. Whilst beneficial from a converter protection perspective, the use of current limiting can make the coordination of network protection more challenging as fault

current may be similar for many fault locations (particularly in compact, low resistance networks). This leads protection in these systems to typically be time-graded with respect to the output of the current limiting converter interface [183], [185]–[190]. The main disadvantage of this approach is a slower operating speed due to the need to set an operating delay between coordinating protection devices. This increase in operating time can have significant consequences for energy delivered at the point of fault, particularly for arcing faults [191], [192]. Within aircraft electrical power systems, prolonged fault exposure can result in detrimental damage to the platform [153].

3.3.6 State-of-the-art in solid-state DC protection

With greater levels of DC distribution in future aircraft electrical systems, there is a need to ensure that protection systems and appropriate switchgear can detect and isolate electrical faults rapidly. Fletcher et al. in [55] categorised the operating times of different circuit breaking technology to determine the most suitable device capable of isolating faulted sections of a compact UAV DC network prior to the peak current discharge of filter capacitors. Operating times of electro-mechanical (EMCB), hybrid (HCB) and solid-state circuit breaker (SSCB) technologies were compared, as shown in the diagram in Figure 3.7. By comparing the circuit breaker operating times to the typical times to reach peak discharge current, it was found that only solid-state circuit breaker technologies are suitable for use within UAV networks.
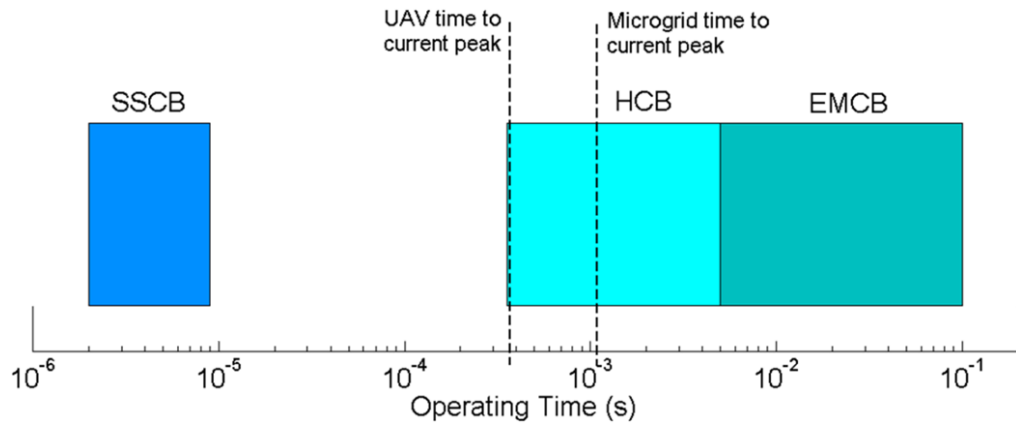
Figure 3.7: Operating times of various circuit breaker technologies [55]

Figure 3.8: COTS SSPC developed by DDC [193]
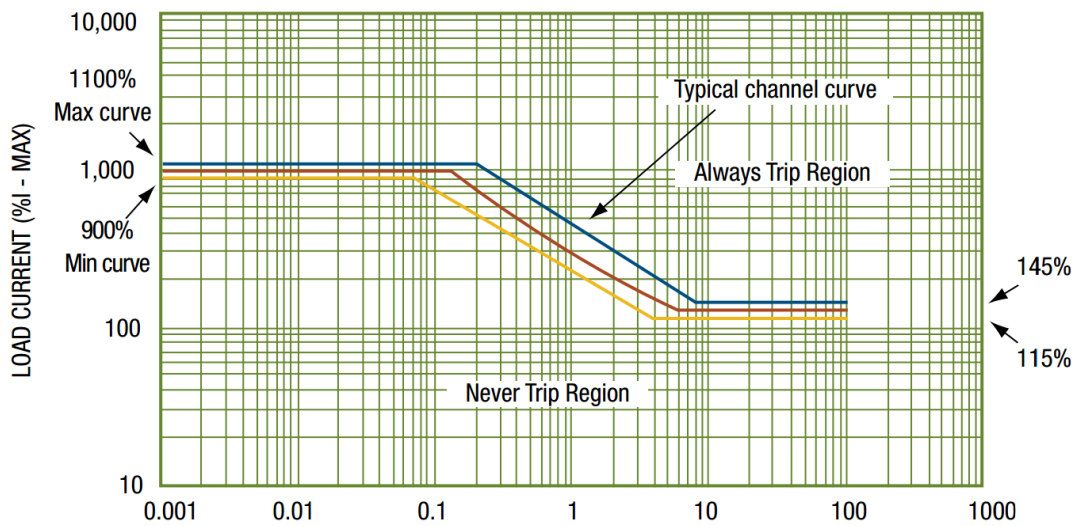
Figure 3.9: SSPC i^2t trip curve characteristic [193]

Solid-state power controllers (SSPC) are state-of-the-art, commercially available, 'smart' power management devices that can enable remote switching and monitoring of loads, and perform circuit protection for primary and secondary power distribution. The advantages of solid state switching relative to electromechanical switching include higher reliability/system availability, reduced weight and volume and improved operation in high vibration environments, making them ideal for aerospace applications [84]. These electronically controlled DC protection devices incorporate solid-state MOSFET switches with rapid isolation functionality. Protection functions offered by commercial SSPCs include instantaneous overcurrent protection and programmable i^2t based overload functionality [141]. Although COTS SSPCs used on recent commercial aircraft are rated for low voltage DC distribution (28V), SSPCs for higher voltage levels are being developed by GE Aviation [194] and Honeywell [195]. A 28V DC SSPC developed by DDC is shown in Figure 3.8. Similar to ELCUs, the trip characteristics of these devices may be modified as a percentage of the current requirements of an individual load channel, as indicated in Figure 3.9.

The individually programmable nature of these advanced solid-state protection devices enables greater flexibility for effective coordination with upstream and downstream devices with improved trip functionality over their electromechanical counterparts. However, trip thresholds are set and fixed for a given configuration of the power system. Furthermore, commercial devices still employ slow i^2t protection algorithms and are only designed for load protection functionality with unidirectional fault current blocking capability [141], [193]. Consequently, the operation of existing solid-state protection devices may be suboptimal for power systems with complex architecture arrangements, that are reconfigurable, and that integrate multiple paralleled sources including advanced energy storage systems.

Within the literature, a more distributed solid-state protection device test bed has been demonstrated in [85] for a marine application, where additional restraint signals between devices have been proposed to improve protection coordination.

However, considerable work is still required to verify the viability of solid-state devices to provide network-wide DC protection.

3.5 Enabling technologies for the integration of high-power ESS

As established in the previous chapter, the two primary and often complimentary functions of high-power, high-bandwidth energy storage systems within compact DC power system applications are to ensure that load demand is met and that network power quality is maintained [89], [91], [94]. The key technological enablers for providing such functionality are bi-directional power electronic converter interfaces and high-bandwidth control systems [196]–[198].

This section provides a literature review of these enabling technologies and analytically derives the functional requirements of the ESS converter interface that will facilitate these functions. Assumptions associated with the internal protection functions of the converter; the characteristics of the converter that define the dynamic behaviour of the overall ESS; and the operating principles of the controller that regulates the ESS response to network transients and load commands are then defined. Finally, the behaviour of the ESS under network fault conditions is analysed. The potential impact of the ESS fault response on the performance of conventional protection systems within future aircraft and other DC power system applications is then established.

3.5.1 Power electronic conversion for energy storage systems

Advanced power electronic converters play a central role in the active regulation of the charging and discharging process of a network integrated ESS. To enable the ESS to meet the demand of high-power loads or to perform power quality functions, the interface must allow a significant quantity of energy to be exported to or absorbed

from the power system within a short period of time. This functional capability may be achieved with the use of a single, bidirectional converter interface that operates in two-quadrants (i.e. sink and source mode). A representative illustration of such a bidirectional converter interface is shown in Figure 3.10.
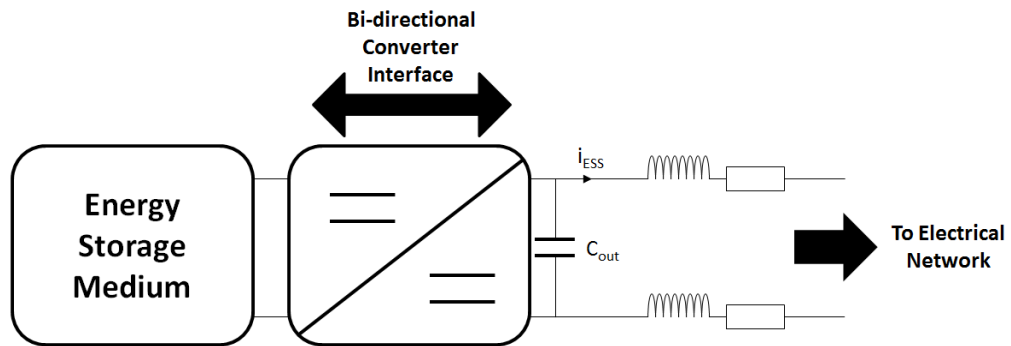
Figure 3.10: Single bi-directional ESS power electronic converter interface

For certain pulse-power applications, two distinct control loops may be required to regulate the charging and discharging process of the ESS. For example, in [199] a low-speed flywheel energy storage system used for meeting the demand of a pulse-load was demonstrated that utilised an active supervisory controller to switch between operating modes when the pulse-load was engaged. Alternatively, tailored power electronic interface configurations may be employed depending on the ESS application needs. For example, Huhman et al. in [200] use a unidirectional DC-DC converter topology to rapidly charge a capacitor bank for a high pulse-power application from an intermediary Li-ion battery ESS to minimise the impact on the rest of the system. A separate secondary converter is used to charge the batteries in this case.

For the systems-level studies performed in this thesis, it is assumed that a single bidirectional ESS converter interface is employed in order to simplify the analysis.

Several characteristics of the ESS converter interface and its control system will influence its response to changing network conditions. One such characteristic is the power rating of the converter interface. Assuming sufficient state-of-charge of the storage medium and operation below the limitations of the medium's internal energy conversion mechanisms, the power rating of the ESS converter will ultimately define the maximum charge / discharge rate of the ESS. The rating of the converter interface itself will be limited by the current and thermal constraints of its constituent power electronic switching transistors / diodes. In order to ensure that these operating constraints are not exceeded, converter systems will incorporate internal protective measures to minimise component damage during overload and short circuit conditions [201]. For example, internal converter protection may be implemented with the use of a fuse or breaker device [202].

However, many advanced power electronic converter topologies are being designed with active current limiting functionality to protect both the converter interface and the network from detrimental current levels [83], [203]. The current-limited threshold may be fixed to a predetermined magnitude and limited duration to prevent physical damage to its internal components [202]. Alternatively, the current-limit threshold may be programmable in more configurable converter interfaces. For example, the 'foldback' protection mechanism introduced in [204] claims to limit and then reduce the current output of converter output linearly to zero in the event of a fault. This internal protection functionality may be broadly referred to as overload or short-circuit protection. An example of this mode of operation is represented in the V-I graph illustrated in Figure 3.11. Under normal operating conditions, the regulated voltage set point of the converter is specified by the steady-state load line, where the 'steady state loading point', as shown on Figure 3.11, may move along this line depending on the load demand. The 'steady state current limit' is the maximum current that the converter can supply under normal operating conditions. Under fault conditions however, the operating point of the converter will increase beyond this point along the 'foldback' line, where voltage and current will be actively decreased to zero in order to minimise the

contribution of fault current supplied by the converter. After the fault is cleared, the operating point is brought back to steady state load line.
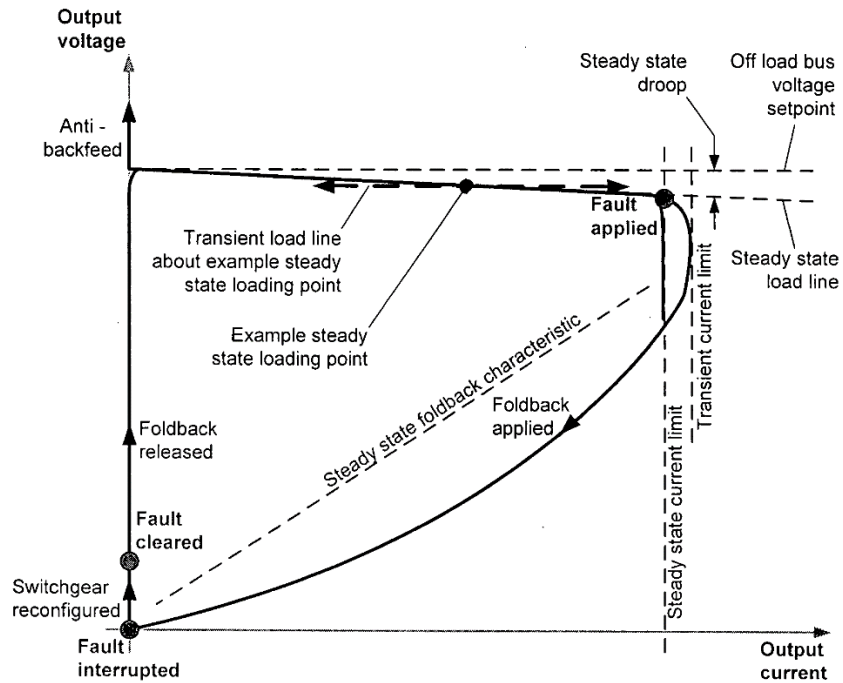
Figure 3.11: Example V-I graph of current limiting converter interface [204]

Converters that offer this functionality will observe a rapid reduction in the output voltage and available power for load demands that exceed the maximum current rating of the converter. Accordingly, a power systems integrator must consider both the upper current limit in addition to the maximum power rating of the ESS converter in the system design process given that the maximum sustained current output from the ESS will limit its capability to support the network voltage.

3.5.1.1 Selection of ESS converter interface

The power rating of the ESS converter may be selected, or its maximum sustained current-limit may be set to a fixed level for a number of reasons. For example, it may be rated to meet the peak demand of a particular load on the network [205]. Alternatively, maximum output current may be limited to a particular magnitude and duration that is sufficient to mitigate a maximum predefined undervoltage transient expected on the network, according to the power quality requirements of the system [206].

In addition, the time constant or minimum response time of the ESS must be defined. The speed of response of the ESS is dictated by its closed-loop bandwidth, which takes into account the switching frequency of its converter interface and the bandwidth of its controller [54], [144], [197]. To fulfil its potential for mitigating transient propagation, the ESS by its nature should be designed to respond rapidly to voltage transients caused by changes in load. It will therefore require operation at a higher bandwidth than that of the primary sources connected to the network. The following section describes the fundamental operation of ESS controllers that enable transient mitigation and power quality functions.

3.5.2 ESS controller operation

The primary function of an ESS controller is to regulate the rate and quantity of energy imported or exported between the power system and the storage medium via the ESS converter interface. Assuming that a single bi-directional DC-DC converter interface is utilised, this primary function is achieved by regulating the magnitude and direction of current on the network facing side of the ESS converter.

The regulation of the output current is achieved via the implementation of a high-bandwidth inner current control loop that relies on the measurement, feedback and comparison of this current with an adjustable reference value. The difference (or error) between the measured and reference current values provides the necessary signal required for the lower level proportional/integral controller to function [54]. The output signal from this lower level controller, known as the modulation index, m, is fed through a pulse-width modulation (PWM) generator which in turn generates the firing signals for the switchgear drive circuitry.

Figure 3.12 provides an illustration of the inner current loop of an example supercapacitor ESS control system integrated to a representative DC power system.
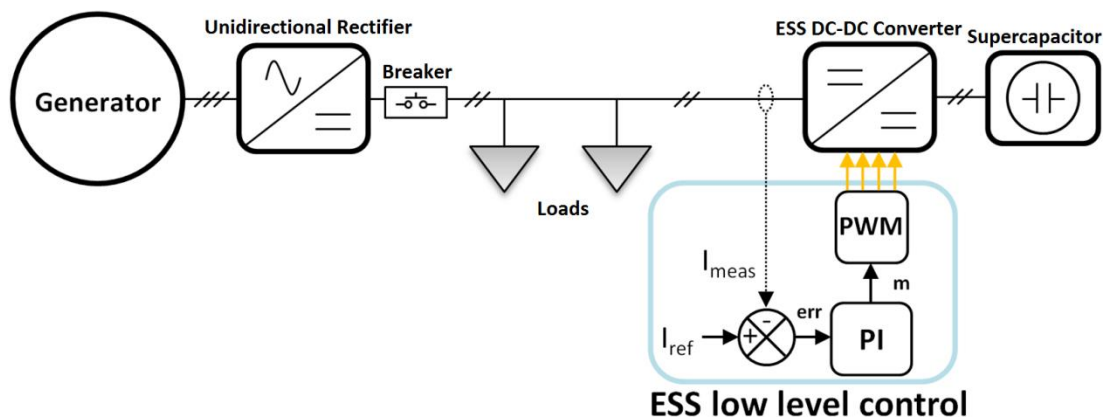
Figure 3.12: Inner current control loop of a supercapacitor ESS

Accordingly, the converter output current may be regulated via adjustment of the reference signal, which in turn modifies the modulation index of the power electronic switching function.

Application of outer control loops that automatically adjust the current reference value as required enables a variety of sub-functions of the ESS to be implemented. For example, secondary sub-functions such as power quality regulation which acts on fast voltage transients, voltage support for when the ESS is commanded to discharge a bulk quantity of energy into the network and SOC control may be superimposed to increase ESS functionality [59]. This is achieved by enabling outer control loops to actively set the reference set point of the inner current control loop.

These ESS control modes may be selected by a hierarchical power management system according the systems-level requirements as depicted in Figure 3.13.
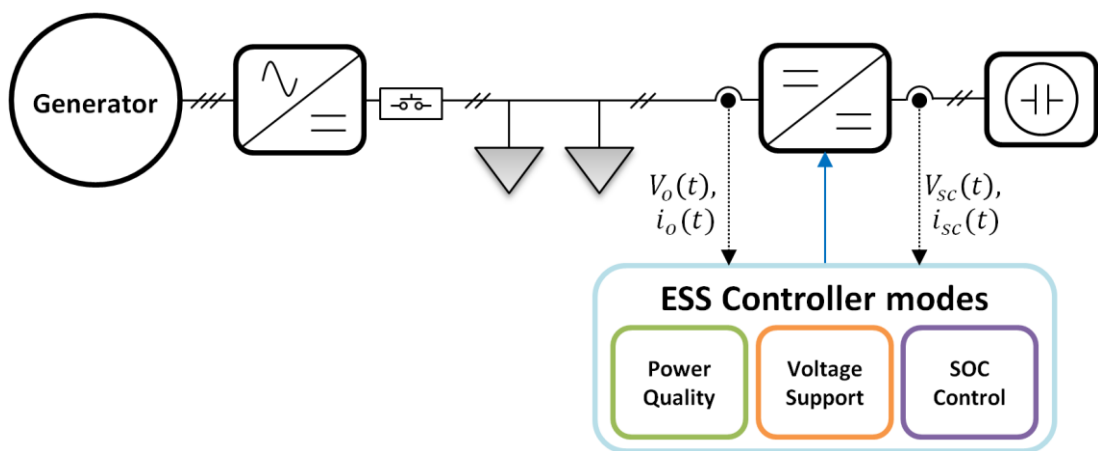
Figure 3.13: ESS controller with selectable modes of operation

3.5.3 Challenges with ESS power quality control operation during network faults

ESS power quality control may be implemented with the use of a voltage tracking controller that enables the ESS to rapidly mitigate large voltage transients on the network. Figure 3.14 shows how this particular control mode may be implemented with appropriate measurement and feedback of system voltage.
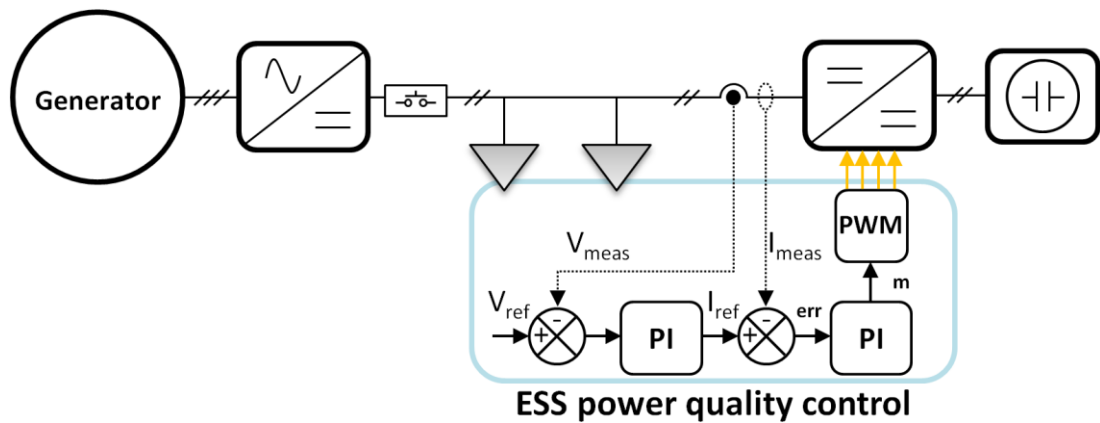
Figure 3.14: ESS controller with outer voltage control loop for power quality

The ESS controller in Figure 3.14 is based on [104], and determines the output current of a power electronic converter, I_{meas}, via cascaded proportional and integral (PI) gain controllers. Assuming ideal operating conditions where the initial steady state network voltage is equal to the reference voltage used by the ESS controller, measurement of the network voltage, V_{meas}, at the terminals of the converter is compared to a fixed reference value, V_{ref}, set to the nominal steady-state voltage of the network. The error (or difference) between the two signals is amplified by a proportional and integral gain to generate a varying reference value, I_{ref}. This reference is used to set the desired output current of the converter. In practice, this control system configuration may result non-ideal behavior given that both the primary generation and the ESS controllers are regulating the same network voltage. A droop control method or a dead zone controller mechanism

applied to the ESS control system may be implemented to minimize this behavior. This is proposed as further work in the conclusions of this thesis.

A second comparator evaluates the difference between the measured output current of the converter to that of the variable reference value. The resultant signal is again amplified through a secondary PI controller and is then used to set the modulation index, *m*, of the converter power electronic switches, thus controlling the output current of the converter based on the measurement of network voltage.

Given that the network voltage is normally set by the primary source of generation, the output of the ESS is typically zero at the nominal network voltage level. During voltage transient events, normally instigated by a disturbance or change in load, the current reference will be automatically adjusted, triggering a change in converter output and prompting the ESS to absorb or export energy onto the network accordingly. As the network voltage settles to the steady state level, the error between the measured voltage and fixed voltage reference decreases to zero, thus causing the ESS current reference to also decay to zero.

It is assumed that the energy storage medium and its corresponding converter interface will have a transient response much faster than that of the primary generation system to enable rapid transient mitigation. This functionality minimizes the propagation of electrical transients throughout the wider electrical network and intrinsically dampens the transient response of the primary generation [59]. Within the context of an aircraft electrical system, the ESS also functions to decouple the electrical system from the mechanical system i.e. reducing the translation of electrical transients into torque transients on the prime mover [142].

However, given the sensitivity of the power quality control mode to the network voltage, the ESS response is intrinsically sensitive to network faults. During this mode of operation, the ESS controller will attempt to regulate the ESS current output using the measurement of the network voltage, as in [54]. In the event of a network fault (such as that applied in Fig. 3.10), the subsequent reduction of

network voltage will trigger a large step in its current reference value and drive the output of the current regulator into saturation (100% duty cycle). This will likely cause the ESS to continuously output current into the fault provided that sufficient stored energy is available to support this and that the power electronic switches withstand the increase in current.
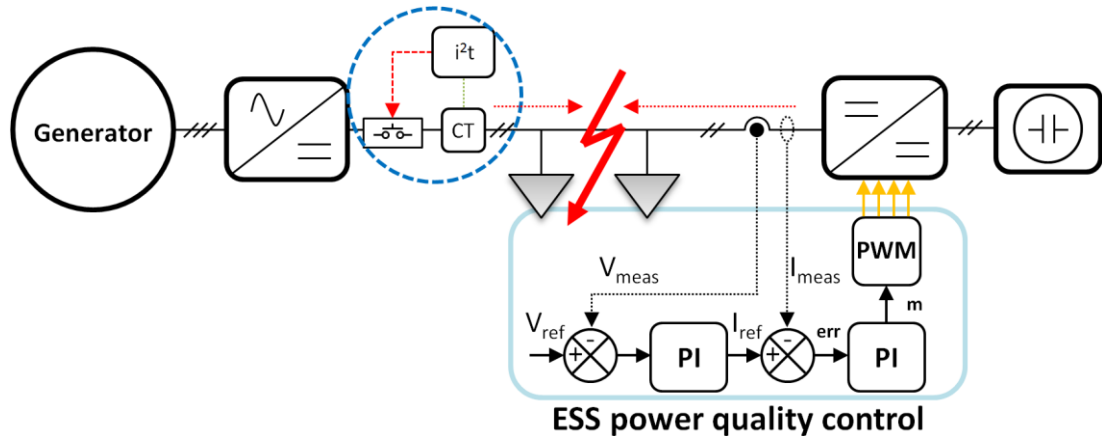
Figure 3.15: ESS operating in power quality control mode under fault conditions

During network fault conditions and in particular in the event of a high-impedance fault, the response of the primary source may be significantly dampened, owing to the coupling that exists between sources via the network voltage. The subsequent damped response of the primary source to the fault may reduce the operational speed of its corresponding overcurrent protection device, causing protection blinding [26] and disrupting protection coordination. Protection blinding is the term commonly used to describe the reduction in overcurrent levels on distribution feeders within grid-based power systems as a result of the fault response of distributed generation. This terminology is therefore adopted to describe the similar effect on the fault response of primary generation within compact power systems as a result of fault current contribution of network integrated energy storage.

A delay in upstream protection operating times may have detrimental effects on the system such as increasing energy delivered at the point of fault (if cleared by the

generator protection device) and increasing time of fault exposure. This may be particularly hazardous in the event of arcing faults [191], [192] resulting in increased fire risk. Furthermore, the magnitude and direction of fault currents measured by the network-wide protection system will vary with ESS availability, changing the fault conditions.

These systems-level integration challenges have received little attention in current literature. For example [89] and [91] demonstrate the use of an ESS to automate power balancing and for voltage sag correction during ac grid side faults on a microgrid. However, the response of these operational modes is not investigated during more severe faults within the DC microgrid. Furthermore, the protection challenges and requirements under such faulted conditions are not discussed.

Reference [146] considers the use of energy storage for fault ride-through of generator phase faults however provides no analysis for how similar ESS control would respond for electrical network faults. Reference [207] describes the beneficial role that a SMES system plays in the integration of wind turbines via an interconnected DC system, whereby stored energy in the SMES helps to maintain the system voltage and supply current during AC and DC-side faults. However, the protection implications of such a response are not considered. In [208], a DC-link integrated supercapacitor based dynamic voltage restorer is considered for restoring voltage during AC-grid faults via a bidirectional DC-DC converter. Again, DC-side faults and protection are not considered. Reference [196] conducts fault studies for a low voltage DC microgrid containing battery storage, where commercial circuit breaker technology is suggested for protecting the battery during network faults. However, the protection selectivity challenges associated with such DC protection devices may cause the ESS protection to operate for faults at various downstream locations, unnecessarily disconnecting the ESS. Similar drawbacks associated with grid connected ESSs are highlighted in [209] where a superconducting fault current limiter is proposed to minimise protection coordination issues caused by the ESS whilst maintaining the availability of the ESS

for post fault recovery. However, the cost and complexities of implementing such systems may limit their use in certain applications.

The evidence therefore suggests that the issue of ESS response on protection system performance is often overlooked and the compatibility of existing network protection systems with networks containing fast acting and power-dense ESS is not well understood. Similar conclusions were also reached by Padullaparti et al in [210] when investigating the impact of large-scale photovoltaic and ESS system installations on network overcurrent protection schemes.

To fully evaluate ESS impact on the protection performance, the technical characteristics of the ESS that govern the coupled behaviour of paralleled sources (through the network voltage) must be assessed.

Accordingly, the following chapters of this thesis investigate the impact of the ESS on the fault response of the primary generation system and derive the network conditions at which conventional protection systems may no longer sufficiently protect the network.

3.6 Conclusions

A literature review of the state-of-the-art in aircraft protection systems was presented in this chapter. The fault response of a high-power ESS will be governed by its corresponding control system and will likely cause the magnitude of fault current delivered by converter interfaced primary sources to be reduced causing problems with the operation of corresponding protection devices, i.e. protection blinding. Minimal work has been carried out in this area within the literature and so the need to investigate the systemic impact of integrating high-power, high-bandwidth energy storage systems within compact DC power systems has been established.

Chapter 4

Characterising the transient response of an electrical system with integrated ESS to electrical faults

4.1 Introduction

This chapter presents a detailed analysis of the behaviour of an electrical power system with high-power ESS operating under electrical fault conditions. The aim of this chapter is to characterise the impact that an ESS has on the transient response of other network integrated electrical sources for a range of electrical fault conditions. This characterisation will enable the subsequent impact on the performance of the network wide protection system to be determined.

The relationship between the fault impedance, ESS controller bandwidth and ESS peak current limit on the rate-of-change of fault energy delivered by the primary electrical source is established and quantified.

A new 'critical fault impedance' term is introduced, derived and validated in this chapter that defines the conditions at which conventional network protection devices will experience protection blinding due to the uninterrupted contribution of fault current from an ESS. A method to rapidly estimate the critical impedance of a DC system that incorporates a high-power ESS is also proposed and verified. This characterisation of the critical impedance is a key contribution of this thesis.

Finally, the experimental validation of protection blinding of a state-of-the-art solid-state power controller (SSPC) protection device, used for aircraft DC applications, is presented.

4.2 Quantification of protection performance of compact DC power systems

A key design objective of any network protection system is to safely provide continuity of supply to loads when other parts of the network are experiencing faults. The ability of the protection system to achieve this objective is measured using various performance criteria including speed, selectivity, stability and sensitivity [155]. Dependability and security of the protection system are also widely used performance criterion by which the reliability of the protection system is measured. IEEE standard C37.100–1992 [211] defines these two facets of protection system reliability as follows:

- Dependability is the facet of reliability that relates to the degree of certainty that a relay or relay system will operate correctly when required, and at the designed speed. Dependability of the protection system is therefore a concern when a fault occurs within a specified protected zone.
- Security is the facet of reliability that relates to the degree of certainty that a relay or relay system will not operate incorrectly, or faster than designed. Security of the protection system is therefore a concern for faults out-with a protected zone or under normal (non-faulted) conditions.

The capability to provide backup protection in the event of a device failure is also an important facet of protection system operation that must be taken into consideration. As a key contribution of this thesis is to demonstrate the impact that ESS integration has on the protection trip-times of a primary electrical source, protection operating speed will be the primary performance criterion of the analysis within this chapter. However, the impact that changes in protection trip-times have on the dependability and security of the overall protection system will also be analysed.

4.3 Simulation of a representative model of a compact DC aircraft electrical power system with high-power ESS under fault conditions

Compact DC electrical power distribution systems are being considered for a number of aerospace applications. An application area that is undergoing a more rapid pace of adoption of advanced power system architectures and integrated subsystems, such as high-power ESS, is unmanned aerial vehicles (UAVs) [212]–[214]. This is due to the greater ease of certification of new technologies for such platforms in comparison to commercial aircraft [215]. Accordingly, a UAV power system is considered for this case study.

This section describes the construction, simulation and analysis of a compact DC power system model with an integrated high-power ESS, representative of a state-of-the-art UAV power system. In order to investigate the impact that the ESS has on the fault response of the power system, multiple simulations of the DC power system model under different fault conditions are conducted. A sensitivity analysis of fault impedance, ESS current limit and ESS controller bandwidth is then performed in section 4.4 to evaluate the impact on the fault response of the primary source.

4.3.1 Model construction and assumptions

Figure 4.1 shows an illustration of the representative model and Table 4.1 presents the relevant network parameters derived from the proposed system in [71]. The system consists of an engine driven electrical generator interfaced with a unidirectional current limited active rectifier with a maximum steady-state current limit set to 200A; a supercapacitor ESS with a bidirectional and current limited DC-DC converter interface with a maximum steady-state current limit set to 200A; and a lumped electrical load of 19.9kW connected in parallel to a common 270V DC bus

bar via appropriate feeders. All supply and load feeders are 5 meters in length, equating to 4.005mΩ feeder resistance and 3.25mH feeder inductance. The closed loop bandwidth of the primary generation converter is set to 1kW, whilst the ESS bandwidth is set to 100kW. The ESS bandwidth is set to this high value to represent a conceptual system on future power systems.

The model is developed within the MATLAB/Simulink environment [216] using an average-value functional-level modelling approach [217] that is ideal for evaluating the dynamic performance of power electronic converters and their corresponding control systems in an integrated power systems context.

Average-value modelling is a process by which the fast switching operation of a power electronic converter device is approximated over a given period (often a single switching interval) in order to represent the time-averaged behaviour of the device. Average-value models are typically less computationally demanding to solve than their detailed switched equivalents and also facilitate the use of larger simulation time steps. Both aspects lead to much quicker completion of simulations, often without the loss of significant accuracy at frequencies of interest [218].
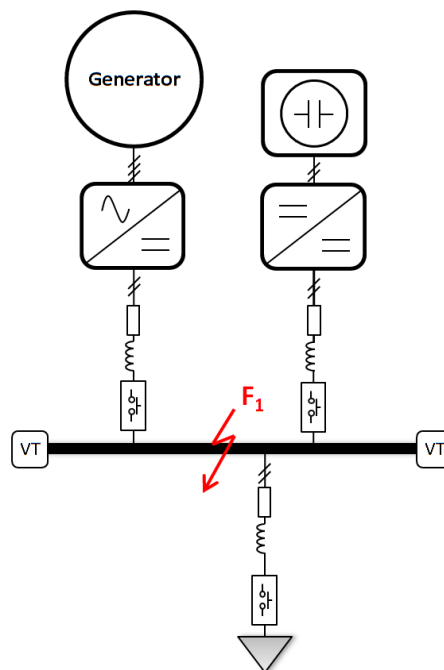
Figure 4.1: DC compact power system model with integrated ESS

Voltage	Max Gen Current	Max ESS Current	R_{cab}	L_{cab}	Total P_{load}	Gen BW	ESS BW
(V)	(A)	(A)	(mΩ/m)	(mH/m)	(kW)	(kHz)	(kHz)
270	200	200	0.801	0.65	19.9	1	100

Averaged models replace all terminal voltages and currents with running averages, where the resulting quantities still respect Kirchhoff's laws, and therefore constitute valid circuit variables. All linear time-invariant components of the original circuit (inductors, capacitors and resistors etc.) impose the same constraints on the average quantities as they do on the original instantaneous variables, and therefore remain the same in the averaged circuit. Switching elements are represented as appropriately controlled voltage or current sources, which are again averaged to represent the output of the converter interface with control relationships involving time-averaged quantities associated with the applied switching input (duty ratios). Figure 4.2 illustrates the time-averaged switching process and Figure 4.3 shows an example of a representative circuit averaged equivalent model of a bidirectional DC-DC converter.
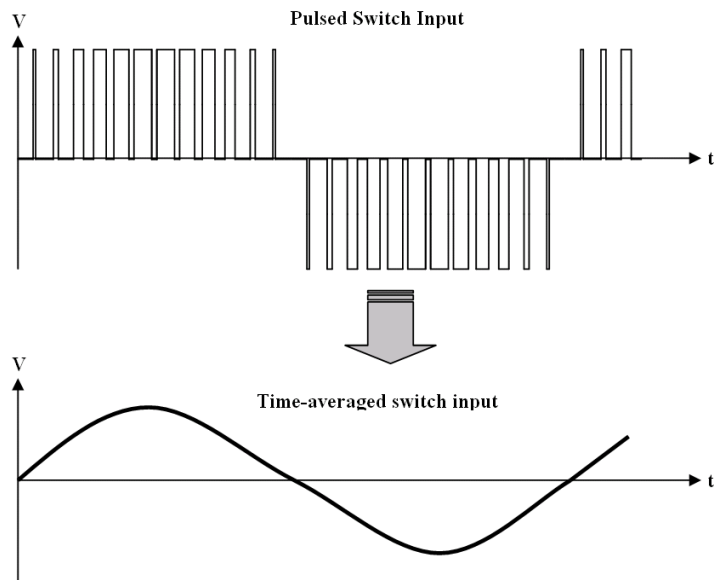
Figure 4.2: Illustration of pulse averaging [219]
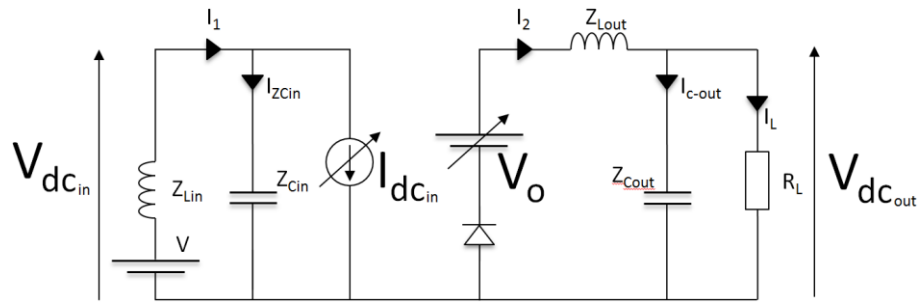
Figure 4.3: Equivalent averaged DC-DC converter model [219]

Average-value models of converters are not normally considered for transient level simulations (i.e. fault studies) of power system components. However, it is assumed that the converters utilised in this system are capable performing sustained current limiting to a predefined level under the range of short-circuit fault impedances conditions evaluated in this thesis. Accordingly, the time-averaged behaviour of these average-value converter models can be considered as being valid under such fault conditions.

4.3.2 Baseline case study of simulated system response under fault conditions

The baseline case study considers only the transient response of the primary source to a fault located at the common bus bar to which the primary source and ESS are interconnected, labelled F1 in Figure 4.1.

The behaviour of the primary source is initially evaluated in isolation to characterize its response to a short-circuit fault (0.001Ω) and to a relatively high-impedance (0.75Ω) fault. These fault conditions are then replicated with the ESS online in order to investigate the impact that the ESS response has on the transient and sustained supply of fault current delivered by the primary source. Within this initial study, the ESS has a nominal closed-loop controller bandwidth two orders of magnitude greater than that of the primary source. It is also assumed that both converters can limit fault current to 200A. Subsequent studies will then explore the sensitivity of varying the fault impedance, ESS current limit and ESS bandwidth on the fault response of the primary source.

Figures 4.4 (a) and (b) show the simulated voltage response and corresponding ESS/primary source response to a low-impedance (0.001Ω) fault applied after 2.5 seconds of simulation time. For both configurations (ESS operational/disconnected), the network voltage collapses rapidly to zero upon fault inception due to the discharge of DC side filter capacitance. When operational, the ESS response saturates at its peak current rating of 200A whilst the response of the primary source reaches its rated maximum of 200A for both configurations. The initial primary source peak current transient is produced by the discharge of its filter capacitor and is also similar in both cases. Given the similarities in both the transient and steady state response of the primary source, it can be inferred that the ESS has minimal impact on the response of the primary source under low-impedance short circuit fault conditions.

Figures 4.5 (a) and (b) show the simulated voltage response and ESS/primary source current response to a high-impedance (0.75Ω) fault on the common bus bar. When

the ESS is operational, the transient undervoltage event that occurs when the fault is applied is observed by the ESS and causes it to rapidly increase its current output to support the network voltage, as anticipated. In comparison to the voltage transient when the primary source is operating in isolation, the dominant ESS contribution of fault current (which again saturates to its maximum level) significantly reduces the depth of the transient undervoltage observed. This results in a reduced transient current response from the primary source. However, if the current traces are extended, the contribution of current from the primary source eventually increases to its maximum limit as it attempts to drive the voltage back up to nominal levels.

The system behaviour when the ESS is disconnected is also illustrated in Figures 4.5 (a) and (b). In this case, the peak primary source fault current is reached more rapidly. In the absence of the ESS, the fault-related voltage transient is far more significant in terms of both magnitude and duration. Consequently, any conventional protection device that operates on a function of the fault current that is used to protect the primary source will observe reduced fault current as a result of ESS integration under high-impedance fault conditions.

The subsequent reduction in the speed of fault detection of protection relays may result in unnecessary prolonged exposure of sensitive electrical subsystems and other healthy sections of the network to the fault. More importantly, it may compromise the safety of the power system with increased fire risk at the point of fault, particularly for high impedance arcing faults
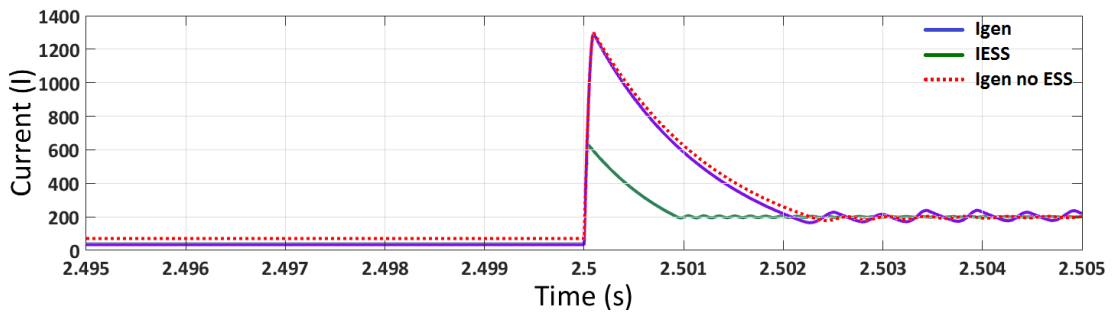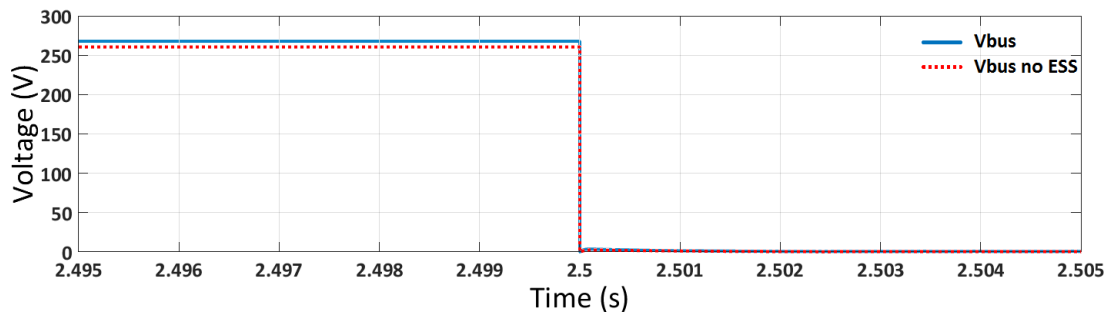
Figure 4.4: (a) Voltage response and (b) primary source/ESS response to a 0.001Ω fault
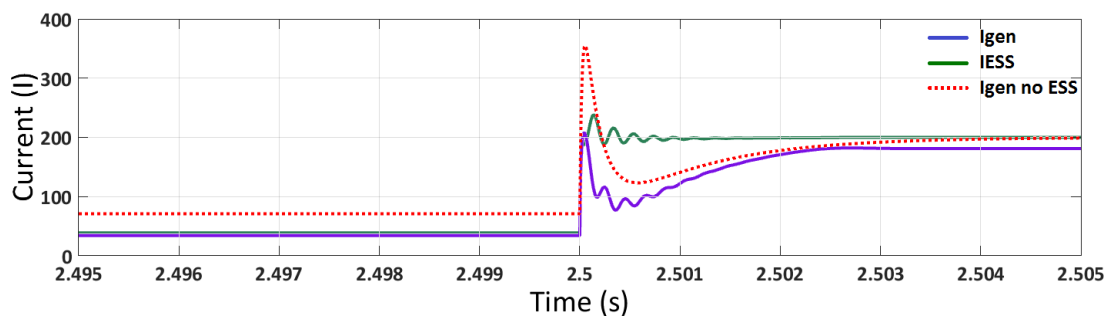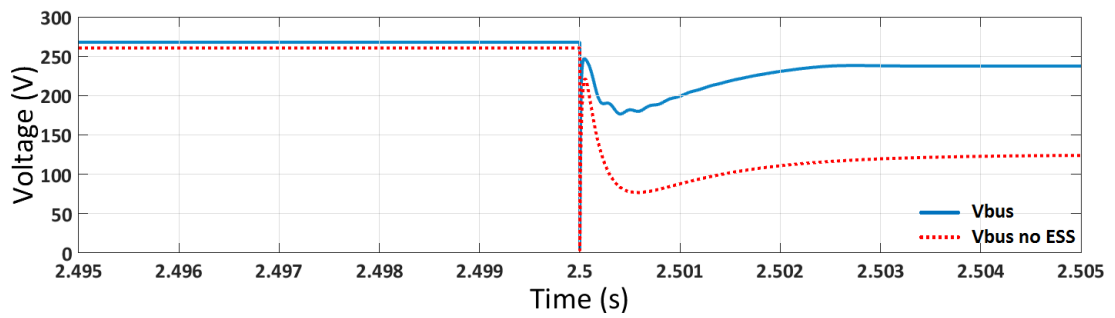
Figure 4.5: (a) Voltage response and (b) primary source/ESS response to a 0.75Ω fault

4.4 Experimental validation of protection blinding

Hardware experimentation was conducted to validate that a state-of-the-art aerospace-grade protection device, configured to protect the primary source operating in isolation within a DC system, does not perform consistently for a given high impedance fault when a high-power ESS is integrated. This thesis contribution is presented in this section.

The scaled down experimental procedure, both in terms of power rating and system voltage, undertaken to validate the protection blinding observations made in the simulation studies of the compact dc power system model is outlined. The observations show that the response of the primary source decreases in the event of a large step change in demand due to the rapid response of the integrated high-power supercapacitor ESS. It is then demonstrated that this dampened response reduces the trip-speed of a state-of-the-art solid-state protection device used in commercial aerospace applications when it is configured to protect the primary source feeder.

The protection device tested in the experiment is a solid-state power controller (SSPC) developed by DDC [141], [193]. This protection device was chosen for this experiment as it is representative of the protection devices being considered for aircraft power system applications, and incorporates a number of reconfigurable protection functions that are embedded in current commercial devices. The protection functions employed in current iterations of commercial SSPC modules include short circuit protection enabling circuit deactivation times in the order of 1μs for 'instant trips' of 10 times rated current, along with i^2t overload protection. Overload trip functions are computed using an embedded processor - individual load channels can be programmed for different rated currents and multiple channels may be paralleled enabling higher current capacities. Measurements of supply voltage, load current and channel temperature are continuously acquired by on-board instrumentation. Communication of these measurements to an external

power management computer is achieved through the built-in and standardised communications channels.

Figures 4.6 and 4.7 show the physical and illustrative experimental setup used to validate the performance of the SSPC placed in series with the primary source feeder. Note that the supercapacitor ESS was connected directly to the system without the need for any power electronics interface (although a separate charging circuit was implemented to bring the supercapacitor voltage up to that of the system prior to connection). This approach was taken as the inherent response of the supercapacitors during transient events was acceptably representative of the desired behaviour of an ESS configured to maintain power quality on a DC system, i.e. the ESS behaves like a low-pass filter and absorbs any high frequency electrical transients caused by load switching events, maintaining the system voltage.
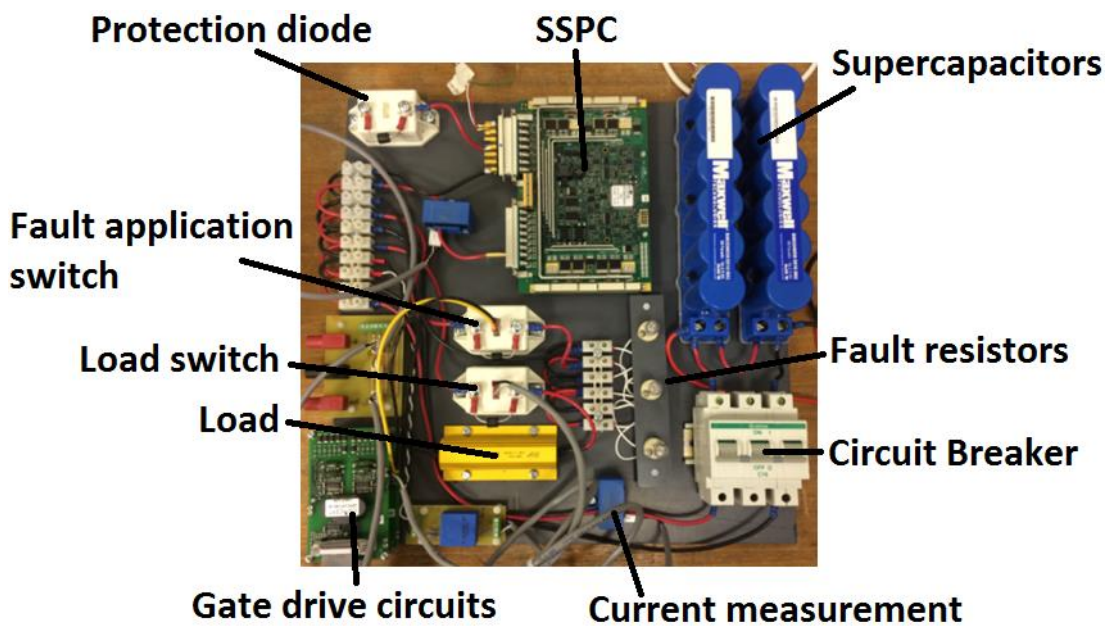
Figure 4.6: Hardware setup with SSPC and supercapacitor ESS
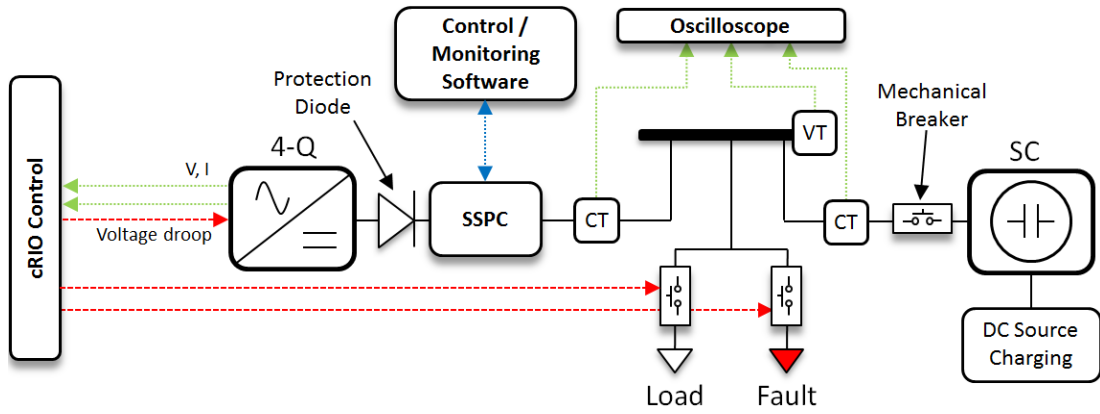
Figure 4.7: Illustrative block diagram of experimental setup to evaluate impact of protection blinding

The performance of the i^2t protection functionality was assessed in this experiment as only high-impedance faults were being considered. The resultant performance of the SSPC was evaluated by comparing its measured trip-time when the ESS is fully operational and when it is disengaged.

The base load for the system was selected to be 10Ω, drawing 2.4A from the main supply. The resistive high-impedance fault introduced to the system is 5Ω, causing the total demand to be approximately 7.5A. The impact that the ESS response has on the network voltage response and the primary source response when the faults are applied was also measured. The nominal network voltage is set by the 4-quadrant amplifier to 24V with the provision of a linear voltage droop profile that ranges from 24.5V for open circuit conditions, to 23.5V for maximum loading. This range was chosen due to upper voltage limitations associated with the supercapacitors used in the experiment. The maximum current limit applied by the DC source is 8A and the controller bandwidth was set to 10 kHz. The voltage droop was implemented to reflect the operation and control action of a converter interfaced primary generation system on an aircraft electrical system, albeit at scaled voltage and power range, whilst also reflecting the configuration of the representative aircraft power system models analysed in the previous section.

Figure 4.8 (a) and (b) show the system voltage and primary source current response to a 5Ω fault when the ESS is connected and when it is disengaged. Note that the protection functions associated with SSPC are disabled in this case in order to measure the uninterrupted fault response of the network.
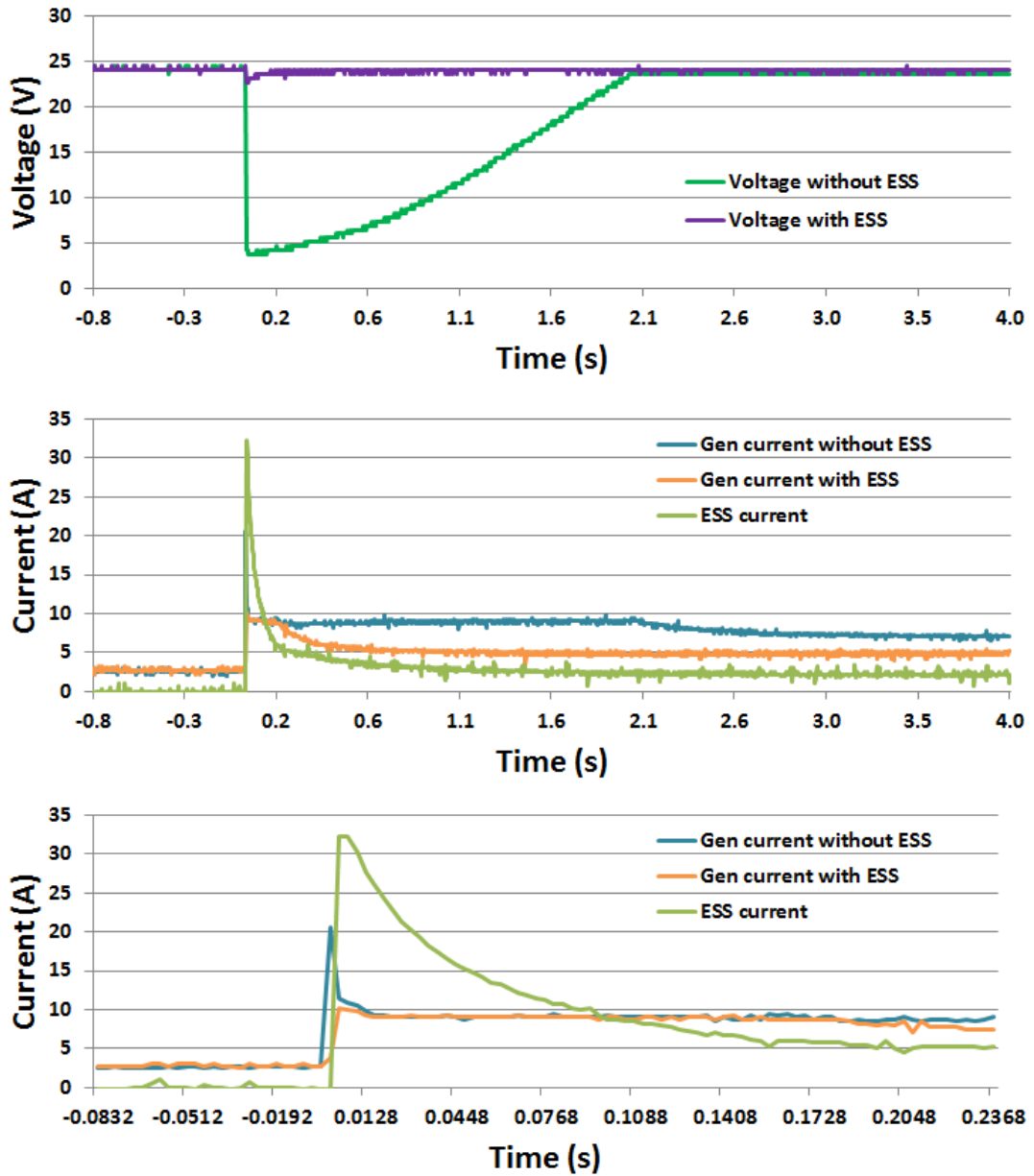
Figure 4.8 Experimental results showing (a) Voltage response and (b) ESS/generator response to a 5Ω high-impedance fault, and (c) fault transient close-up

With the ESS is offline, the undervoltage observed in Figure 4.8 (a) when the fault is applied is caused by the discharge of the output filter capacitor associated with the primary DC source (representing the converter fed generator system). The primary source responds by supplying its maximum rated current (limited to 8A) in order to drive the voltage back up to nominal levels in accordance to its voltage droop set point. The limited current response explains the linear increase of the voltage during the transient period. Figure 4.8 (a) and (b) also show the voltage and primary source response to the 5Ω fault respectively, with the ESS engaged. Contrary to the previous case, the network voltage response illustrates the effectiveness of the ESS in minimising undervoltage during network transient events. Figure 4.8 (b) shows that the rapid response of the ESS sustains the network voltage to nominal levels. As a result, the primary source controller that governs its response by the measurement of network voltage, does not observe as much of a voltage dip and therefore reacts by supplying a reduced steady-state fault current.

It is this reduced response that causes protection blinding – the rate of energy supplied by the primary source decreases due to the rapid contribution of fault energy delivered by the ESS. Given that the computation of i^2t determined by a protection device is in effect a measurand of energy, the time to reach a fixed i^2t threshold will inherently increase if the rate of energy supplied by the primary source is reduced. The SSPC begins the i^2t computation when the supply current exceeds the user defined current threshold (the i^2t threshold is a function of this current threshold).

Figure 4.9 illustrates the impact of protection blinding by comparing the trip times when a fixed threshold of 3A is selected for the SSPC to protect the primary source. The total steady-state fault current is approximately 7.5A when the 5Ω fault is applied.
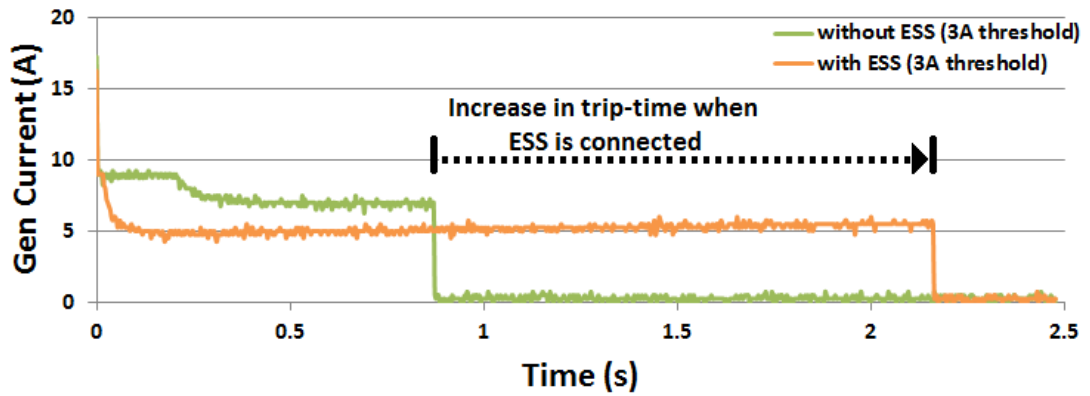
Figure 4.9: SSPC trip times with and without ESS

From Figure 4.9, it can be seen that the trip-time when the ESS is disconnected from the network is 0.87 seconds. When the ESS in engaged, the trip time increases to 2.18 seconds. This corresponds to an increase of 1.31 seconds associated with the SSPC i^2t protection function using a fixed threshold of 3A for both network configurations. Within the context of aircraft power system applications, this increase in trip-time will result in a fault being present on the system for a longer period of time than intended by the protection system. Indeed, this protection blinding behaviour may even disrupt system wide protection coordination. Accordingly, it is vital that this problem is addressed prior to the integration of high-power ESS into safety critical power systems.

4.4.1 Discussion on experimental results

The results shown in Figures 4.8 and 4.9 validate the protection blinding effects associated with integrating a fast acting ESS at a location downstream of the primary feeder on a compact DC power system. The results prove that a protection device with a fixed threshold associated with the primary source may take longer to detect a fault when there is energy storage on the network.

The reduced performance of this protection device may have a detrimental effect on the operation of the network wide protection system and may compromise the operational safety of the power system. Coordination with downstream protection devices may be disrupted, prolonging fault exposure and increasing the risk of physical damage. In particular, the combination of a downstream load fault together with a failure of its load protection device may leave the fault on the system for a considerably longer period of time than would normally be expected. Similarly, the ESS may mask the presence of a fault if it was located on the common bus bar to which the ESS and primary feeder are interconnected. This behaviour will decrease the dependability of the protection system operation. The subsequent safety implications may ultimately lead to the catastrophic failure of the platform. Although the results produced in this experiment are discussed within the context of an aircraft power system application, it is anticipated that they will apply to other compact DC power system applications that have overcurrent based protection systems that may be negatively impacted by the response of a high-power ESS.

4.5 Sensitivity analysis of fault energy delivered by primary source to fault impedance, ESS current limit and ESS controller bandwidth

This section presents the results of a sensitivity analysis carried out to determine the impact of the ESS response on the quantity of fault energy delivered by the primary source for a range of fault impedances and different ESS behavioural characteristics.

To fully evaluate ESS impact on the fault response of the primary source and in turn the performance of its corresponding protection device, the technical characteristics of the ESS that govern the coupled behaviour of paralleled sources (through the network voltage) must be assessed. The two key behavioural characteristics of ESS which influence this are described below.

First, the maximum sustained current output from the ESS will determine its ability to support the network voltage. This peak current may be due to the storage device itself or its converter interface (assuming current limiting capability). It may be rated to output a maximum current close to that of the demand from a peak load on the network, or limited to a fixed level to prevent physical damage to internal components [94], [202].

Second, the speed of response of the ESS will determine its ability to respond to transient voltage changes. This is dictated by its internal impedance and the converter's closed-loop bandwidth, which takes into account the switching frequency of its converter interface and its controller gains [54], [144], [197]. To fulfil its potential for mitigating transient propagation, the ESS by its nature should be designed to respond rapidly to voltage transients. It should therefore operate at a higher bandwidth than that of the primary source. Therefore in the event of a fault, the response of the ESS will likely impact the initial fault behaviour of other connected sources and the subsequent protection response.

The following subsections will illustrate the impact of the ESS on the fault response of the primary source for various fault scenarios, considering both changes in ESS behavioural characteristics and network fault conditions. The degree of protection blinding is inferred from the rate-of-change of fault energy (i^2t) delivered by the primary source upon fault inception. Sensitivity of the rate-of-change of fault energy to fault impedance is first investigated in subsection 4.4.1. Then, sensitivity to the peak ESS current limit is presented in subsection 4.4.2. Finally, subsection 4.4.3 discusses the impact of varying the ESS controller bandwidth.

Subsequent sections then derive relationships between these behavioural (designed) and conditional (variable) characteristics to identify the conditions in which protection performance is degraded.

4.5.1 Sensitivity of fault impedance on fault energy output of the primary source

The sensitivity of fault impedance on the degree of protection blinding caused by the response of the ESS is determined in this subsection by investigating the impact on the fault energy (i^2t) delivered by the primary source for a broad range of fault impedances. Fault impedances of 100mΩ, 250mΩ, 500mΩ, 750mΩ and 1Ω are applied. Figures 4.10 and 4.11 present a range of simulation results that show the i^2t output of the primary source for increasing fault impedances located on the common bus bar to which the ESS and primary source are connected, as shown in Figure 4.1. The impact of the ESS contribution on the primary source response is illustrated separately within Figure 4.10 (a) and (b), whereas both sets of traces are contrasted within Figure 4.11 to compare the initial transient behaviour of the i^2t response over a shorter timeframe.

From these figures, it can be seen that the influence of the ESS serves to progressively reduce the fault current from the generator system for increasing fault impedances. During lower impedance faults (up to 500mΩ), the output of the generator system is limited according to the rated current output of the converter. In these cases the contribution of the ESS only has the effect of moving the i^2t curve associated with the generator and converter along the time axis during the initial fault transient. This would introduce a relatively inconsequential increase in trip-time in reaching a specified overcurrent threshold. However, for higher impedance faults, the contribution from the ESS actually serves to reduce the steady state gradient of the generator system output i^2t curve. This effect could significantly increase the trip-time of any associated protection devices.

To highlight how this trip time can be extended, the i^2t response can be compared to relevant operating thresholds. Table 4.2 presents some examples of the time-to-threshold that are expected for the primary source operating as the single source of fault current, and operating in tandem with the ESS. The results show that for greater i^2t thresholds the increase in time, as a result of the ESS contribution to the

fault, becomes significantly greater with increasing fault impedance. These are consistent with previous observations in Figures 4.10 and 4.11. For example, if the primary source protection was to operate within 70μs (corresponding to the time at which a 50% decrease in voltage occurs following a short circuit on the bus bar), the i^2t threshold would be set to 60 A^{2}s. The time to reach this threshold during a higher impedance (1Ω) fault would increase from 2.2 ms without the ESS, to 4.5 ms when the ESS is operational (over doubling the operating time). Furthermore, Table 4.2 indicates that operating times for a higher trip threshold of 300 A^{2}s (selected arbitrarily to emphasise the impact of increased thresholds) are increased even further, as the reduced i^2t gradient dominates the change in operating time.
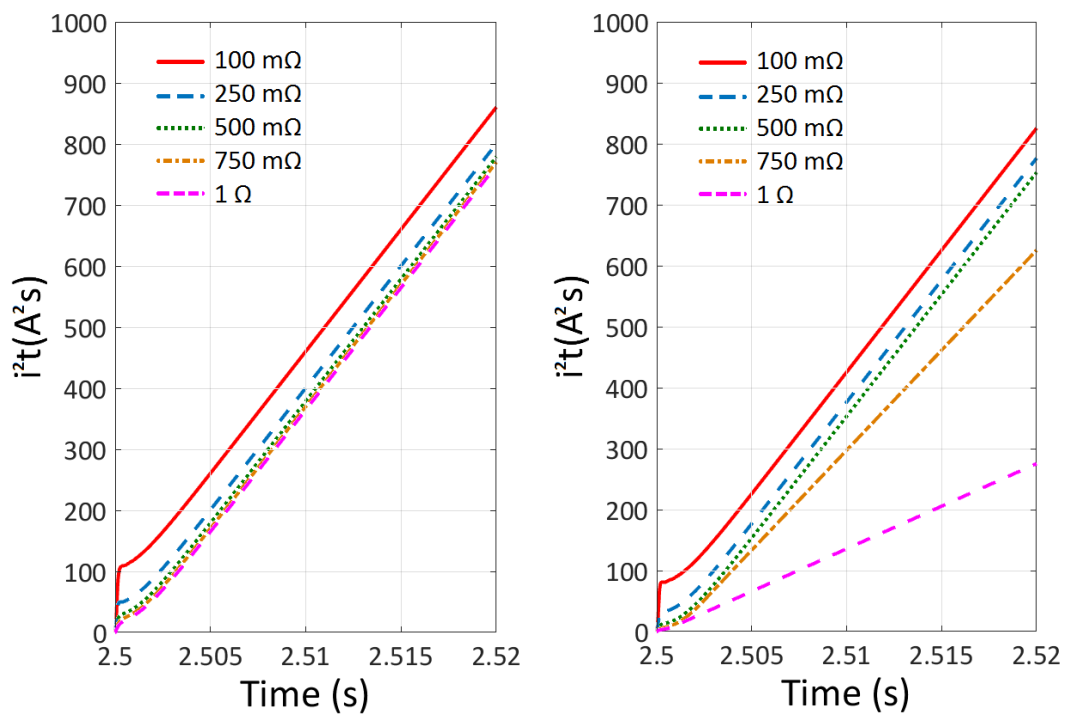
Figure 4.10: Steady state i^2t response for increasing fault impedances at F1 with (a) no ESS and (b) with ESS
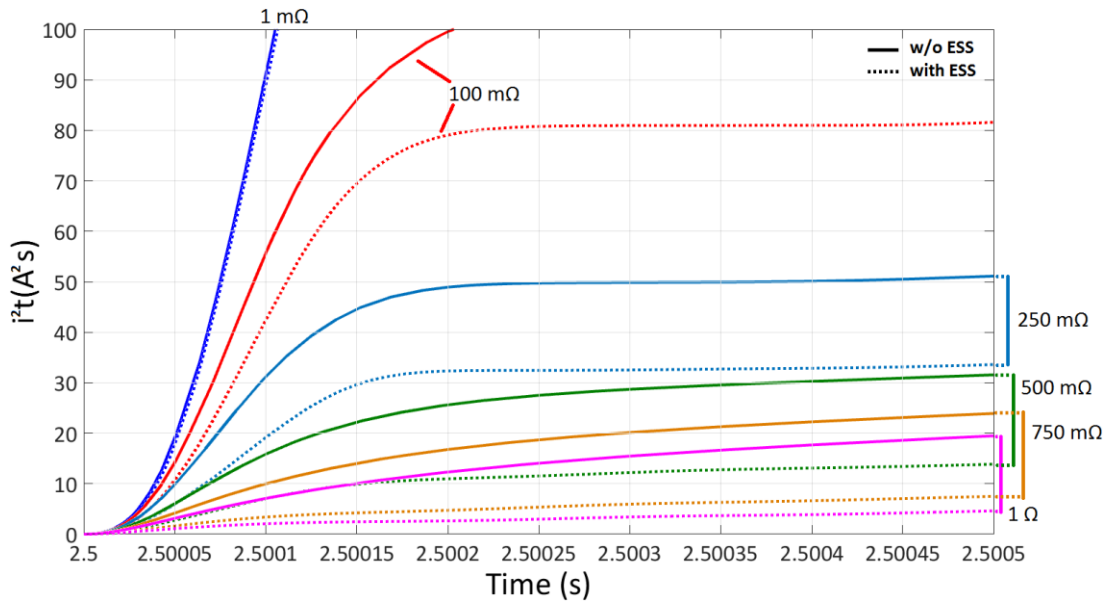
Figure 4.11: Transient period of primary source i²t response for increasing fault impedances

Table 4.2: Time to i²t threshold for increasing fault impedance

Fault impedance at F_1 (mΩ)	Time to 60A²s (no ESS)	Time to 60A²s (with ESS)	Time to 300A²s (no ESS)	Time to 300A²s (with ESS)
1	70µs	70µs	250µs	250µs
100	100µs	150µs	6ms	7ms
250	100µs	1.8ms	7ms	8.1ms
500	1.8ms	2.5ms	7.5ms	8.5ms
750	2ms	2.8ms	8ms	10ms
1000	2.2ms	4.5ms	8.2ms	23ms

4.5.2 Sensitivity of sustained ESS peak current limit on fault energy output of the primary source

For all fault impedances investigated within section 4.5.1, the steady state ESS current output reached its limit of 200A. This sensitivity analysis investigates the impact of varying the ESS peak current limit from 100A – 300A (50% – 150% of the peak generator limit) on the i^2t response of the primary source for a fixed fault impedance of 750 mΩ. This impedance value is selected as it appears from Figure 4.10 that it is the first incremental impedance at which the voltage coupling between the primary source and ESS becomes evident. The change in gradient at this particular impedance value is discussed further in section 4.6. Figure 4.12 illustrates a selection of simulation results that show the i^2t response of the primary source when operating in parallel with the ESS at discrete peak current ratings. These are compared to a baseline trace with the ESS disengaged.

Figure 4.12 clearly shows that increasing the peak current limit of the ESS relative to that of the primary source serves to reduce the gradient of the primary source i^2t contribution. Moreover, it is evident that the primary source response is most sensitive to changes in the ESS peak current limit when this exceeds the primary source peak current (i.e. >100%). When the ESS peak current limit is less than that of the primary source (i.e. <100%), the impact on the primary source fault response is more marginal. Although the reduced depth of discharge of the primary source filter capacitor causes a slight displacement of the primary source output i^2t trace, there is no effect on its steady state output (as indicated by only minor/no changes in the gradient of the corresponding i^2t traces).

Illustrating this further, Table 4.3 provides examples of time-to-threshold values that will be expected for the primary source output if particular ESS peak current limits were to be applied. It shows that for both 60 A^2s and 300 A^2s threshold levels, there is relatively minimal impact on the time-to-threshold for ESS peak current ratings less than the primary source rating. For example, a maximum increase of 0.2ms is observed for the 60 A^2s threshold whereas an increase of 1.3ms is

observed to reach 300 A^{2}s. In contrast, notable increases in the time-to-threshold for the primary source are observed when the ESS peak current rating is equal or greater to the primary source. In particular, a threefold increase is noted when the ESS is rated at 150% of the peak current output of the primary source.
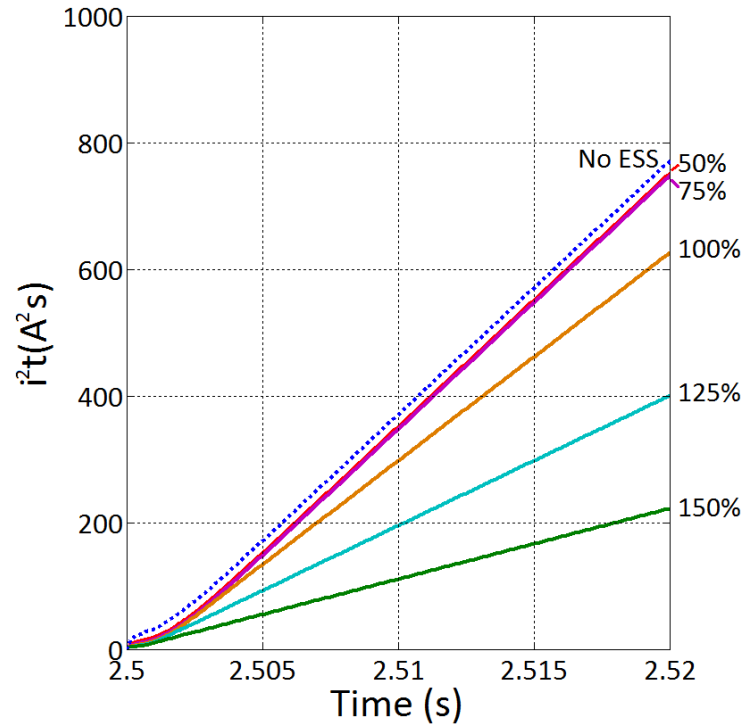
Figure 4.12: Primary source i^{2}t response for 750mΩ at F1 with variable ESS current limit

Table 4.3: Time to primary source i^{2}t threshold for varying ESS peak current limits and fixed fault impedance (750mΩ)

ESS current limit as a percentage of Gen peak current (%)	Time to 60A^{2}s	Time to 300A^{2}s
No ESS	2ms	8ms
50	2.6ms	8.7ms
75	2.7ms	8.8ms
100	2.8ms	10ms
125	3.4ms	15.2ms
150	5.5ms	27ms

4.5.3 Sensitivity of ESS bandwidth on fault energy output of the primary source

The final characteristic considered is the ESS closed-loop bandwidth. Figure 4.13 illustrates the fault energy produced by the primary source when the ESS is operating with different closed-loop bandwidths (for a fixed fault impedance of 750mΩ and fixed sustained current output of 200A). The bandwidth of the primary source in this case study is kept constant at 1kHz, whilst the ESS bandwidth is varied logarithmically from 100Hz to 1MHz. A baseline trace where the ESS is inactive is again included for comparison.

Figure 4.13 indicates that increasing the bandwidth of the ESS has the effect of introducing an increasing time-delay on the i^2t response of the primary source. For lower ESS bandwidths, corresponding to larger time-constants, the primary source i^2t exhibits a characteristic ripple caused by the discharge of its associated filter capacitor and that of the ESS filter capacitor. As the ESS bandwidth is increased to two orders of magnitude greater than that of the primary source and beyond (i.e. 100kHz and 1MHz), the corresponding ripple is smoothed as the ESS time-constant becomes lower than that of the ESS filter capacitor. This eliminates the interaction between both filter capacitors resulting in a smoother discharge of the primary source filter capacitor. Accordingly, a maximum shift along the time axis of 900μs is evident at these higher bandwidths in relation to the generator system operating independently.
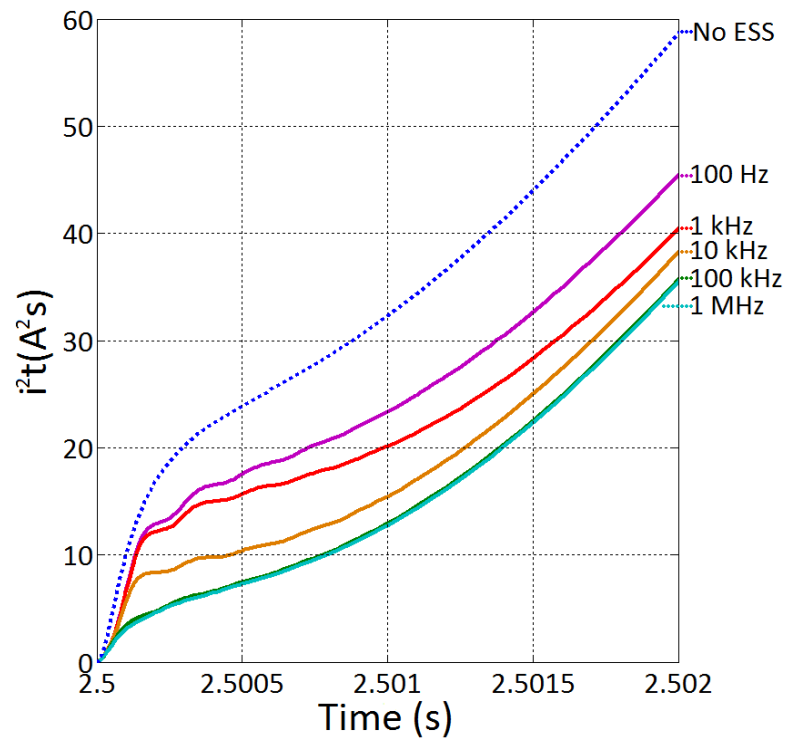
Figure 4.13: Primary source i²t response for varying ESS bandwidth from 100Hz to 1MHz for 750mΩ at F1

4.6 Quantification of network operating and fault conditions under which protection blinding is likely

The effects of the fault impedance and ESS peak current output on the development of the primary source i^2t response can be combined to determine the conditions at which protection blinding becomes evident. Whilst this sensitivity analysis is system specific, the findings are applicable to a wide range of compact DC systems. Figure 4.14 depicts a graph of the steady state gradient of the primary source i^2t curve measured when the fault impedance is modified from 1mΩ to 1Ω and the ESS peak current output is adjusted from 50% - 150% of the primary source peak current limit.

Figure 4.14 shows that the gradient (or rate-of-change) of fault energy (i^2t) delivered by the primary source is consistent for relatively low fault impedances, supporting previous observations. This region of the plot is indicative of the network conditions at which the primary source is delivering its peak sustainable fault current. The ESS has thus had little impact on its response compared with the system operating with the ESS disconnected. Alternatively, the region of the surface plot where the i^2t gradient decreases is indicative of the network conditions where the coupling between the primary source and ESS (through the network voltage) becomes evident, and the response of the primary source to the fault is dampened. Consequently, it is within this region that protection blinding will occur as a result of ESS fault current contribution.
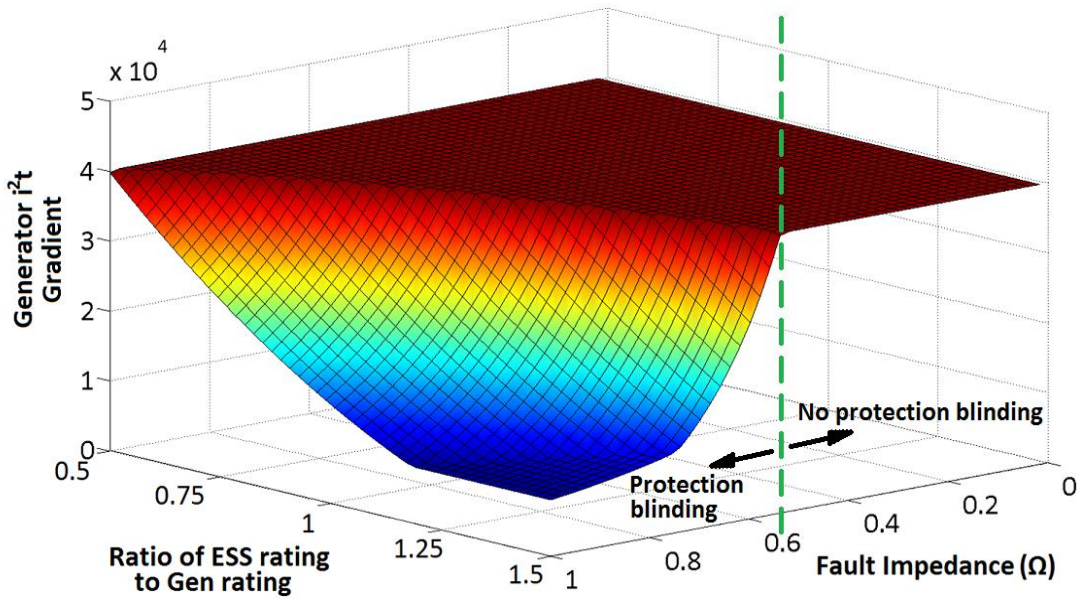
Figure 4.14: Steady state gradient of primary source i^2t response

As indicated in [144], the dynamic response of an ESS to a load or fault transient is dependent on the proportional and integral gain parameters of the outer control loop that govern the behavior of its converter interface. The converter interface will also be limited to how much current it can physically output, according to its rating. A high proportional gain will correspond to a large initial change in the output for a given change in the error, whereas a smaller proportional gain will lead to a less responsive and less sensitive controller. Given that the ESS control system operates directly on the measurement of the network voltage which (during faulted conditions) is analogous to the fault impedance, the ESS current output will naturally be driven to its maximum rated limit for a wide range of fault impedances. However, for ever increasing levels of fault impedance (that may even approach the equivalent impedance of high-power loads) the magnitude of current output from the ESS will become lower than its rated limit. Therefore, the ESS response will be determined by the combination of the ESS peak current limit and its controller gains under these faulted conditions. This will have the effect of reducing the gradient of the primary source i^2t to a constant level for a given high impedance fault, independent of the ESS rating. However, this does not affect the impedance at

which protection blinding starts to occur as this is still dependent on the peak current limit of the ESS. This impedance can be defined as the critical impedance of the system. To derive the critical impedance of the system, consider the simplified equivalent circuit shown in Figure 4.15. The primary generation and ESS are represented by current sources that feed the effective impedance, R_e, prior to the application of the fault, which is represented by resistance R_f.
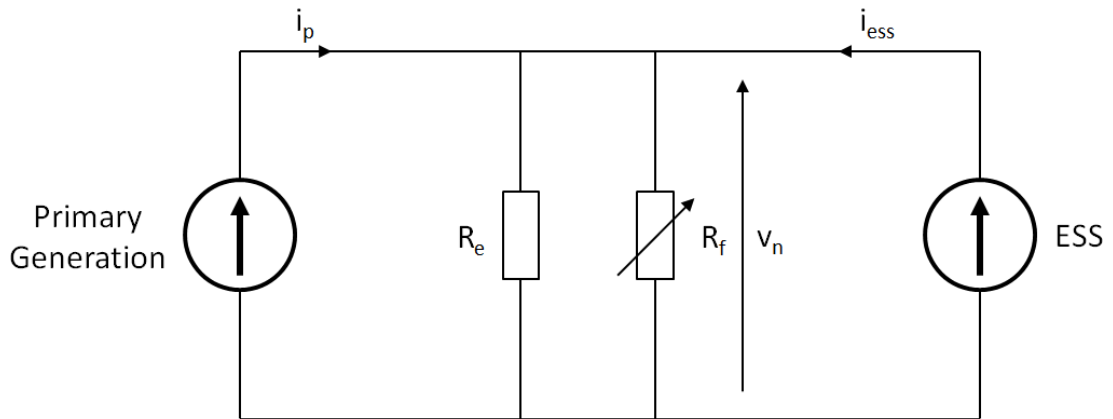
Figure 4.15: Simplified equivalent circuit diagram of primary generation and ESS feeding effective system resistance and fault resistance

The critical impedance R_c at which the gradient of the primary source fault energy output (i^2t) will start to decrease (indicating the occurrence of protection blinding) can be estimated as

$$R_c \approx \frac{v_n}{i_p + i_{ess}}$$

(4.1)

where v_n is the nominal network voltage, and i_p and i_{ess} are the maximum sustained current magnitudes that the primary source and ESS respectively would supply to a short circuit at their terminals.

The total equivalent impedance R_T of the network during faulted conditions can be estimated as

$$R_T \approx R_e // R_f \qquad (4.2)$$

where R_f is the impedance of the fault itself and R_e is the effective impedance of the network (excluding the fault), and in this case defined as

$$R_e \approx \frac{v_n^2}{P_L}. \qquad (4.3)$$

The term P_L is the total load power drawn by the network prior to the fault. If $R_T \gg R_c$ the ESS will likely mask the presence of the fault from a conventional overcurrent protection device used to protect the primary source. Given that R_e (which is determined by the total loading on the network) and R_f are variable, it may be difficult to determine R_T for a suitable range of potential fault conditions. However, it may be possible to determine the minimum possible fault impedance that will cause protection blinding. Under no load conditions, the effective impedance R_e will tend to infinity and the total impedance R_T will therefore be equivalent to the fault impedance. Accordingly, R_c will determine the minimum fault impedance R_f at which protection blinding will occur.

Based on the above approximations R_c will also provide the conditions for maximum power transfer to a fault. This can be shown by rearranging equation (4.1) so that

$$\frac{1}{R_c} \approx \frac{i_p}{v_n} + \frac{i_{ess}}{v_n}. \qquad (4.4)$$

Substituting for the resistance of both sources within (4.4) gives

$$\frac{1}{R_c} \approx \frac{1}{R_p} + \frac{1}{R_{ess}}. \qquad (4.5)$$

Within (4.5) it is apparent that critical resistance R_c is the parallel combination of the equivalent internal resistances of the primary source, R_p, and ESS, R_{ess}, with the internal resistances representing the effects of current control. These are the same conditions for maximum power transfer.

This relationship is verified by evaluating the total power dissipated across a fault for the range of fault impedances and ESS peak current magnitudes considered in the previous section. The resultant surface plot is shown in Figure 4.16.

From Figure 4.16, it is evident that as the ESS rating is increased as a percentage of the primary generation rating for any given fault impedance, the power dissipated across the fault changes. However, the maximum steady-state power is shown to be dissipated at the critical impedance of the system.
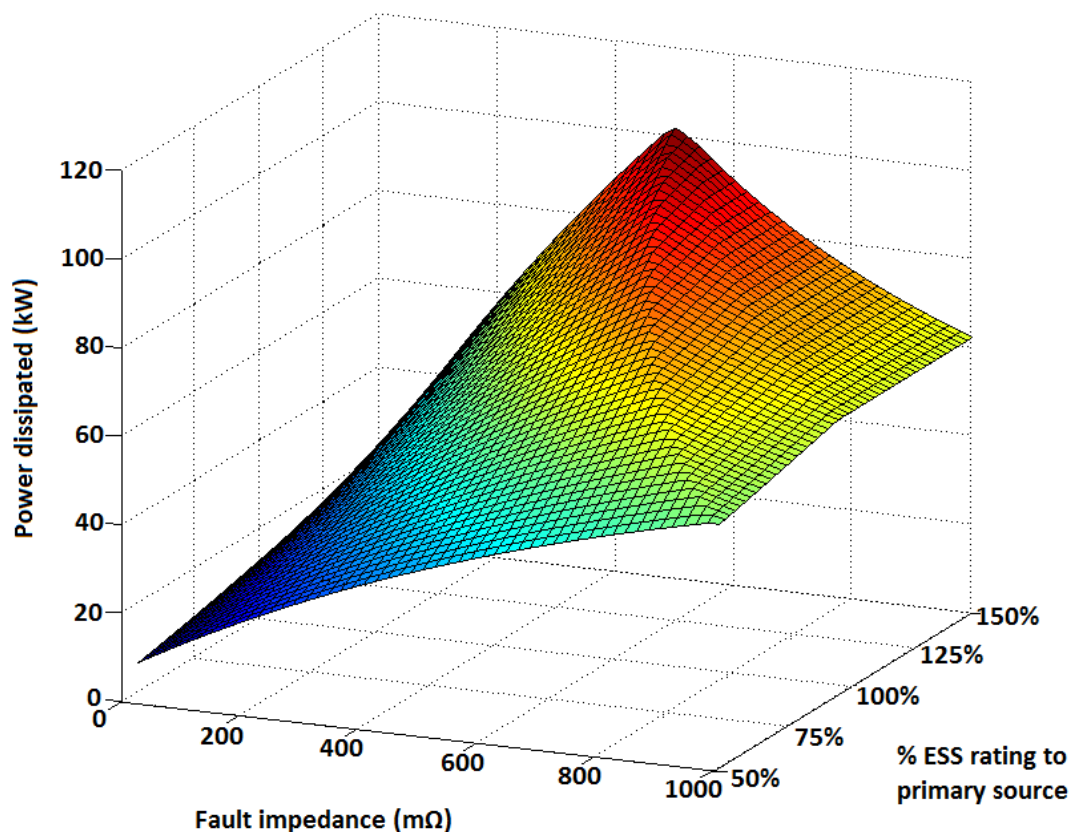
Figure 4.16: Power dissipated across the fault for the range of fault impedances and ESS peak current limit magnitudes

94

4.7 Impact on the performance of conventional protection operation

Altogether, Figures 4.10 – 4.15 and Tables 4.2 and 4.3 define the degree of protection blinding effects on the primary source as a result of integrating a high-power, high bandwidth ESS. It was found that an increase in ESS bandwidth causes a relatively insignificant delay in the development of the i^2t response of the primary source; whereas the dominant variable shaping the behavior of the primary source fault response is the ESS peak current rating. A higher ratio of ESS to primary source rating is found to result in an increase in the time-to-threshold of conventional protection devices that operate on i^2t.

Consequently, if the trip threshold of the primary source protection is set based on its fault response when operating in isolation, it may not be suitable for all fault conditions during paralleled operation with the ESS. Depending on the peak current rating of the ESS, the response of the ESS for fault impedances beyond the critical fault impedance (as described by (4.1)) will temporarily mask the presence of the fault from the primary source. It is under these conditions that the coupling between the sources via the network voltage becomes evident. As a result, fault current levels will be reduced and fault detection times of the primary source protection device will increase. If the fault occurs at a location that requires the use of the blinded device to interrupt fault current this may expose the wider system to the fault for an extended period and potentially compromise the safety of the power system with increased fire risk at the point of fault. It is plausible that faults of higher impedance, such as arc faults, may induce such behavior. Accordingly, the ESS will reduce the dependability of the protection system under these conditions due to its slower than designed operation.

If instead the i^2t threshold for the primary source protection device is set at a lower threshold to reflect its damped response resulting from ESS operation, coordination issues with downstream protection may occur when the ESS is then disconnected or

has a depleted state of charge. Under these conditions, the security of the protection system may be reduced.

Furthermore, it is anticipated that the additional fault current supplied by the ESS for faults that occur at a downstream location will actually serve to improve the fault-detection times of downstream protection devices.

Thus, it will be difficult to predict how the ESS will respond during network fault conditions, in terms of both the magnitude and duration of fault current contribution, and subsequently how this will impact on the system response as a whole. It is therefore essential to be able to define the acceptable limit of impact (in relative terms) that the ESS will have on the primary source fault response in order to identify where conventional protection approaches are acceptable and where alternative protection approaches are required. The analysis laid out in this chapter will help to define these limits.

4.8 Conclusions

The simulation studies and analysis presented in this chapter have enabled the impact of high-power energy storage integrated within a compact power system on the fault response of a primary source to be quantified. The impact of protection blinding on a commercial DC protection device used in aircraft applications was then validated on scaled laboratory experimental demonstrator. A new 'critical fault impedance' term which defines the conditions when protection blinding occurs on a system was then proposed and mathematically derived in this chapter, enabling a rapid assessment of protection risk on a given system.

Based on the protection challenges this case study identifies, Chapter 5 identifies alternative protection strategies which will help to minimize the impact of energy storage integration on protection system performance.

Chapter 5

ESS protection solutions

5.1 Introduction

Key contributions to the state-of-the-art in the protection of DC power systems with integrated high-power energy storage are made in this chapter. The research challenge being addressed is the development of a systems-level protection strategy that enables the ESS to be used more effectively under fault conditions.

A reference DC power system model and baseline protection system is first defined and evaluated in this chapter. The performance of this protection system under fault conditions is then assessed when an ESS is integrated at different locations on the network. Then the novel application of a number of existing protection approaches is considered. Each protection approach is assessed to evaluate its ability to meet the following two broad design objectives:

1. To minimise (or to prevent the exacerbation of) the adverse impact of ESS integration where possible, and
2. To enhance the overall performance of the system when feasible

These protection strategies assessed include:

- A permanent reduction in the trip-threshold settings of devices exposed to protection blinding
- The rapid disconnection of the ESS under all network fault conditions irrespective of fault impedance and fault location
- A modification of the baseline protection system to enable the simultaneous disconnection of the ESS via inter-tripping

- The novel application of adaptive protection (in combination with inter-tripping) to enable the modification of trip-thresholds of particular devices as a function of ESS availability

- The application of differential unit protection for rapid fault discrimination and isolation

A description of the operating principles and limitations of each protection approach are outlined together with a justification for their application within this context. The performance of each approach is then compared to the performance of a baseline protection system.

5.2 Reference DC power system model

The proposed protection solutions evaluated in this chapter are applied to a reference DC power system model constructed within the MATLAB SimPowerSystems environment. A diagram of this power system is illustrated in Figure 5.1. The system is structured to form a radial network architecture that provides a reference evaluation platform to assess the performance of each protection method. Relevant network parameters, such as equivalent cable resistance and inductance per meter, are shown in Table 5.1 and were obtained from a real UAV power system demonstrator being developed by R-R. All feeder lengths are modelled as being 5 meters in length. Simulation results of each protection method are presented in either graphical or tabular formats within this chapter.

The power system consists of a single generator coupled with an active power electronic rectifier with current limiting capability [220] feeding a DC distribution system. This choice of source is used to ensure fault current is limited, preventing damage to internal power electronic switchgear devices. This subsystem is henceforth referred to as the primary source. The distribution system consists of two distribution buses, labelled B_1 and B_2. Three sequential protection layers,

labelled P_1, P_2 and P_3 comprise breakers that can be tripped via their corresponding feeder or load protection relays to appropriately sectionalise the network in the event of a fault.
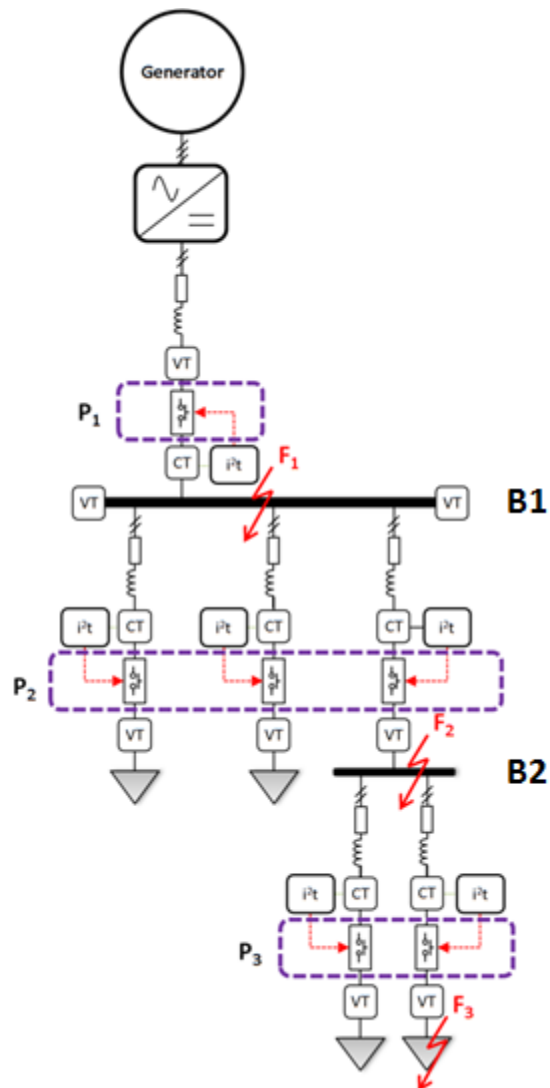
Figure 5.1: DC radial power system architecture reference model

Table 5.1: Parameters of reference model based on a 270V DC aircraft electrical power system

Voltage (V)	Max Source Current (A)	R_{cab} (mΩ/m)	L_{cab} (mΩ/m)	Total P_{load} (kW)
270	200	0.272	0.63	19.9

Under short circuit conditions, it is assumed that the maximum steady-state DC fault current supplied by the primary source is limited to 200A via its corresponding converter interface. Alternatively, if a passive rectification stage such as an autotransformer rectifier unit (ATRU) is used, steady-state fault current will be limited by the saturation current of the generator under fault conditions provided that the diodes withstand the delivered fault current. Protection of fault current limited power systems is normally time-graded as discussed in following sections.

A high bandwidth ESS can be integrated at two locations on this power system: at either B_1 or B_2, as illustrated in Figure 5.2. It is assumed that the supply of current from the ESS is also limited to 200A. The function of the ESS under normal operation is to maintain power quality by tracking the system voltage and supplying or absorbing energy as demanded to mitigate any voltage transients caused by load transitions and network disturbances. The results of simulations in Chapter 4 show that a sustained drop in the network voltage due to a rail-to-rail fault can result in a sustained supply of fault current from the ESS. This behavioural response can reduce the expected magnitude of steady state fault current from the primary source if fault impedance is greater than the critical impedance of the network.

Accordingly, there can be two sources of fault current on the network, depending on ESS availability. However, the employed protection system must perform effectively under both configurations, i.e. when the ESS is active or disengaged. When the ESS is operational, the critical impedance of this DC network can be approximated by (1) to be:

$$R_c \cong \frac{V_n}{I_{gen} + I_{ESS}} \cong \frac{270}{200 + 200} \cong 0.675\Omega .$$

To fully capture the system behaviour for a range of network faults that encompass the critical impedance, simulations of the power system model are performed with

0.5Ω, 0.75Ω and 1Ω faults applied at the three locations on the network, as indicated in Figure 5.2. Given the compact nature of the modelled system, and hence the low resistance of the network cables, fault location does not affect the critical fault impedance of the system. These fault case scenarios will be used to evaluate both the performance of the baseline protection scheme and the proposed solutions.

The following section describes the baseline protection scheme selected for this case study.
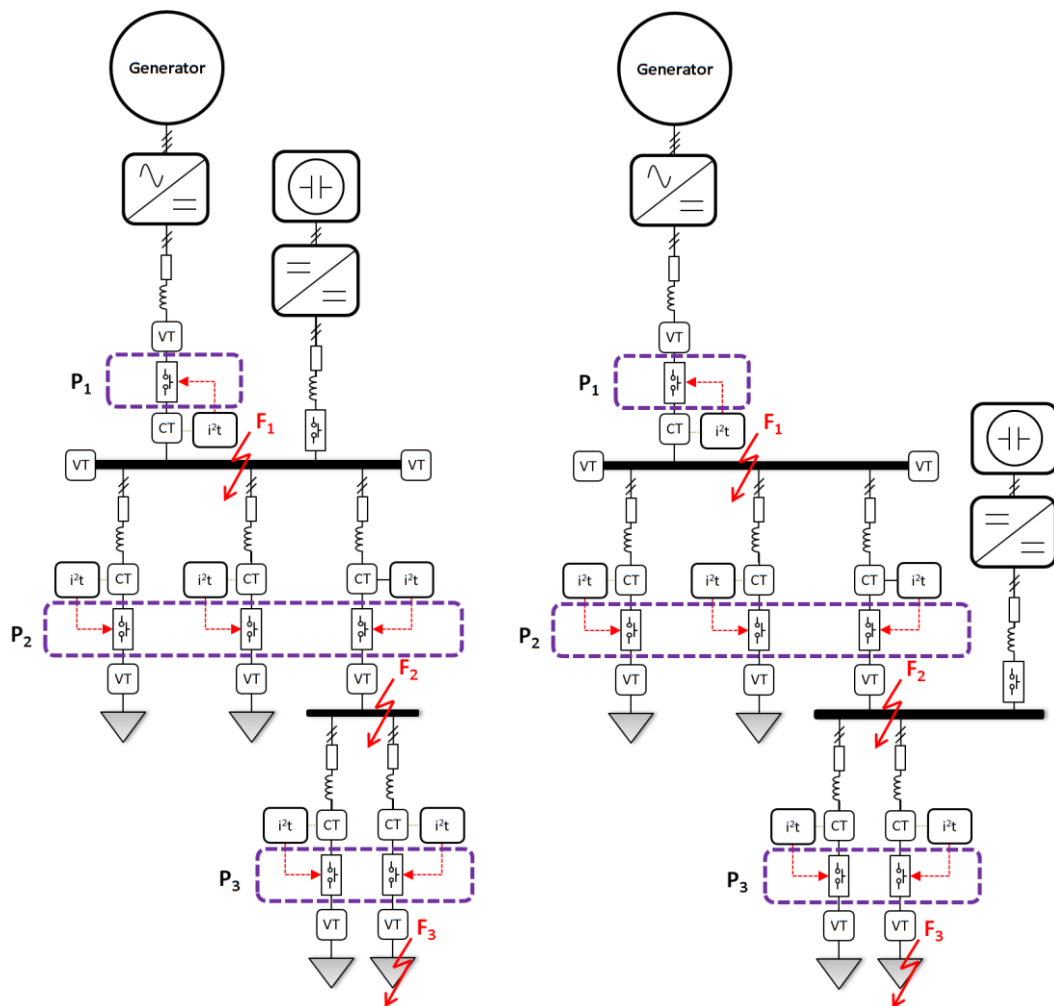
Figure 5.2: DC radial power system architecture with ESS at Bus 1 and Bus 2

5.3 Baseline protection system

The baseline protection system for the reference DC power system illustrated in Figure 5.1 consists of distributed relays and switchgear located within protection layers P_1, P_2 and P_3 that enable the power system to be appropriately sectionalised in the event of a fault. Protection settings of each relay are assumed to be fixed. Normal operation of the protection system requires that the relays operate in a coordinated manner such that only the device immediately upstream from the fault operates first. All devices in parallel branches, i.e. in layer P2 and P3, are assumed to operate within the same timeframe.

Time-graded coordination with respect to the primary source operating in isolation has been selected as the baseline protection approach to which the performance of each proposed solution is compared [155], [181]. This selection has been made due to the following two assumptions:

1. Given the current limited nature of the primary power supply, current-graded coordination of network protection devices is particularly challenging as fault current may be uniform across the system, irrespective of fault location. This is especially true for compact, low resistance networks. This leads protection in these systems to be typically time-graded with respect to the output of the current limiting converter interface. The main disadvantage of this approach is a slower operating speed due to the need to set an operating delay between coordinating protection devices. However, provision of strict trip-time intervals is required to minimise spurious tripping and ensure protection security is maintained. This enables effective fault discrimination using independently operating devices [155], [181].

2. Given that the ESS, by its nature, is a finite and intermittent source of energy on the network, the default configuration of the power system assumes no energy storage is available. The ESS is therefore considered to be

disconnected from the network when it is operating in a secondary control mode (i.e. bulk charging); when insufficient stored capacity is available to perform transient mitigation (i.e. depleted SOC); or when it is permanently offline. Accordingly, fixed protection settings for all coordinating devices have been selected assuming that the primary supply is operating in isolation and is therefore the only source of fault current on the network.

The individually operating protection relays that form the overall baseline protection system are assumed to employ i^2t fault detection algorithms. i^2t based protection has been selected as it is widely utilised within aircraft electrical power systems and is employed on state-of-the-art solid-state protection devices for low voltage DC sections of the network. Local measurement of current at each relay location is obtained via appropriate instrumentation, forming the input to the relay. After appropriate signal processing, the computation of i^2t is instigated when the instantaneous measurement of current is greater than a pre-set and user programmable threshold. The relay generates a trip signal via the associated logic circuitry when its i^2t threshold is exceeded. Figure 5.3 shows a diagram of the constituent components of the relay.
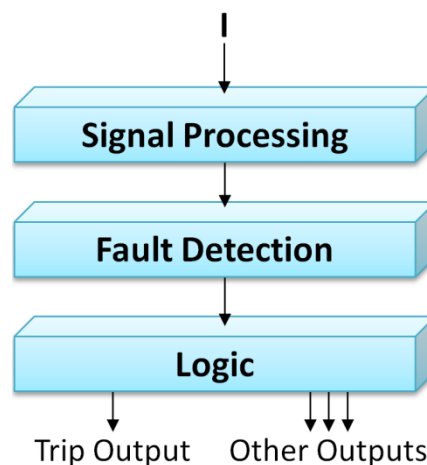
Figure 5.3: Constituent components of a protection relay

5.3.1 Time-graded coordination of independently operating devices

The distributed relays within the system are configured to operate in a coordinated and sequential manner such that any relay in layer P_3 will trip before a relay in layer P_2. Similarly, a relay in layer P_2 will be configured to trip before any relay in layer P_1. For example, a fault at F_3 would cause relay P_3, P_2 and P_1 to initiate the computation of i^2t. However, to ensure that a device in layer P_3 operates before P_2, its trip threshold is set to a lower threshold than that of the device in layer P_2. The relay in layer P_1 is set to the highest threshold. In this manner, the protection system offers inherent backup protection functionality for faults at any location on the network in the event of a failed downstream relay/breaker trip action, minimising the disruption to healthy sections of the network.

It is assumed that all protection switchgear within the system is appropriately rated to withstand the maximum magnitude of fault current along the fault path. It is also assumed that the maximum user-configurable load current setting associated with each feeder protection device is exceeded during all fault scenarios investigated in this case study. Accordingly, it can be assumed that the computation of i^2t is instigated precisely when the fault is applied.

Given that the maximum fault current at any location on the network is limited to 200A for the default system configuration, i^2t thresholds of 300A^{2}s, 200A^{2}s and 100A^{2}s have been arbitrarily selected for relays within sections P_1, P_2 and P_3 respectively to ensure appropriate delay between protection layers.

5.3.2 Evaluation of baseline protection system performance

Assumptions associated with the evaluation of the baseline protection system performance are presented within this subsection. Performance is evaluated using the trip-time measurement of the protection relay directly upstream from the fault (with respect to the primary power source) that is used to trigger the opening of its corresponding switchgear device. This is the length of time that it takes for the relays computational measurement of i^2t to exceed its trip threshold from the moment of fault inception. Latency associated with any instrumentation and digital-sampling is assumed to be negligible. Similarly, latency associated with the communication of these measurements is also assumed to be insignificant. Fault clearance time associated with opening of protection switchgear used to physically isolate the fault is assumed to be rapid in comparison to the operation of the fault detection algorithm, and is therefore not taken into consideration within this case study.

The performance of the baseline protection scheme is first evaluated for the default network configuration, whereby no ESS is integrated. Then, with the ESS connected, the performance is re-evaluated under the following configurations of the power system:

- Network configuration 1 – ESS integrated on B_1
- Network configuration 2 – ESS integrated on B_2

A simplified version of the three configurations of the network is illustrated in Figure 5.4.
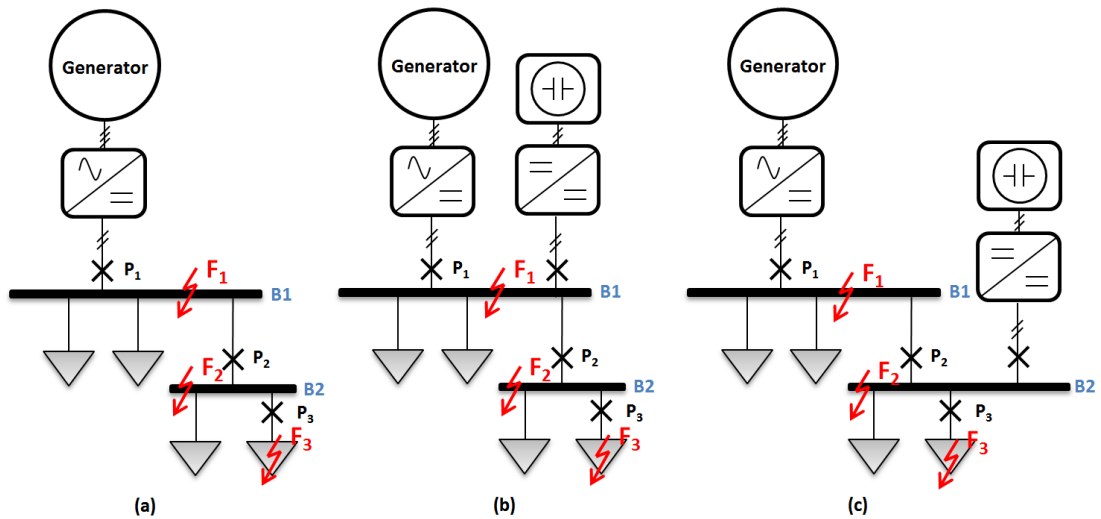
Figure 5.4: (a) Default configuration, (b) Configuration 1 and (c) Configuration 2

Given that protection blinding has been identified to occur under relatively high impedance fault conditions, only 0.5Ω, 0.75Ω and 1Ω faults at locations F_1, F_2 and F_3 are considered in this investigation.

The response of the ESS during relatively low impedance (short circuit) fault conditions has been shown in Chapter 4 to have negligible impact on the fault response of other network integrated sources. It can therefore be assumed that the performance of baseline protection system will not be impacted as a result of ESS integration under these conditions.

5.3.3 ESS protection assumptions

Simulations of the DC power system model operating under fault conditions for network configurations 1 and 2 are performed with no ESS protection device employed. The ESS is assumed to have sufficient capacity to supply fault current for the duration of the fault and does not disconnect from the network. The network is considered to revert back to the default configuration if the ESS SOC has depleted. This systems level functional behaviour is initially assumed for the evaluation of the baseline protection system performance as the optimal protection strategy for the ESS is unknown. Indeed, the ESS protection requirements may be application specific. For example, the ESS may be commanded to supply maximum available power to a high-power load for a duration that is longer than the expected operating time of all coordinating downstream protection devices. Under these conditions, the ESS current output may be equivalent to the magnitude of its current-limited fault current output. This would mean that the employment of a conventional protection device that uses an i^2t based fault detection algorithm (with fixed settings) would require a significantly higher trip-threshold setting to prevent nuisance tripping of the ESS under such operating conditions.

Accordingly, the performance and limitations of the baseline protection scheme and alternative protection strategies are investigated in subsequent sections of this chapter that address this challenge and enable a more optimised use of the ESS during fault conditions.

5.3.4 Simulation results of baseline protection system performance

This section presents the simulations results of fault studies of all three configurations of the reference DC power system model shown in Figure 5.4. The baseline protection system is first evaluated with no ESS connected to the system (default configuration) and then with the ESS integrated at the predefined locations. The implications of utilising the baseline protection system design with no modification to settings when considering the integration of a high-power ESS is then discussed in section 5.3.5.

Simulation results have been categorised by fault location (F_1, F_2 and F_3) and show the quantity of fault energy (i^2t) measured at the location of the corresponding upstream protection relay (P_1, P_2 and P_3) for 0.5Ω, 0.75Ω and 1Ω faults. These results are then used to determine the inferred trip-time of the protection relay for the default configuration of the network in comparison to when the ESS is operational for both network configurations 1 and 2.

Figure 5.5 (a) shows the quantity of fault energy measured by protection relay P_1 for 0.5Ω, 0.75Ω and 1Ω faults at location F_1 when the primary power source is operating in isolation (default configuration) and when the ESS is connected to bus B_1 (configuration 1). Similarly, Figure 5.5 (b) compares the fault energy at P_1 for the default configuration of the network and when the ESS is located on B_2 (configuration 2). The threshold of protection layer P_1 is set to $300A^2s$, as indicated on Figure 5.5.
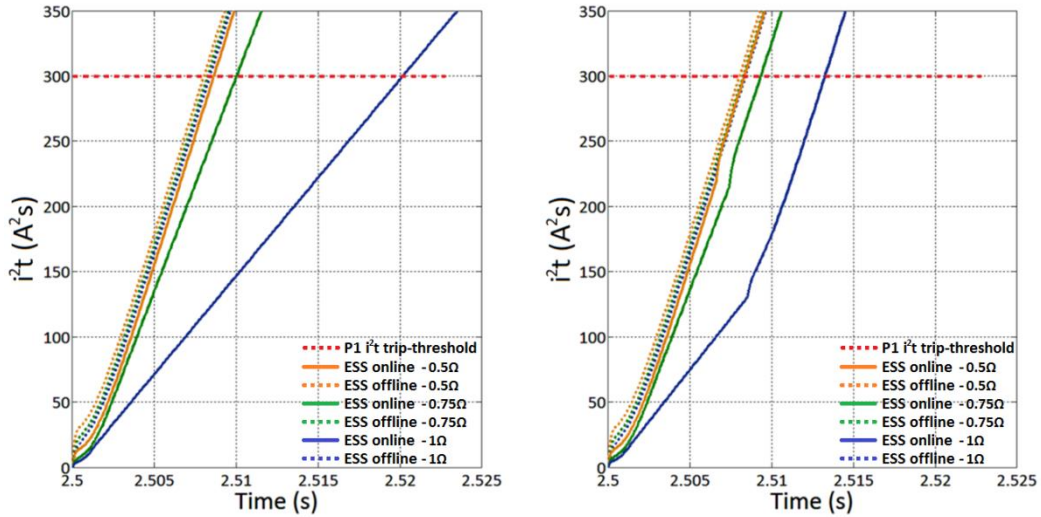
Figure 5.5: Fault energy at protection relay P_1 for 0.5Ω, 0.75Ω and 1Ω faults located at F_1 for (a) default / configuration 1 and (b) default / configuration 2

From Figures 5.5 (a) and (b), it is clear that the performance of protection relay P_1 is degraded when the ESS is operational for fault impedances greater than the critical impedance of the network (i.e. longer trip-time) in comparison to the protection performance when the primary source is operating in isolation. It is also evident that a fault impedance lower than the critical impedance (i.e. 0.5Ω) has minimal impact on the performance of protection device P_1. For instance, a trip-time increase of 0.7ms is observed for a 0.5Ω fault when the ESS is integrated at bus B_1 whereas the trip-time increases by 1.8ms and 11.8ms respectively for 0.75Ω and 1Ω faults. Similarly, when the ESS is integrated at bus B_2 for configuration 2, there is a 0.3ms increase in trip-time observed for a 0.5Ω fault at F_1 in comparison to the default configuration of the network. However, for 0.75 Ω and 1Ω faults the trip-time increases by 1.1ms and 4.9ms respectively.

Note that when the ESS is integrated to bus B_2 (configuration 2) the protection relay P_2 trips due to the fault current contribution from the ESS. It trips before relay P_1 due to its lower trip threshold and, as a result, interrupts the ESS fault current by triggering the opening of the switchgear device. This can be better visualised in the

current path diagram illustrated in Figure 5.6. This operation is reflected in Figure 5.5 (b) where the rate of change of fault energy (i^2t) delivered by the primary source increases in response to the opening of protection device P_2.

For faults at location F_2, protection relay P_2 is used to interrupt the fault current from the primary source. The trip-time of P_2 is therefore used to determine the performance of the protection system. The diagram shown in Figure 5.7 visualises the direction of fault current for all three configurations of the system.

Figure 5.8 (a) shows the quantity of fault energy measured by protection relay P_2 for 0.5Ω, 0.75Ω and 1Ω faults at location F_2 for the default configuration of the network and when the ESS is connected to bus B_1 (configuration 1). Similarly, Figure 5.8 (b) compares the fault energy at P_2 for the default configuration of the network and when the ESS is located further downstream at bus B_2 (configuration 2). The threshold of protection layer P2 is set to 200A^{2}s, as indicated on Figure 5.8.

Comparing the inferred trip-times of the protection device P_2 when the system is operating in the default configuration to when it is in configuration 1, it is clear from Figure 5.8 (a) that the baseline protection system performance is enhanced by the additional fault current contribution from the ESS for faults at F_2, irrespective of fault impedance. For example, when the ESS is engaged, the P_2 trip-time for 0.5Ω, 0.75Ω and 1Ω faults is approximately 4.3ms, 4.5ms, and 4.ms faster than its trip-time for the default configuration of the network.

In contrast, when the system is arranged in configuration 2, P_2 trip-time increases as a result of the ESS fault current contribution. Again, faults greater than the critical impedance of the power system causes significant protection blinding as the rate of change of fault energy from the primary source is reduced due to the ESS response. This can be observed in Figure 5.8 (b) where the elapsed time for i^2t to exceed the P_2 threshold of 200A^{2}s increases from 6.6ms to 9.7ms for a 0.75Ω fault, and from 7ms to 25ms for a 1Ω fault.
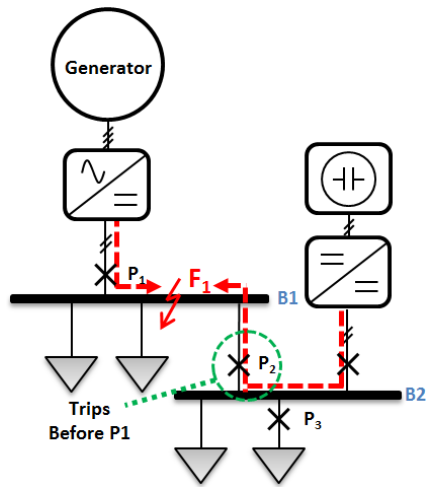
Figure 5.6: Fault current path for configuration 2 for a fault at F₁
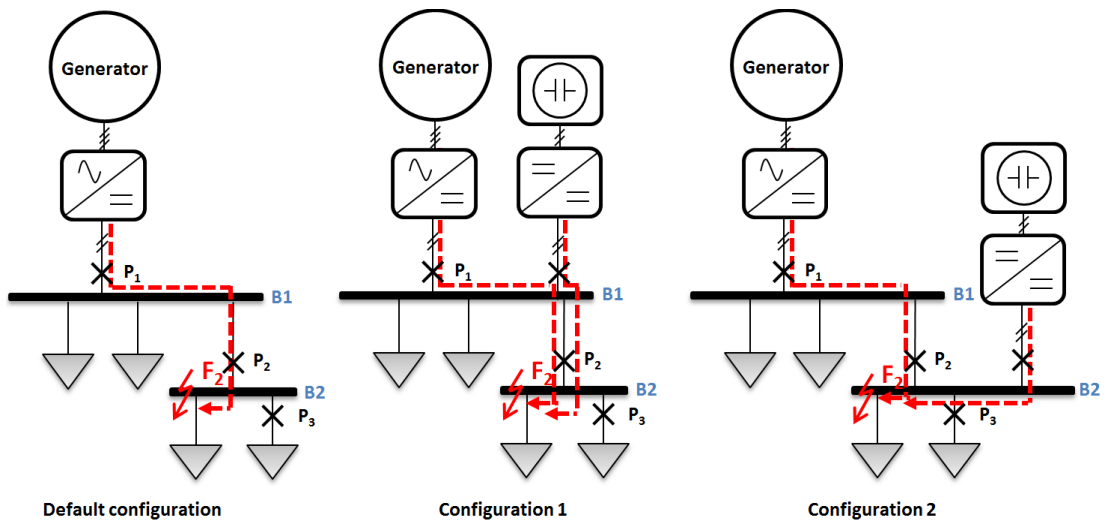
Figure 5.7: Fault current paths for all three network configurations for a fault at F₂
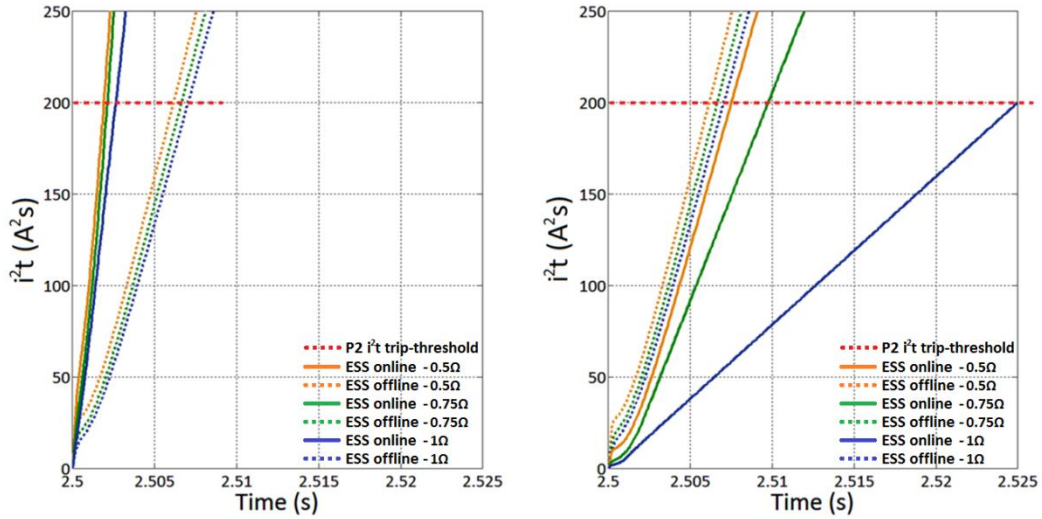
Figure 5.8: Fault energy at protection relay P_2 for 0.5Ω, 0.75Ω and 1Ω faults located at F_2 for (a) default / configuration 1 and (b) default / configuration 2

This response is similar to the previous fault scenario where the performance of protection relay P_1 is degraded for F_1 faults due to the supply of fault current from the ESS from a location that is downstream from the considered protection device.

For F_3 faults, protection relay P_3 is used to interrupt the fault current from the primary source. Figures 5.9 (a) and (b) compare the quantity of fault energy measured by protection relay P_3 for 0.5Ω, 0.75Ω and 1Ω faults when the system is operating in the default configuration and when it is arranged in configurations 1 and 2. The threshold of protection layer P_3 is set to 100A^{2}s, as indicated on Figure 5.9.

It is clear from both Figures 5.9 (a) and (b) that the performance of the baseline protection system is improved as result of the additional fault current contribution from the ESS in the event of a fault at location F_3. Given that the ESS is integrated at an upstream location relative to protection relay P3 for both configurations 1 and 2, the trip-time decreases significantly in comparison to the default operation of the system, irrespective of fault impedance.

A summary of the simulated performance of the baseline protection system for all considered fault locations and fault impedances, Table 5.2 displays the trip-times of the appropriate protection devices that are triggered in the event of a fault.
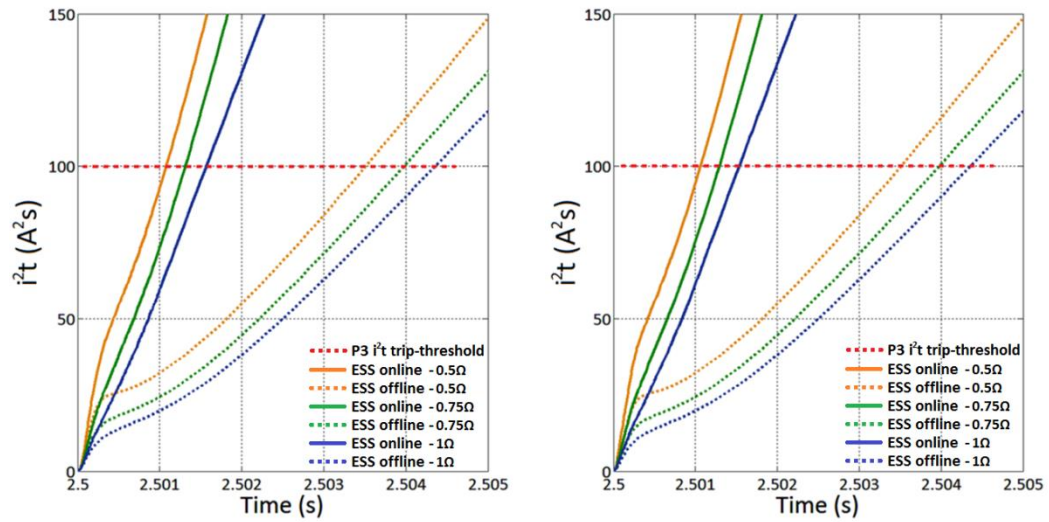
Figure 5.9: Fault energy at protection relay P₃ for 0.5Ω, 0.75Ω and 1Ω faults located at F₃ for (a) default / configuration 1 and (b) default / configuration 2

Table 5.2: Summary of baseline protection system performance

Fault location	Fault impedance (Ω)	Default configuration		Configuration 1		Configuration 2	
		tripped device	trip time (ms)	tripped device	trip time (ms)	tripped device	trip time (ms)
	0.5	P1	8	P1	8.7	P2 then P1	8.3
F1	0.75	P1	8.2	P1	10	P2 then P1	9.3
	1	P1	8.3	P1	20.1	P2 then P1	13.2
	0.5	P2	6.1	P2	1.8	P2	7.5
F2	0.75	P2	6.6	P2	2.1	P2	9.7
	1	P2	7	P2	2.6	P2	25
	0.5	P3	3.5	P3	1	P3	1
F3	0.75	P3	3.9	P3	1.3	P3	1.2
	1	P3	4.3	P3	1.5	P3	1.5

5.3.5 Discussion on the performance of the unmodified baseline protection system with ESS integration

The results of the unmodified baseline protection system presented in Table 5.2 show that for a consistent set of fault conditions (i.e. fault location and fault impedance), the additional fault current supplied by the ESS can either improve or impair the overall performance of the baseline, depending on where on the network that ESS is located in relation to the fault.

Accordingly, applying no change to the baseline protection system design may be a viable solution under certain conditions when considering the integration of a high-power ESS. For example, if faults are likely to only occur at the particular locations where performance is improved, no change to the baseline system is required. Indeed, if the impedance of faults located anywhere on the network are likely to be lower than the critical impedance, the fault response of the ESS will have minimal impact on the performance of the baseline system. For instance, this may be the case if the rating of the ESS is relatively low, increasing the critical impedance according to equation 4.1. However, the impedance and location of faults within a number of critical power system applications may be difficult to predict, and so continued use of the baseline protection solution will not be appropriate for such systems.

The results of the baseline performance evaluation show that the protection devices that experience protection blinding are those that are in series with the primary source with respect to the location of the ESS. Consequently, a fault that is greater than the critical impedance and is located within this series path will result in a slower overall protection system performance. It is this impaired performance for these particular fault locations that the novel application of alternative protection solutions needs to address. On the other hand, any protection device on a parallel feeder with respect to both sources benefits from the additional fault current supplied by the ESS. Thus, any fault that develops downstream from these devices, irrespective of its impedance, will be detected faster. This improvement in

performance for these particular fault locations is another aspect of the system behaviour that a more optimised protection system must enable.

For example, consider the trip-times of protection device P_2 for all evaluated F_2 faults, in all three configurations of the network. With the ESS located at bus B_1, P_2 trip-times for all F_2 faults are significantly reduced in comparison to the default configuration. This is because protection device P_2 is located on a parallel feeder with respect to the ESS and primary source. Hence, the additional fault current supplied by the ESS into fault F_2 accelerates fault detection and enhances the overall performance of the protection system. The additional ESS i^2t contribution for accelerated performance for a fault at this location is $72A^2s$ for the 0.5Ω fault, $84A^2s$ for the 0.75Ω fault and $104A^2s$ for the 1Ω fault.

However, the same fault condition results in a slower response of P_2 when the ESS is located at bus B_2. In this instance, P_2 is in series with the primary source with respect to the ESS, and hence is exposed to protection blinding for an F_2 fault. This reduction in operating speed prolongs fault exposure and heightens the risk of physical damage to the system and its surroundings. The length of time that the ESS is delivering 200A into the fault prior to the tripping of protection device P_2 is 7.5ms for a 0.5Ω fault (additional i^2t contribution of $300A^2s$), 9.7ms for a 0.75Ω fault (additional i^2t contribution of $388A^2s$) and 25ms for a 1Ω fault (additional i^2t contribution of $1000A^2s$). Therefore, by the time that the appropriate protection device trips, the total quantity of energy at the point of fault increases substantially as a result of its slower operation.

This behaviour is also observed in the evaluation of P_1 trip-times for all F_1 faults. For either location of the ESS (at bus B_1 or bus B_2) protection device P_1 is in series with both sources, and hence has impaired performance due to the protection blinding caused by the ESS for F_1 faults in comparison to its performance in the default configuration. The i^2t contribution of the ESS for an F_1 fault on configuration 1 is $348A^2s$, $400A^2s$ and $804A^2s$ for 0.5Ω, 0.75Ω and 1Ω faults respectively. For configuration 2, it is an additional i^2t contribution of $332A^2s$, $372A^2s$ and $528A^2s$.

5.4 Permanent reduction of protection settings to accommodate for protection blinding

Figure 5.10 highlights the relays within the baseline protection system that are exposed to protection blinding as a result of ESS integration for configurations 1 and 2. It is proposed that the trip-settings of these relays are permanently reduced so that the trip-times match those of the baseline system when operating in the default configuration of the network in order to minimise the adverse effect of ESS integration.

As evident in the results of the fault studies performed in section 5.3, only protection device P_1 would benefit from a trip threshold reduction if the ESS is connected to bus B_1 (configuration 1). However, if the ESS is integrated to bus B_2 (configuration 2) both P_1 and P_2 settings would require a reduction in trip thresholds to improve the overall protection system performance to match that of the baseline system performance when primary source is the only source of fault current on the network (default configuration).
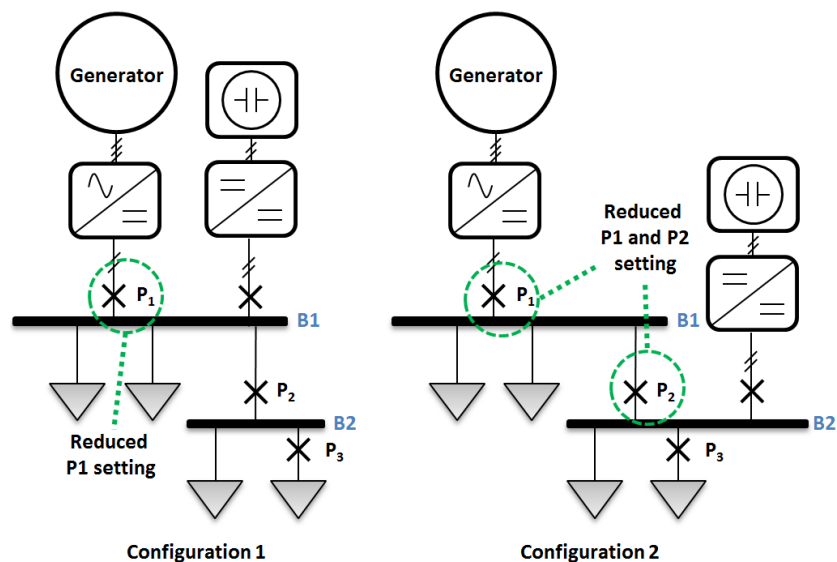
Figure 5.10: Protection devices exposed to protection blinding for (a) configuration 1 and (b) configuration 2 of the network

The following case study considers network configurations 1 and 2 individually, and aims to evaluate the potential improvement in trip-times of the affected protection relays by reducing their corresponding trip thresholds. A discussion on the limitations of this solution in enabling consistent protection system performance to that of the baseline protection system is then presented.

5.4.1 Configuration 1

For configuration 1 of the DC power system model shown in Figure 5.10, P_1 settings are arbitrarily reduced from 300A^{2}s to 250A^{2}s. In practice, the level to which the protection settings may be permanently reduced may be restricted by the coordination requirements between protection tiers and is discussed further in section 5.4.6. This case study is performed to simply demonstrate the impact of reduced settings. The times taken for the relay measurement of i^2t to exceed this new trip threshold for F_1 faults of 0.5Ω, 0.75Ω and 1Ω are presented in Table 5.3.

The results presented in Table 5.3 indicate that reducing the trip threshold settings of relay P_1 will improve the trip-time of the protection device, as expected, when the ESS is engaged. However, the trip-times of P_1 for high-impedance faults greater than the critical impedance of the network are still significantly increased. For example, a 1Ω fault at F_1 results in a trip-time of 16.9ms for the lower trip-threshold of 250A^{2}s in comparison to 20.1ms when the setting is 300A^{2}s. Although there is a clear improvement in the time taken to detect the fault when the ESS is engaged, this trip-time is still more than 100% greater than the trip-time of P_1 in the baseline system during the default configuration of the network. This is due to the reduced rate of change of fault energy being delivered by the primary source for higher-impedance faults as a result of the ESS contribution (i.e. the root cause of protection blinding). The i^2t contribution of the ESS with the modified settings is 296A^{2}s, 340A^{2}s and 676A^{2}s for the given fault impedances.

Table 5.3: Trip-times of P_1 with reduced trip threshold of $250A^2s$

Fault location	Fault impedance (Ω)	Default configuration		Configuration 1		Configuration 1 (modified)	
		P1 threshold	trip time (ms)	P1 threshold	trip time (ms)	P1 threshold	trip time (ms)
	0.5	$300A^2s$	8	$300A^2s$	8.7	$250A^2s$	7.4
F1	0.75	$300A^2s$	8.2	$300A^2s$	10	$250A^2s$	8.5
	1	$300A^2s$	8.3	$300A^2s$	20.1	$250A^2s$	16.9

5.4.2 Configuration 2

For network configuration 2, it is proposed that the trip thresholds of P_1 and P_2 are both reduced to accommodate for the protection blinding caused by the response of the ESS under fault conditions. In this case, the P_1 trip setting is reduced from $300A^2s$ to $250A^2s$, whilst the P_2 trip setting is reduced from $200A^2s$ to $150A^2s$. Table 5.4 shows the trip-times of these devices in comparison to the default cases.

Table 5.4: Trip-times of P_1 and P_2 with reduced thresholds of $250A^2s$ and $150 A^2s$

Fault location	Fault imped. (Ω)	Default configuration		Configuration 2		Configuration 2 (modified)	
		tripped device	trip time (ms)	tripped device	trip time (ms)	tripped device	trip time (ms)
	0.5	P1 - $300A^2s$	8	P2 then P1 $200A^2s$ - $300A^2s$	8.3	P2 then P1 $150A^2s$ - $250A^2s$	7.1
F1	0.75	P1 - $300A^2s$	8.2	P2 then P1 $200A^2s$ - $300A^2s$	9.3	P2 then P1 $150A^2s$ - $250A^2s$	7.8
	1	P1 - $300A^2s$	8.3	P2 then P1 $200A^2s$ - $300A^2s$	13.2	P2 then P1 $150A^2s$ - $250A^2s$	10.8
	0.5	P2 - $200A^2s$	6.1	P2 - $200A^2s$	7.5	P2 - $150A^2s$	6
F2	0.75	P2 - $200A^2s$	6.6	P2 - $200A^2s$	9.7	P2 - $150A^2s$	7.6
	1	P2 - $200A^2s$	7	P2 - $200A^2s$	25	P2 - $150A^2s$	18.9

The results presented in Table 5.4 show that a reduction in the trip threshold of protection device P_2 enables faster fault detection of all F_2 faults in comparison to the baseline P_2 settings for configuration 2. The reduction of the P_1 trip threshold is also implemented to compensate for the protection blinding effects caused by the ESS when providing backup protection functionality in the event of a P_2 trip-failure.

In this situation, P_1 will operate faster in comparison to the unmodified P_1 settings for configuration 2.

Similar to the previous case, it is clear that F_2 faults greater than the critical impedance of the network result in P_2 trip-times that are significantly longer than the baseline protection system performance during default network configuration operation. For example, a trip-time increase of 1ms is observed when the P_2 trip threshold is set to 150A^2s for a 0.75Ω in comparison to the baseline case. This is an improvement over the 3.1ms increase if the P_2 settings are unmodified. Similarly for a 1Ω fault, a 11.9ms increase is observed with the lower threshold in comparison to a 18ms increase in the unmodified case. Although the lower trip threshold of P_2 modestly improves the performance of the protection relay, the ESS fault current contribution still causes protection blinding by reducing the rate of change of fault energy delivered by the primary source.

For F_1 faults, the overall protection system performance using the lower P_1 and P_2 settings is improved in comparison to the baseline system performance when the ESS is operational. This is due to the faster operation of P_2, which interrupts the ESS supply of fault current due to its lower trip-threshold, leaving P_1 to disconnect the primary source. However, despite the lower P_1 and P_2 trip settings to compensate for the ESS during operation in network configuration 2, the overall performance of the protection system (in terms of the time taken for P_1 to operate) is still slower than the baseline protection performance for a 1Ω fault at F_1 in the default configuration of the network.

Given the improved trip times of P_2 for a fault at F_2, the i^2t contribution of the ESS with the modified P_2 settings is 60A^2s less for a 0.5Ω fault, 84A^2s less for a 0.75Ω fault and 244A^2s less for a 1Ω fault in comparison to the original settings. For an F_1 fault, the i^2t contribution of the ESS is 48A^2s less for a 0.5Ω fault, 60A^2s less for a 0.75Ω fault and 96A^2s less for a 1Ω fault in comparison to the original settings.

The implications of decreasing the trip thresholds even further are described in the discussion in section 5.4.6.

5.5 Novel protection approaches to improve system performance under fault conditions

It is evident from the case studies presented in sections 5.3 and 5.4 that the availability and operation of the ESS under fault conditions plays a significant role in shaping the protection system performance. It is clear that under certain fault conditions, the rapid disconnection or shutdown of the ESS will benefit the overall protection system performance whilst avoiding the unnecessary dissipation of available stored energy. However, the removal of the ESS from the network for all faults significantly limits the benefits of the ESS. In other cases, allowing the ESS to continue supplying fault current into a fault will improve fault detection times of downstream relays. However, this may not always be necessary if the protection performance already meets the minimum safety requirements of the power system application.

Accordingly, this section evaluates the performance of candidate protection approaches that may minimise or prevent the exacerbation of the adverse impact of ESS integration where possible, and that enhance the overall performance of the system when feasible.

5.5.1 Rapid ESS disconnection for all fault conditions

A relatively crude ESS protection approach to enable the baseline protection system to operate as intended for all fault conditions, irrespective of the ESS location, is to implement the rapid disconnection of the ESS in the event of any network fault condition. This approach is being considered as it enables the network to rapidly reconfigure in the event of a fault and revert back to the default configuration enabling the baseline protection system that is optimised for this particular configuration to operate as intended.

This ESS fault behaviour may be implemented through the use of a low-voltage-disconnect function that will trigger the ESS protection device when the network voltage drops below a fixed and predefined threshold for a fixed period of time. For example, if the network voltage drops below 50% of nominal levels for longer than 1ms, then the ESS will be prompted to disconnect from the network.

Although this will lead to a guaranteed optimal operation of the baseline protection solution (albeit with a minimal delay associated with the time taken to disconnect the ESS), it leads to a suboptimal use of the ESS under fault conditions. This is because it prevents the ESS from being used for fault ride through or post-fault recovery. This protection approach also prevents the ESS from being used to accelerate the performance of downstream relays where the additional fault current being supplied by the ESS will enable the downstream protection devices to trip faster.

Furthermore, this functionality may be sensitive to high-power load transitions or the switching of highly capacitive loads that may cause a prolonged undervoltage condition. This undervoltage may be observed by the protection function and disconnect the ESS unnecessarily. Thus, as a solution it meets the design criteria of preventing the exacerbation of protection blinding, however it does not allow for the protection performance to be enhanced. Nor does it allow for the ESS to be used more effectively during fault conditions.

5.5.2 Inter-tripping

Inter-tripping, or the use of a single protection relay to trigger the operation of more than one switchgear device, is being considered to reduce the impact of protection blinding caused by the ESS and to enable the ESS to disconnect from the system to prevent the continued dissipation of stored energy into a fault. Interrupting the fault current contribution of the ESS is necessary under the conditions where no network protection device within the series fault path of the ESS is available to sectionalise the network. For example, Figure 5.11 illustrates the cases in the previous fault studies where the ESS supply of fault current must be interrupted to prevent the continual discharge of stored energy into the fault.
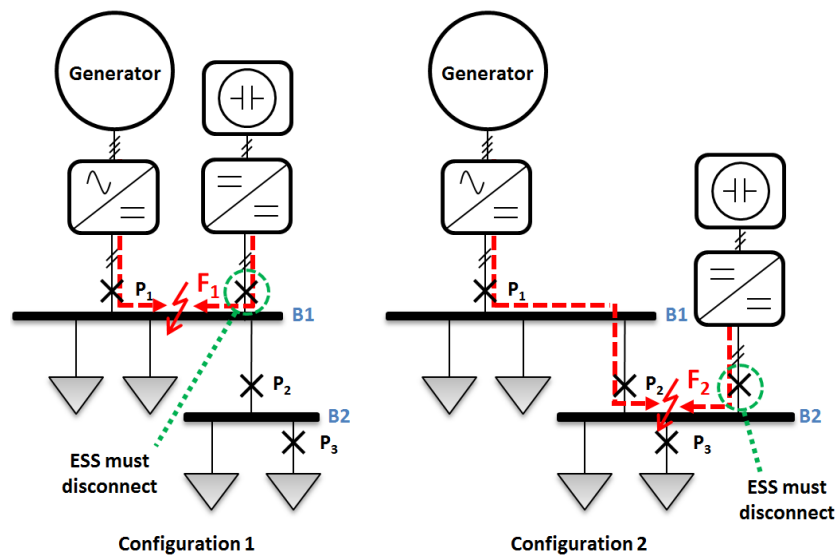
Figure 5.11: Fault cases where ESS must be disconnected to prevent unnecessary energy dissipation into fault

From Figure 5.11, it is clear that for network configuration 1, a fault at location F_1 requires the opening of protection switchgear P_1 to interrupt the primary source contribution of fault current in addition to the disconnection of the ESS. Similarly

for network configuration 2, the ESS must be disconnected to interrupt its contribution to a fault at location F_2.

One method to achieve this desired behaviour is to employ a protection relay with inter-tripping functionality that enables a fault-detection trip condition at one location to trigger the opening of more than one circuit breaker across the network. This may be implemented with a modification to the baseline protection system to enable an appropriate protection relay to simultaneously isolate the ESS in the event of a fault. Disconnection of the ESS may be achieved using a dedicated switchgear device to physically isolate the system, or it may be performed by a controlled shutdown function of ESS converter interface, that is triggered via an external trip signal.

For network configuration 1, this inter-trip function may be performed by relay P_1. This added functionality allows the ESS to disconnect from the system for all network fault events that cause relay P_1 to trip. However, when implemented the resultant ESS protection behaviour will have no impact on the fault-detection time of P1 as the protection blinding effects caused by the ESS response will still occur.

For configuration 2, implementation of an inter-trip from relay P_1 to isolate the ESS in the event of a trip event will not provide the desired ESS protection behaviour. This is apparent when considering a fault at location F_2. For this fault case, protection layer P_2 is configured to operate before P_1. Assuming the opening of P_2 does not fail, protection device P_1 should not operate at all. Therefore, an inter-trip pairing with this relay to the ESS protection device would still cause the ESS to unnecessarily discharge into the fault.

Alternatively, implementation of an inter-trip pairing with protection relay P_2 will deliver the desired ESS protection functionality under normal operating conditions. A fault at location F_2 will result in a P_2 relay trip whilst also enabling the disconnection of the ESS from the network. The overall performance of protection system will again be unaffected as the P_2 trip-time will remain the same. However,

for a fault at location F_1 relay P_2 will trip to trigger the opening of its corresponding protection device, as evident in the fault studies earlier in the chapter, and consequently disconnect the ESS. In this particular scenario, it may be more desirable to continue having the ESS available to supply power to healthy sections of the network. This may be achieved by blocking the trip signal being sent to the ESS protection device and may be implemented as a function of P_2 fault current direction. Figure 5.12 illustrates the two different functions that this inter-trip can perform, depending on fault location. This inter-trip functionality will minimise the unnecessary discharge of stored energy into an F_2 fault, whilst blocking this inter-trip for an F_1 fault will improve its availability for post fault recovery.
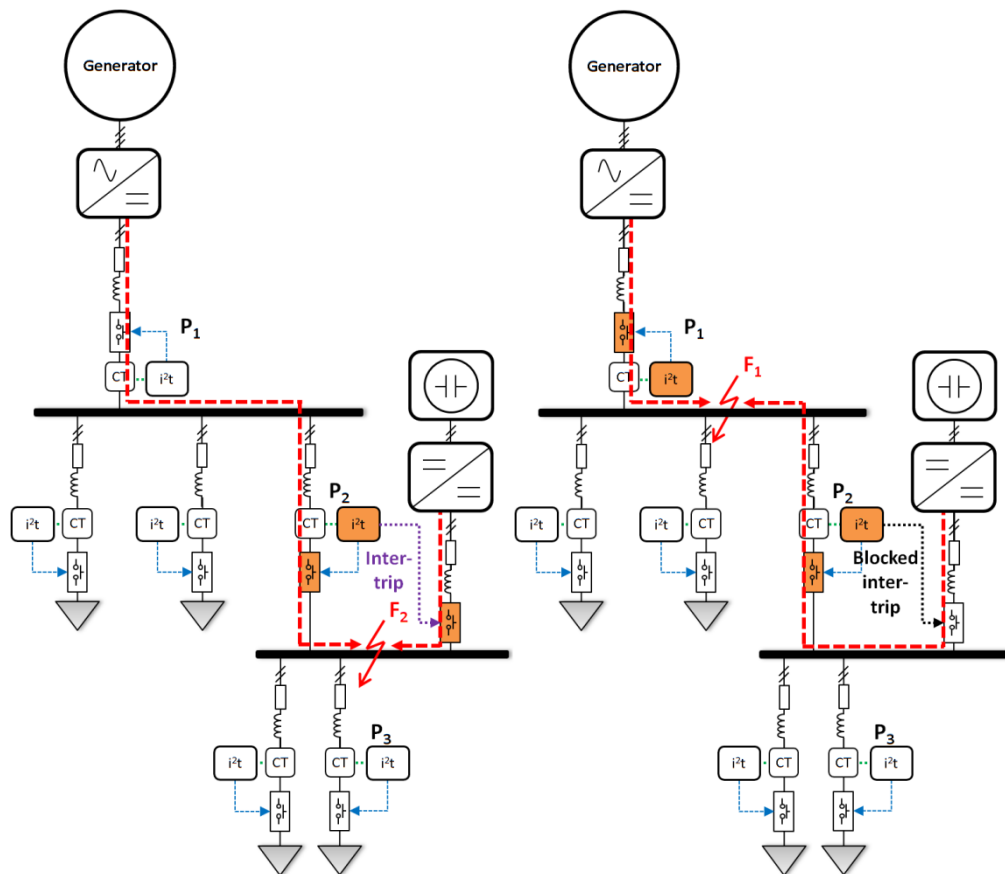
Figure 5.12: Inter-trip functionality of ESS protection

Accordingly, the performance of the baseline protection system will still be impaired for faults in the series path between the ESS and primary source in this case; however, the overall performance of the system is improved as the ESS will now be prohibited from unnecessarily dissipating stored energy. In addition, the ESS may still be used to continue supplying fault current to accelerate fault detection for downstream faults.

5.5.3 Adaptive protection settings

Adaptive protection schemes can enable the effective protection of power systems that are reconfigurable or change operating state [27]. Adaptive protection is a well-established method that has received considerable attention within academic literature and operates on the principle of utilizing distinct or variable protection settings that can be selected depending on predefined network states. Adaptive protection relays operate in a similar manner to conventional protection devices with the exception of an adaptive element that can change the operation of any of the three principle parts of the relay – the signal processing, fault detection algorithm/threshold setting, or the trip logic. A representative diagram of an adaptive protection relay is shown in Figure 5.13(a).
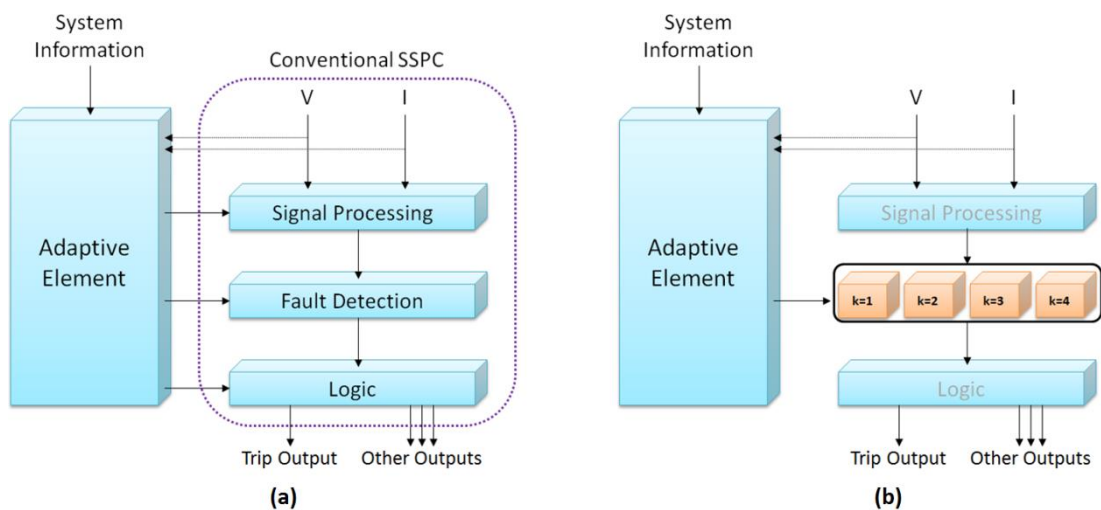
Figure 5.13: (a) Constituent components of an adaptive protection relay and (b) selectable predefined fault detection thresholds

Information associated with the power system such as the open/close status of certain contactors, or other power system configuration changes (such as the disconnection of an ESS) may be identified by a supervisory control and data acquisition system, or by other direct detection methods. This information is then

communicated to the adaptive element to implement the appropriate changes to its overall operation. For example, an adaptive relay may be configured to switch between distinct and predefined fault detection thresholds depending on collected information, as represented in Figure 5.13(b).

The distinct thresholds can be optimised to meet the requirements of the overall protection system performance for the predefined system states. In this manner, time graded co-ordination with downstream devices may be preserved for backup protection. Implementing adaptive protection in hardware would normally require relatively low cost, low bandwidth communications. In addition, existing relays that are compatible may be modified to accommodate an adaptive element with minimal additional weight and cost.

5.5.3.1 Modification of baseline protection system to incorporate adaptive settings

A modification to the baseline protection system is proposed that enables the trip threshold of each relay exposed to protection blinding to be automatically adjusted when the ESS is active to ensure similar overall protection system performance as the baseline system under the default network configuration. Figure 5.14 illustrates the relays that are modified to include this adaptive element on configuration 1 and 2 of the reference DC power system model. For network configuration 1, the i^2t trip threshold of device P_1 is adapted depending on the functional state of the ESS. For network configuration 2, both P_1 and P_2 thresholds are modified.

For simplicity, it is assumed that only two functional states of the ESS are determined by the adaptive element: ESS fully operational and ESS unavailable. In practice, there may be other functional states of the ESS that may impact the selection of protection settings, such as when the ESS is charging and when the ESS is operational but has depleted SOC. However, for the relevance to this case study, it is assumed that the ESS will be operating at full capacity. It is assumed that the adaptive element determines the availability of the ESS by acquiring knowledge of

the operating state of the ESS contactor (on/off) or converter interface (online/offline) and the SOC of the ESS. It is assumed that if the ESS SOC is depleted to a level that will render it incapable of impacting the fault response of the primary source, it can be regarded as unavailable.

Given that these system level functional states are Boolean in nature, it is assumed that a low bandwidth communications system is suitable to transmit system information to the adaptive elements incorporated within the protection devices. The identification of ESS availability may therefore be determined with the use of a simple AND gate logic function.

Accordingly, only two distinct protection settings for each upstream relay are proposed. When the ESS is determined to be fully operational, relay trip thresholds are decreased from default levels to ensure similar trip times. When the ESS is offline, the settings revert back to the default baseline settings. Table 5.5 shows the performance of the baseline protection system with fixed default settings ($300A^2s$, $200A^2s$ and $100A^2s$ for protection layers P_1, P_2 and P_3 respectively), whilst Table 5.6 shows the performance of the system with automatically reduced adaptive settings when the ESS is engaged. The adapted P_1 and P_2 settings have been reduced to $250A^2s$ and $150A^2s$ respectively.

Maloperation of the adaptive element may result in the wrong protection settings being applied for the wrong configuration of the network. For example, if the reduced settings were selected when the ESS is offline, protection coordination may be impaired. However, a failsafe mode may be incorporated into the system to ensure that the default settings are used in the event of an inoperative component, such as a failure to detect that the ESS is operational or a failure or that the SOC of the ESS is uncertain. The default settings in this is case are the original higher trip thresholds that will not accommodate for the protection blinding effects, but will at least provide protection, albeit with degraded performance. This will result in a similar protection system performance as the baseline when the ESS is engaged, and may prove to be easier to certify.
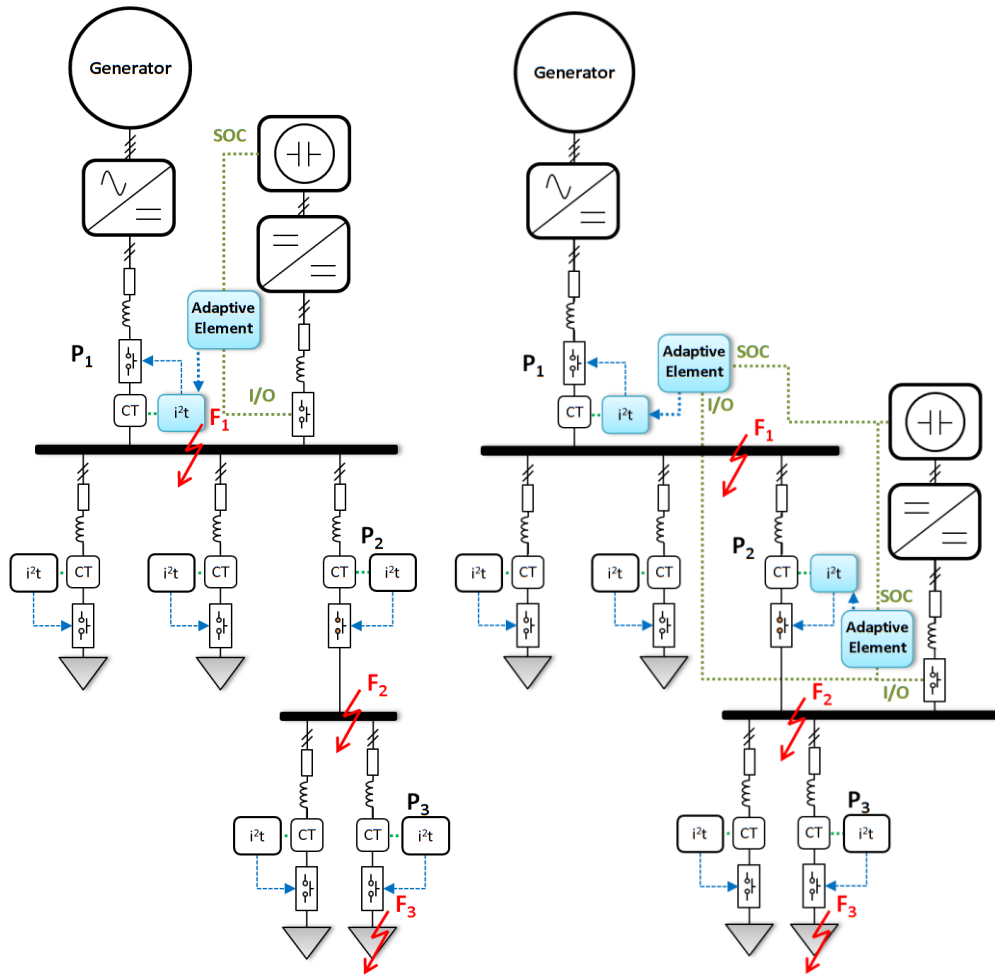
Figure 5.14: Adaptive element incorporated into modified baseline protection system for (a) network configuration 1 and (b) configuration 2

Table 5.5: Summary of baseline protection system performance

Fault location	Fault impedance (Ω)	Default configuration		Configuration 1		Configuration 2	
		tripped device	trip time (ms)	tripped device	trip time (ms)	tripped device	trip time (ms)
F1	0.5	P1 ($300A^2S$)	8	P1 ($300A^2S$)	8.7	P2 ($200A^2S$) then P1 ($300A^2S$)	8.3
	0.75	P1 ($300A^2S$)	8.2	P1 ($300A^2S$)	10	P2 ($200A^2S$) then P1 ($300A^2S$)	9.3
	1	P1 ($300A^2S$)	8.3	P1 ($300A^2S$)	20.1	P2 ($200A^2S$) then P1 ($300A^2S$)	13.2
F2	0.5	P2 ($200A^2S$)	6.1	P2 ($200A^2S$)	1.8	P2 ($200A^2S$)	7.5
	0.75	P2 ($200A^2S$)	6.6	P2 ($200A^2S$)	2.1	P2 ($200A^2S$)	9.7
	1	P2 ($200A^2S$)	7	P2 ($200A^2S$)	2.6	P2 ($200A^2S$)	25
F3	0.5	P3 ($100A^2S$)	3.5	P3 ($100A^2S$)	1	P3 ($100A^2S$)	1
	0.75	P3 ($100A^2S$)	3.9	P3 ($100A^2S$)	1.3	P3 ($100A^2S$)	1.2
	1	P3 ($100A^2S$)	4.3	P3 ($100A^2S$)	1.5	P3 ($100A^2S$)	1.5

Table 5.6: Summary of adaptive settings baseline protection system performance

Fault location	Fault impedance (Ω)	Default configuration		Configuration 1		Configuration 2	
		tripped device	trip time (ms)	tripped device	trip time (ms)	tripped device	trip time (ms)
F1	0.5	P1 ($300A^2S$)	8	P1 ($250A^2S$)	7.4	P2 ($150A^2S$) then P1 ($250A^2S$)	7.1
	0.75	P1 ($300A^2S$)	8.2	P1 ($250A^2S$)	8.5	P2 ($150A^2S$) then P1 ($250A^2S$)	7.8
	1	P1 ($300A^2S$)	8.3	P1 ($250A^2S$)	16.9	P2 ($150A^2S$) then P1 ($250A^2S$)	10.8
F2	0.5	P2 ($200A^2S$)	6.1	P2 ($200A^2S$)	1.8	P2 ($150A^2S$)	6
	0.75	P2 ($200A^2S$)	6.6	P2 ($200A^2S$)	2.1	P2 ($150A^2S$)	7.6
	1	P2 ($200A^2S$)	7	P2 ($200A^2S$)	2.6	P2 ($150A^2S$)	18.9
F3	0.5	P3 ($100A^2S$)	3.5	P3 ($100A^2S$)	1	P3 ($100A^2S$)	1
	0.75	P3 ($100A^2S$)	3.9	P3 ($100A^2S$)	1.3	P3 ($100A^2S$)	1.2
	1	P3 ($100A^2S$)	4.3	P3 ($100A^2S$)	1.5	P3 ($100A^2S$)	1.5

Comparing Table 5.5 and 5.6, it is evident that automatically reducing the thresholds of protection device P_1 for configuration and 1, and P_1 and P_2 for configuration 2 when the ESS is available delivers better overall protection system performance than the baseline. As anticipated however, it is difficult to exactly match the response times for both network configurations and all potential fault impedances. In particular, trip times with the reduced settings are still notably longer for 1Ω F_1 faults on configuration 1, and 1Ω F_2 faults on configuration 2 of the network. Accordingly, although the application of adaptive protection settings can improve the trip speeds of upstream protection devices for fault that are close to the critical impedance of the network, the improvement is marginal for faults significantly greater than the critical impedance. Therefore, it can be concluded that the incorporation of adaptive settings does not significantly improve the dependability of the protection system for all potential fault conditions. This is because the accommodation of protection blinding using adaptive protection settings does not eliminate the cause blinding itself, i.e. the fault response of the ESS still remains the same under these fault conditions. Accordingly, adaptive protection would not be a suitable primary protection solution and may be better suited as a secondary or tertiary backup protection system.

5.5.3.2 Experimental verification of adaptive protection using a commercial SSPC

In order to verify the performance improvements of an SSPC when an ESS is connected to a compact DC power system, the experimental procedure described in Chapter 4, section 4.4 was repeated with the protection setting of the SSPC adapted to incrementally decreasing thresholds. These new trip-times were then compared with the fixed 3A threshold results with the ESS disengaged in order to determine the optimum setting that delivers similar performance for each network configuration. Table 5.6 shows a summary of the trip-times using the adapted settings.

Table 5.7: Comparison of trip-times with adapted protection settings

Fault impedance (Ω)	Adapted generator system trip threshold (A)	Trip time with ESS (s)	Trip time without ESS (3A threshold) (s)
5	3	2.18	0.87
	2.9	1.77	
	2.8	1.53	
	2.7	1.33	
	2.6	1.07	
	2.5	0.79	

The results in Table 5.7 verify that adapting the settings to a reduced threshold for the SSPC when the ESS is operational, the trip-time of the protection device can be tuned to give similar performance when the ESS is disengaged. This is reflected in Figure 5.15. This was found to be between 2.6A and 2.5A. It was found that decreasing the trip thresholds further than this level would correspond to a faster trip time when the ESS is connected to the network. In practice, this may also disrupt protection coordination with downstream devices and reduce the security of the overall protection system. Given that the SSPC software only allowed the user to configure the current threshold for the device, it is difficult to optimise the performance of the SSPC for all possible fault scenarios.

Alternatively, an adaptive current and time setting associated with the SSPC may provide a more precise means of matching trip times for different network configurations, for example using an IDMT trip curve. A device with this flexibility may be a valuable component in the design of a more effective DC protection system for a number of applications. Expanding this concept further, an adaptive protection device operating at a higher voltage and power level may provide an unprecedented combination of power system flexibility and protection functionality.
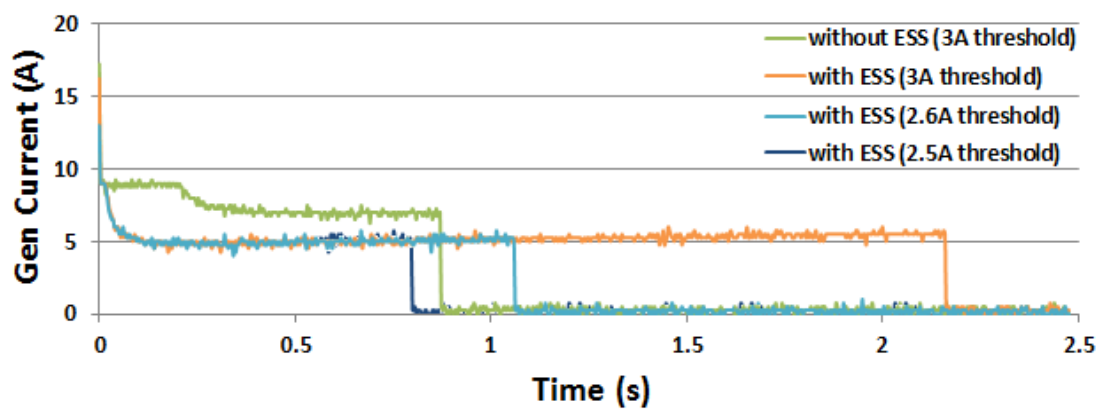
Figure 5.15: Trip-times with 3A and adapted 2.6A and 2.5A protection setting

5.5.4 Differential unit protection

Differential (or unit) protection [20] is a highly discriminative protection method that exploits the fundamental principal of conservation of electrical charge, based on the theory of Kirchhoff's Current Law. Differential protection requires appropriate current measurements (such as current transformers or Hall Effect transducers) to be located at each end of a feeder, bus bar or section of network that is being protected. These measurements of current are then communicated to a centralised differential protection relay that compares the current measurements and calculates the difference between the two (or more) measurement points. A fault that occurs within the protection zone is detected if the sum of these current measurements $\sum I_{bus} \neq 0$. The output from the fault detection algorithm can then be used to trigger the opening of any contactors or breakers on the faulted feeders.

Differential protection is inherently insensitive to fault impedance and can therefore enable the rapid detection, discrimination and isolation of a faulted section of a network. In contrast, the insensitivity of differential protection to faults out-with the protected zone makes it very suitable for protecting points of common coupling (e.g. for bus bar protection) where multiple sources of generation and loads may be interconnected.

In this manner, a differential protection scheme around the common bus bar to which the ESS is integrated may help to resolve some of the integration challenges associated with such sources. The network diagram illustrated in Figure 5.16 shows an example of how this differential protection scheme me be configured on network configuration 1 and 2. The performance of the differential unit protection is given in Table 5.8.
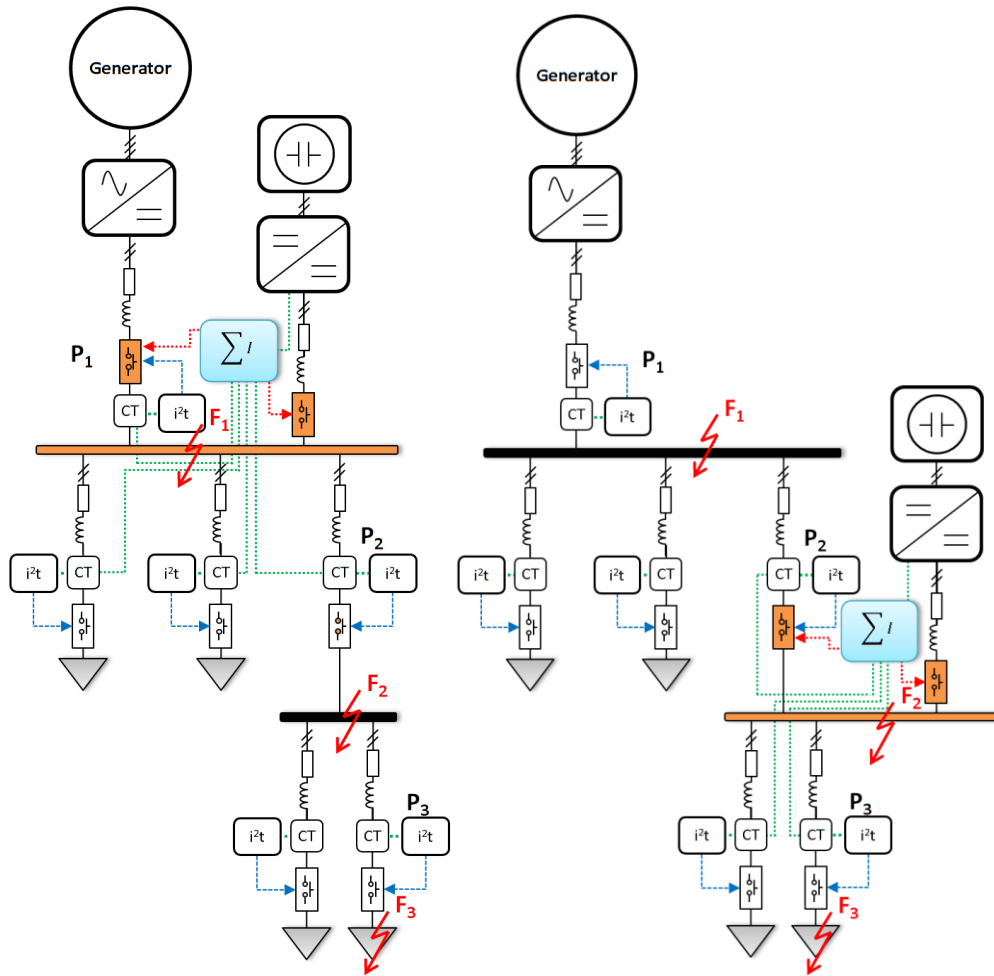
Figure 5.16: Differential unit protection around (a) bus B1 and (b) bus B2

Table 5.8: Summary of differential unit protection performance

Fault location	Fault impedance (Ω)	Configuration 1		Configuration 2	
		tripped device	trip time (ms)	tripped device	trip time (ms)
F1	0.5	P1 and ESS	0.1	P2 then P1	8.3
	0.75	P1 and ESS	0.1	P2 then P1	9.3
	1	P1 and ESS	0.1	P2 then P1	13.2
F2	0.5	P2	1.8	P2 and ESS	0.1
	0.75	P2	2.1	P2 and ESS	0.1
	1	P2	2.6	P2 and ESS	0.1
F3	0.5	P3	1	P3	1
	0.75	P3	1.3	P3	1.2
	1	P3	1.5	P3	1.5

As shown in Figure 5.16, this type of protection system can be practically implemented on the network by summing measurements of current from all source and load feeders connected to the common bus bar. A fault located within this zone (e.g. fault F_1 in configuration 1 and fault F_2 for configuration 2) will be detected and isolated by opening the appropriate switchgear to interrupt the fault current. Faults located within sections of the network further downstream, for example faults F_2 and F_3 in network configuration 1, will not be identified by the differential scheme, however may be detected and isolated using conventional overcurrent (i^2t) methods.

The principal advantage of implementing this differential protection scheme is that it enables the simultaneous isolation of multiple sources of fault current operating in parallel that may be feeding a fault. This alleviates the requirement for both the ESS and primary source to continue supplying fault current to actuate their corresponding protection devices and minimises the total fault energy dissipated into a fault located within this network section. The sensitivity of differential protection to faults of high impedance also makes it particularly advantageous in minimising the protection blinding effects of conventional protection devices associated with slower acting sources integrated within the network. Furthermore, the highly selective nature of differential protection enables the ESS to continue supplying fault current for faults further downstream to increase the speed of detection of conventional downstream protection, thus improving the overall performance of the wider protection system. Additionally, such a system will further enhance the effectiveness of integrating ESS onto a compact network as the highly selective principle of unit protection will enable the optimal response of the ESS for close up faults. This would prevent the ESS from unnecessarily adding to the energy delivered at the point of fault, thus preventing the dissipation of additional energy stored within the ESS, and increasing the ability of this system to support the post-fault recovery of the network and its loads.

The significant improvement in protection performance in comparison to the previous protection methods is evident in the results presented in Table 5.8. For configuration 1, F_1 faults are detected and isolated within 100μs irrespective of the fault impedance. This corresponds to an i^2t contribution of 4A^{2}s from the ESS into this fault, which is significantly lower than previous methods for the same fault condition. This system behaviour also eliminates any measurable impact of protection blinding. Furthermore, faults downstream of the bus B_1 (F_2 and F_3) are detected faster due to the additional contribution of fault current from the ESS. Similar performance improvement is achieved with configuration 2. However, in this case P_1 will still be subject to protection blinding for a F_1 fault as shown in the results. The performance of P_1 in this case is equivalent to the performance of the baseline. This may be alleviated by deploying an additional differential unit zone around this particular section of the network.

Accordingly, differential protection is an ideal primary protection mechanism. By being largely insensitive to fault current magnitude, a unit protection scheme offers similar advantages to adaptive protection for relatively low impedance faults over conventional protection methods (i.e. increased speed).The fast acting capabilities of differential unit protection have been experimentally demonstrated in [225] and support the ethos of enabling the ESS to be used for fast fault recovery.

The key drawback of differential protection however is the lack of provision of backup protection functionality. This would have to be provided through conventional overcurrent approaches (which may be enhanced by the adaptive protection philosophy described previously). Furthermore, this solution would be significantly more reliant on communications than adaptive protection with the need for incorporating high-bandwidth feedback systems for the current measurements. Similarly associated drawbacks include additional weight, complexity and cost of the overall network protection system. However, differential protection is an established method for protecting critical sections of aircraft electrical systems as described in Chapter 3. Accordingly, the certification of

differential protection for DC systems on future platforms may be more achievable than certifying adaptive settings.

5.4.6 Discussion on the novel application of existing protection strategies

The protection solutions applied to the DC power system with integrated high-power ESS proposed in this chapter were evaluated on their ability to meet the following two objectives:

1. To minimise the adverse impact of the ESS on the fault response of the network, and
2. To enable the ESS to be used more effectively under fault conditions where feasible.

Integrating the ESS with no change to the baseline solution enabled faster detection of F_2 and F_3 faults in configuration 1, and F_3 faults in configuration 2, meeting the second objective of the protection system design. However, the increased trip-times for F_1 faults in configuration 1 (worst case increase of 11.8ms for 1Ω) and F_2 faults in configuration 2 (worst case increase of 18ms for 1Ω) in comparison to the default configuration proves that the no change solution does not minimise the adverse effect of the ESS fault response on the overall protection system performance. However, this solution is still viable for a system application where sensitivity to only low-impedance faults is required.

Permanently reducing the settings of devices P_1 and P_2 did reduce the trip-times when the ESS was engaged. Compared to the default configuration, a smaller worst case increase of 8.6ms was observed for 1Ω F_1 faults in configuration 1, and an increase of 11.9ms for 1Ω F_2 faults in configuration 2. However, there are two main limitations or drawbacks associated with permanently reducing the trip thresholds of the respective protection devices that are exposed to protection blinding as a result of ESS fault current contribution to network faults.

The first drawback is that a reduction in trip-threshold settings of the corresponding protection devices does not prevent protection blinding from occurring. Although reducing the settings may improve the trip-times of the protection devices, the improvements are only modest when considering relatively high-impedance faults. This is because the ESS response to faults greater than the critical impedance of the network still causes a reduction in the rate of change of fault energy delivered by the primary source. Hence, a reduction in protection trip thresholds will not change the fault response of interconnected sources. Therefore, network protection systems consisting of individually operating protection devices that employ i^2t based fault detection algorithms, that may be configured to deliver optimal performance for a particular network configuration, will never perform consistently for all possible network configurations, fault locations and fault impedances.

Secondly, given that relay settings are fixed for all configurations of the network, ensuring accurate time-graded coordination using reduced trip thresholds may be challenging as the system reverts back to its default configuration and the ESS is offline. For instance, an over-reduction in the trip thresholds of upstream protection devices may increase the probability of unintentional trips when the sole contribution of fault current is supplied by the primary source. This behaviour may reduce the security of the protection system.

Furthermore, the level to which the protection trip thresholds may be reduced may be significantly constrained. For instance, the assumption that there is sufficient headroom for reducing upstream relay trip thresholds for the case study presented in this chapter may not be applicable in certain applications as the trip thresholds of the coordinating layers were arbitrarily set. However, in a practical system there may be a minimum delay requirement between coordinating protection layers that is application specific. Under these conditions, it can be assumed that the individual trip thresholds of the coordinating devices would already be set to the lowest possible setting to comply with the time-grading requirements. It can also be assumed that these settings will be optimised for the default configuration of the

network. Therefore, the option to reduce the protection settings of upstream devices to a level lower than the optimised settings for the default configuration of the network may not be feasible for all scenarios.

However, similar benefits of permanently decreasing the i^2t trip-thresholds of the baseline system to reduce the trip-times of the system when the ESS is operational can be achieved with the employment of automatically adapting to lower settings when the ESS is online. This protection approach eliminates the drawbacks associated with increased risk of nuisance tripping and coordination issues when the network reverts to the default configuration. Again, a worst case trip-time increase of 8.6ms was observed in configuration 1 for a 1Ω F_1 fault, and an increase of 11.9ms in configuration 2 for a 1Ω F_2 fault. However, the adverse protection blinding effects caused by the ESS fault response are not eliminated using this protection approach.

The protection approach of rapidly disconnecting the ESS from the network for all fault conditions guarantees the optimal operation of the baseline protection solution (with a minimal delay associated with the time taken to disconnect the ESS). This behaviour meets the first objective of the protection system design as protection blinding is effectively eliminated. However, this approach also leads to a suboptimal use of the ESS under fault conditions. This is because it prevents the ESS from being used for fault ride through or post-fault recovery and prevents the ESS from being used to accelerate the performance of downstream relays where the additional fault current being supplied by the ESS will enable the downstream protection devices to trip faster.

Incorporating inter-tripping to enable the ESS to disconnect from the network alongside the breaking of fault current from the primary source improves the overall performance of the system as the ESS is prohibited from unnecessarily dissipating stored energy into the fault post-clearance. However, this additional functionality does not improve the trip-time performance of the baseline protection system. Indeed, the performance is the same as the 'no change' approach as the

system is still impaired for faults in the series path between the ESS and primary source. However, the ESS may still be used to continue supplying fault current to accelerate fault detection for downstream faults.

The most effective protection method applied to the DC system eliminating protection blinding caused by the ESS and enabling the ESS to accelerate downstream protection performance is differential unit protection. This protection method enables all F_1 faults in configuration 1 and all F_2 faults in configuration 2 to be detected within 100µs. This corresponds to a decrease in trip-time of 8.2ms and 6.9ms for configuration 1 and 2 respectively in comparison to the baseline system performance operating in the default configuration.

A chart of the respective worst case trip-time performances for 1Ω F_1 faults for configuration 1 and 1Ω F_2 faults for configuration 2 for all evaluated protection approaches are shown in Figure 5.17.
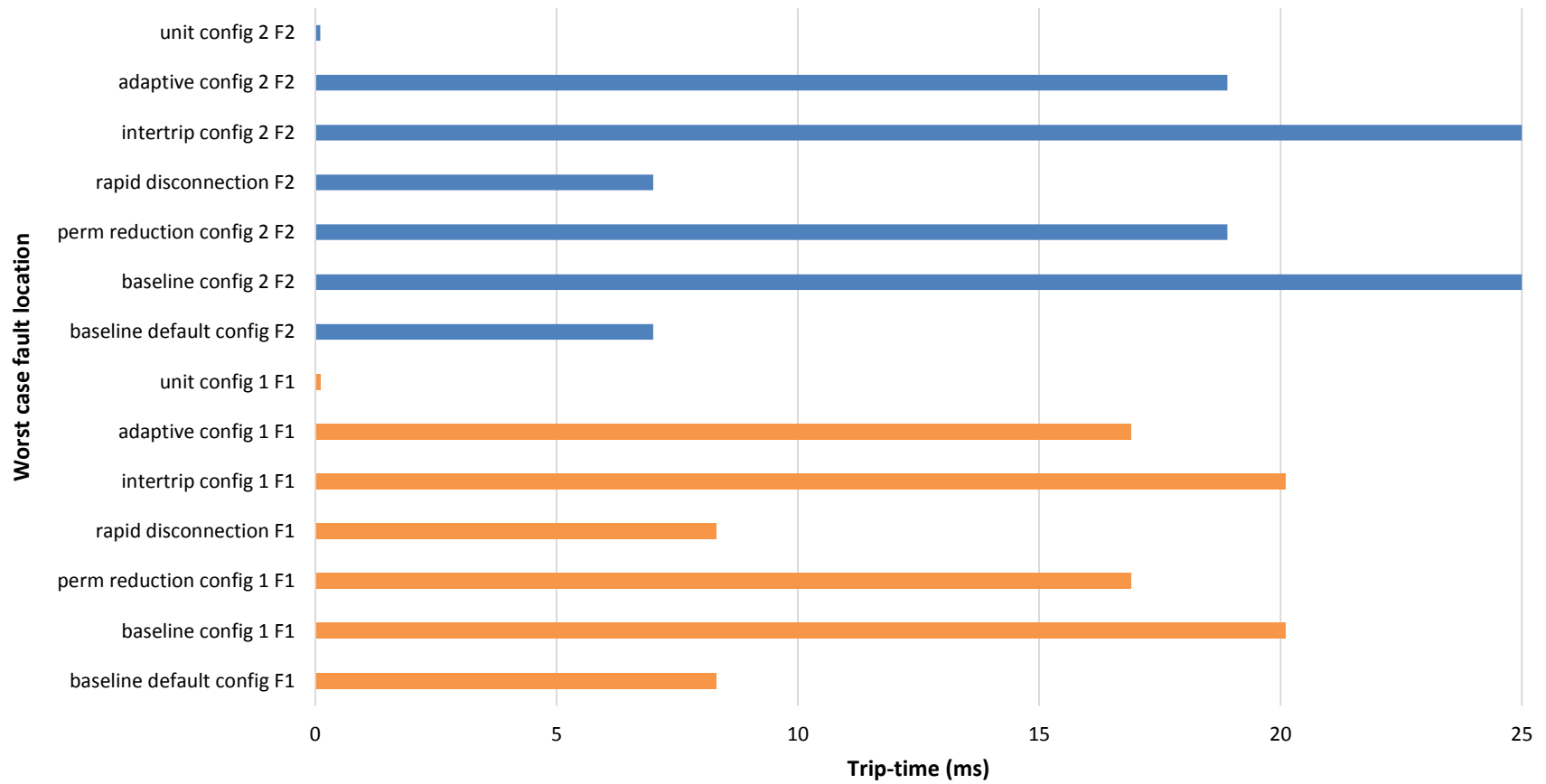
Figure 5.17: Respective worst case trip-time performances for 1Ω F₁ faults for configuration 1 and 1Ω F₂ faults for configuration 2 for all protection approaches

5.6 Conclusion

Through extensive simulations of a number of protection techniques applied to the DC power system model with integrated high-power ESS to evaluate their performance under fault conditions, it is evident that differential unit protection enables the most effective use of the ESS under fault conditions. Within the context of an aircraft power system, this type of protection method will be ideal for primary protection of exposed sections of the DC distribution system to prevent protection blinding, allowing for the safer integration of a high-power ESS with substantially less fault current contribution to faults within protected zones. Due to the maturity of using differential unit protection for critical sections of an aircraft electrical network, certification of such a system for DC systems on future aircraft is plausible.

Adaptive trip settings for i^2t based time-graded protection systems together with inter-tripping functionality is a viable backup protection method that will secure better overall protection system performance than utilising the baseline approach with no change.

Chapter 6

ESS fault mode control

6.1 Introduction

The application of a novel ESS fault mode control (FMC) is proposed and evaluated in this chapter. ESS FMC is a protection function and supplementary mode of operation of the ESS converter controller that overrides its normal operational modes. FMC adapts the response of the ESS to a network fault as a function of its location and also offers inherent backup protection functionality. The tailored ESS fault behaviour enables both protection system design objectives defined in chapter 5 to be met and surpasses the performance of the evaluated existing protection approaches.

ESS FMC is shown to enable better utilisation of available energy under fault conditions to accelerate fault detection of downstream faults, whilst minimising protection blinding of upstream devices by rapidly interrupting ESS fault current for close-up faults. The inherent backup functionality offered by the ESS FMC in the event of a network protection device trip-failure is also demonstrated.

6.2 Principle of operation of ESS FMC

The FMC commands the ESS to perform one of the two following functions:

1. To shut down or disconnect the ESS immediately in the event that a 'close-up' fault is detected (as defined below).
2. To allow the ESS to continue supplying maximum fault current for a fixed period of time for faults that are identified as being 'downstream' with respect to the ESS point of integration. If the fault is not cleared within this timescale, then the ESS will be commanded to shut down.

143

Close-up faults are those that occur at a network location where there is no network protection device in series with the ESS fault path to interrupt its fault current contribution. For example, a fault that develops across the terminals of the ESS or on the bus bar to which it is integrated is considered to be a close-up fault. Downstream faults are those that occur at a location where there is a network protection device available within the fault path of the ESS to sectionalise the network.

Function 1 mitigates protection blinding of upstream protection devices and minimises unnecessary discharge of stored energy, whist function 2 improves the performance of downstream network protection devices. Figure 6.1 provides an illustration of the ESS fault response for these two functions.

Upon fault inception, the ESS converter filter capacitor will discharge into the fault. The ESS FMC protection algorithm must then determine if there is a fault on the network, and then decide what FMC function must be triggered in response to the fault. Accordingly, the FMC must have a mechanism to detect and then discriminate between 'close-up' and 'downstream' faults. The following sections describe how this may be implemented.
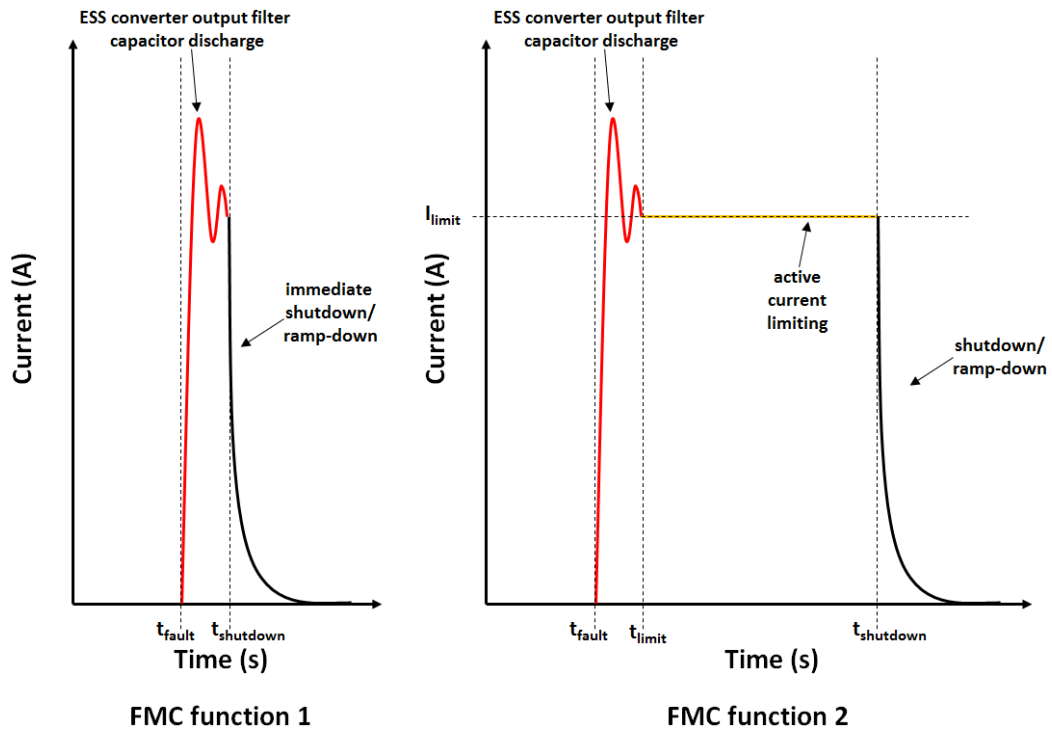
Figure 6.1: Representation of the ESS fault response for FMC functions 1 and 2

6.2.1 Categorisation of faults

F_1, F_2 and F_3 faults on configuration 1 and 2 of the reference DC power system model can be categorised as either close-up or downstream faults with respect to the ESS, as illustrated in Figure 6.2.

For configuration 1, fault F_1 is considered to be a close-up fault, whilst F_2 and F_3 are considered to be downstream faults due to the availability of protection devices P_2 and P_3 to interrupt the fault path. Accordingly, P_2 and P_3 would benefit from an additional supply of fault current from the ESS to increase fault detection speed, thereby improving the overall performance of the baseline protection system. Conversely, for a F_1 fault, an immediate shutdown of the ESS would eliminate P_1 protection blinding, enabling its performance to match that of the baseline system when operating under the default configuration of the network. The use of inter-tripping between the ESS and P_1 protection devices will enable the protection

performance of the baseline to be surpassed, whereby the detection and discrimination of a close-up fault by the ESS is the trigger to trip the network device.

Categorisation of F_1, F_2 and F_3 faults for configuration 2 is more challenging. Given that the ESS is integrated to bus B_2, fault F_2 is considered to be a close-up fault as the immediate disconnection of the ESS in this scenario would mitigate blinding of protection devices P_2 and P_1. F_3 is clearly a downstream fault with respect to the ESS as the additional fault current contribution from the ESS would improve the fault detection speed of P_3.

For fault F_1, the immediate shutdown of the ESS will prevent blinding of protection device P_1, enabling the equivalent performance to the baseline when the network is configured in default arrangement. However, this ESS behaviour will prevent protection device P_2 from tripping, leaving F_1 exposed to healthy sections of the network and preventing the ESS to be used for post fault recovery.

To enable P_2 to open as fast as possible for this fault event, the FMC should command the ESS to continue supplying fault current even though this additional fault current contribution will lead to a slower P_1 performance in comparison to the baseline in the default network configuration. Accordingly, fault F_1 should be categorised as a downstream fault with respect to the ESS connected to bus B_2. Although this will result in a prolonged exposure of F_1 to any B_1 connected loads, this will not impair their ability to be resupplied post clearance, as the primary source will always require to be disconnected under this fault condition. This ESS fault behaviour and protection system response will, however, improve ESS availability for loads connected to bus B_2 post fault clearance, leading to a better overall protection system performance.
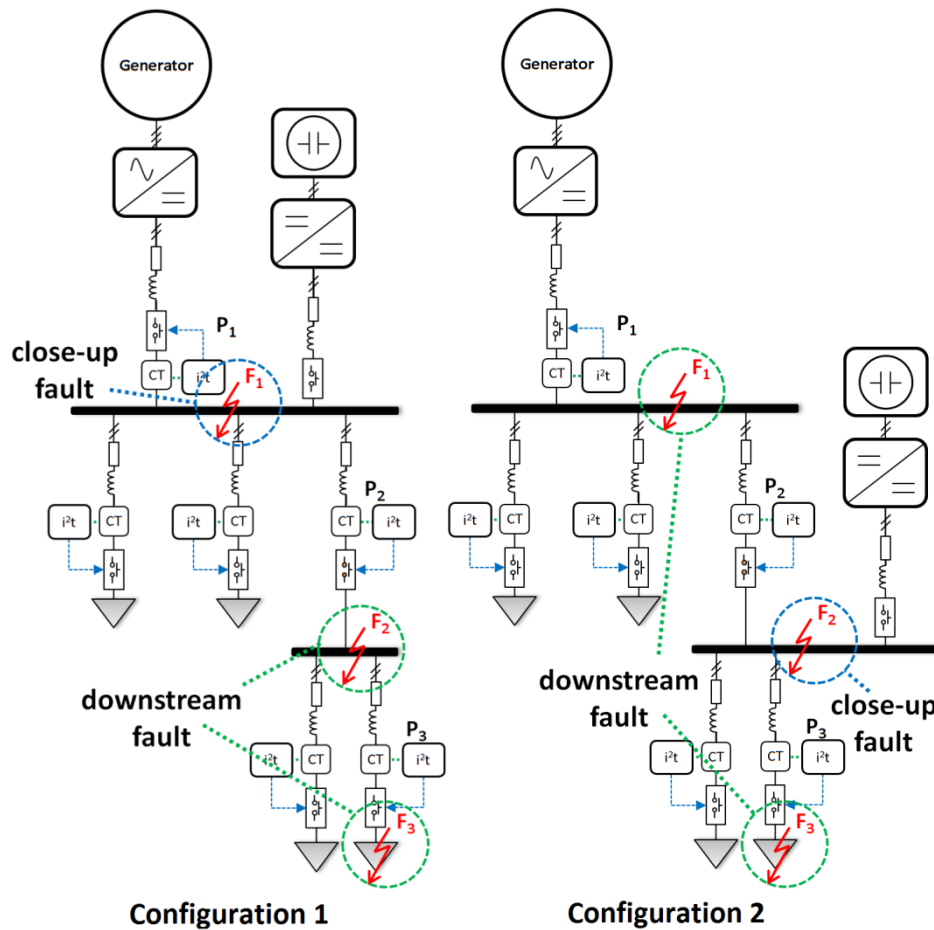
Figure 6.2: Categorisation of close-up and downstream faults with respect to the ESS for configuration 1 and 2

6.3 Methods for enabling rapid fault detection and discrimination

Two methods to enable rapid fault detection and discrimination for the purpose of initiating ESS FMC are proposed. These are:

1. The differential measurement of current of all nodes feeding the bus bar to which the ESS is connected, exploiting Kirchhoff's current law, and

2. The utilisation of a highly novel fast fault detection technique [226] to measure the initial rate-of-change of current at the terminals of the ESS filter capacitor at the time of fault

6.3.1 Current differential method

The first proposed method to enable rapid fault detection and discrimination for triggering ESS FMC exploits Kirchhoff's current law in a similar manner demonstrated in Chapter 5 for differential current protection. Figure 6.3 provides an illustration of the additional communications infrastructure required on network configuration 1 and configuration 2 to implement this system. A fault within the differential zone will result in a non-zero sum of currents enabling rapid fault detection and discrimination of close-up faults, irrespective of fault impedance. A fault outwith the current differetial zone, characterised as a downstream fault, will not impact the sum of currents, meaning $\sum I_{bus} = 0$. This can be observed in the results presented in Figure 6.4 that shows $\sum I_{B1}$ for 0.01Ω, 0.5Ω, 0.75Ω and 1Ω faults at locations F_1, F_2 and F_3 on network configuration 1, and similarly, $\sum I_{B2}$ for configuration 2 on Figure 6.5.

Accordingly, this technique may be used to instigate the activation of function 1 (rapid shut down) of the proposed ESS FMC if the fault is found to be within the differential zone.

However, faults out with this zone will not be picked up by this discrimination method. Therefore, a secondary means of discriminating 'downstream' faults is required to instigate function 2 of the ESS FMC. One such method that may be relatively simple to implement is the use of a time-based overcurrent algorithm, whereby function 2 of the ESS FMC is triggered if the ESS output is equal to its maximum current-limited magnitude for greater than a predefined period. Alternatively, the $\delta i / \delta t$ fault detection approach described in the following section may be used in conjunction with this method to initially detect a fault.
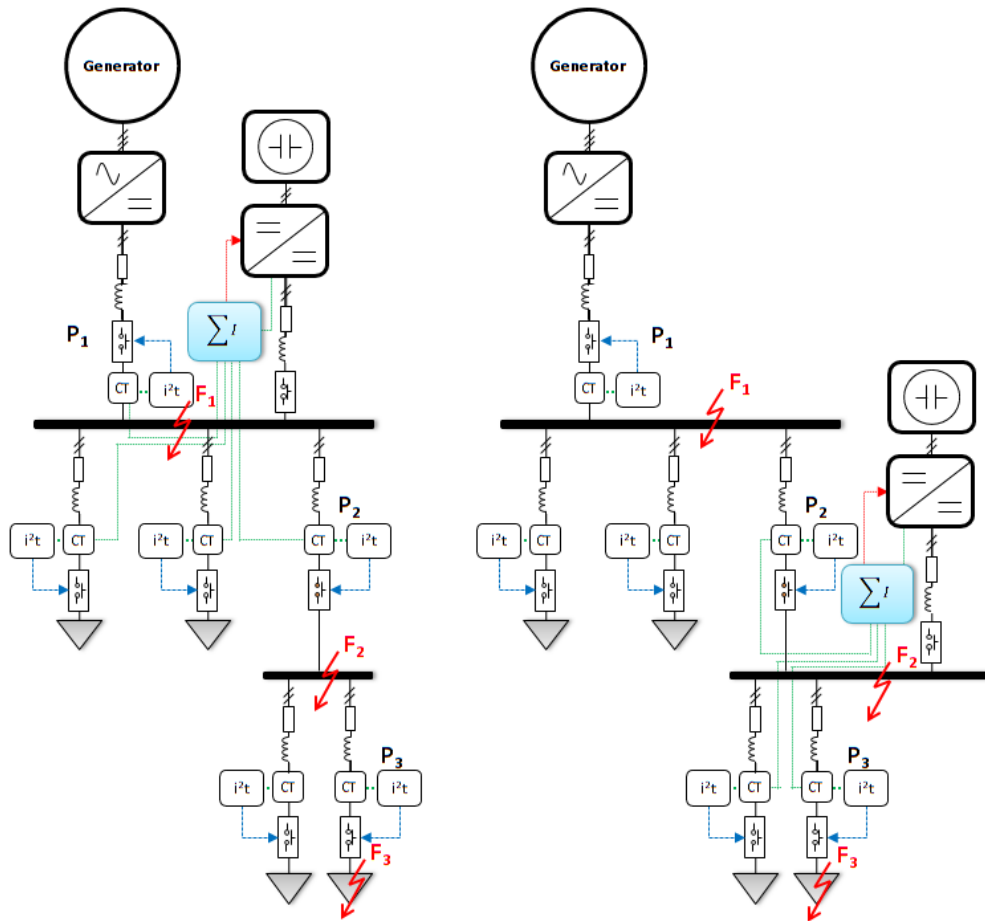
Figure 6.3: Additional communications infrastructure required to enable current differential fault discrimination method
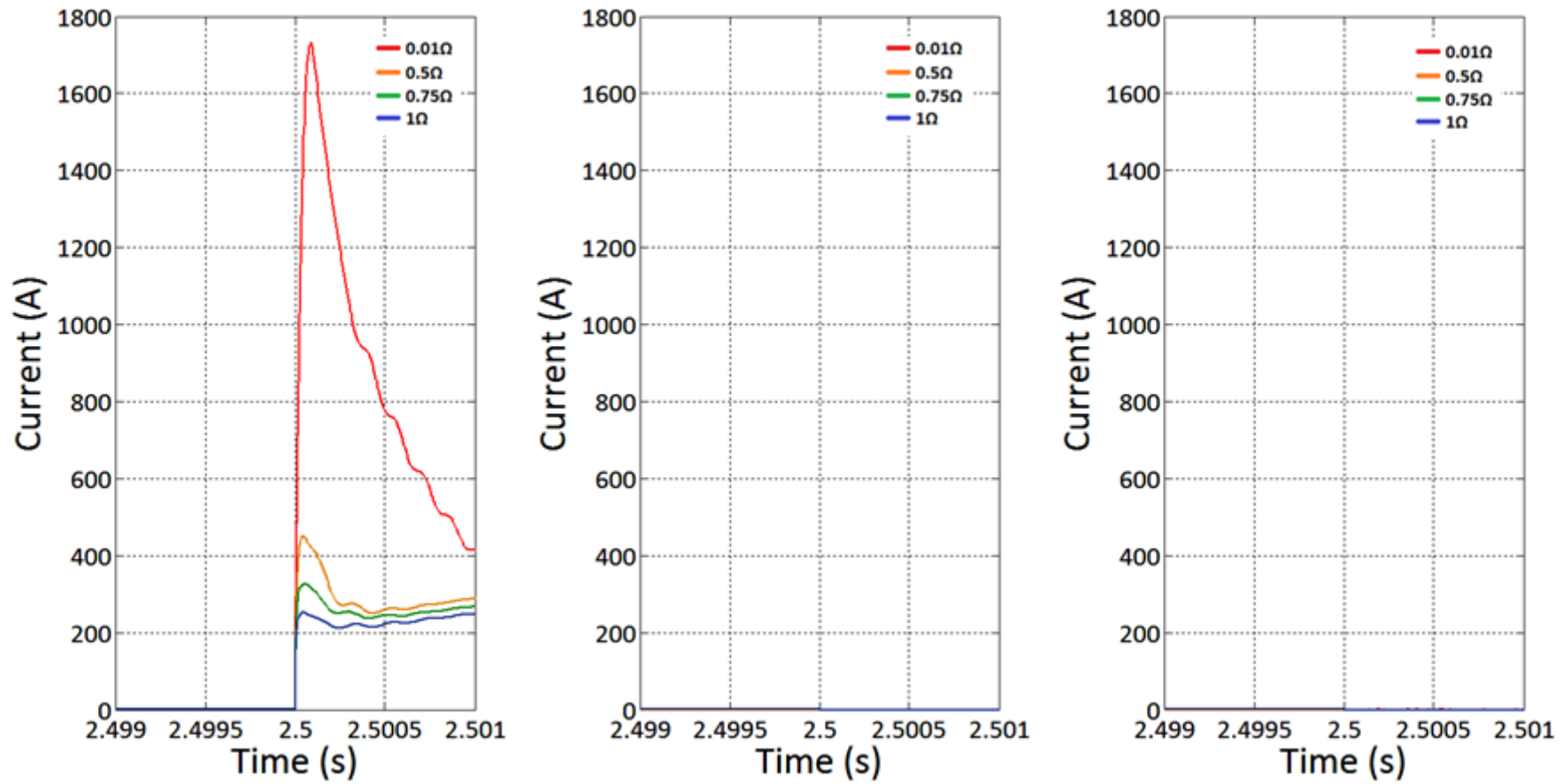
Figure 6.4: Differential current around Bus 1 for 0.01Ω, 0.5Ω, 0.75Ω and 1Ω faults at locations F1, F2 and F3 on network configuration 1
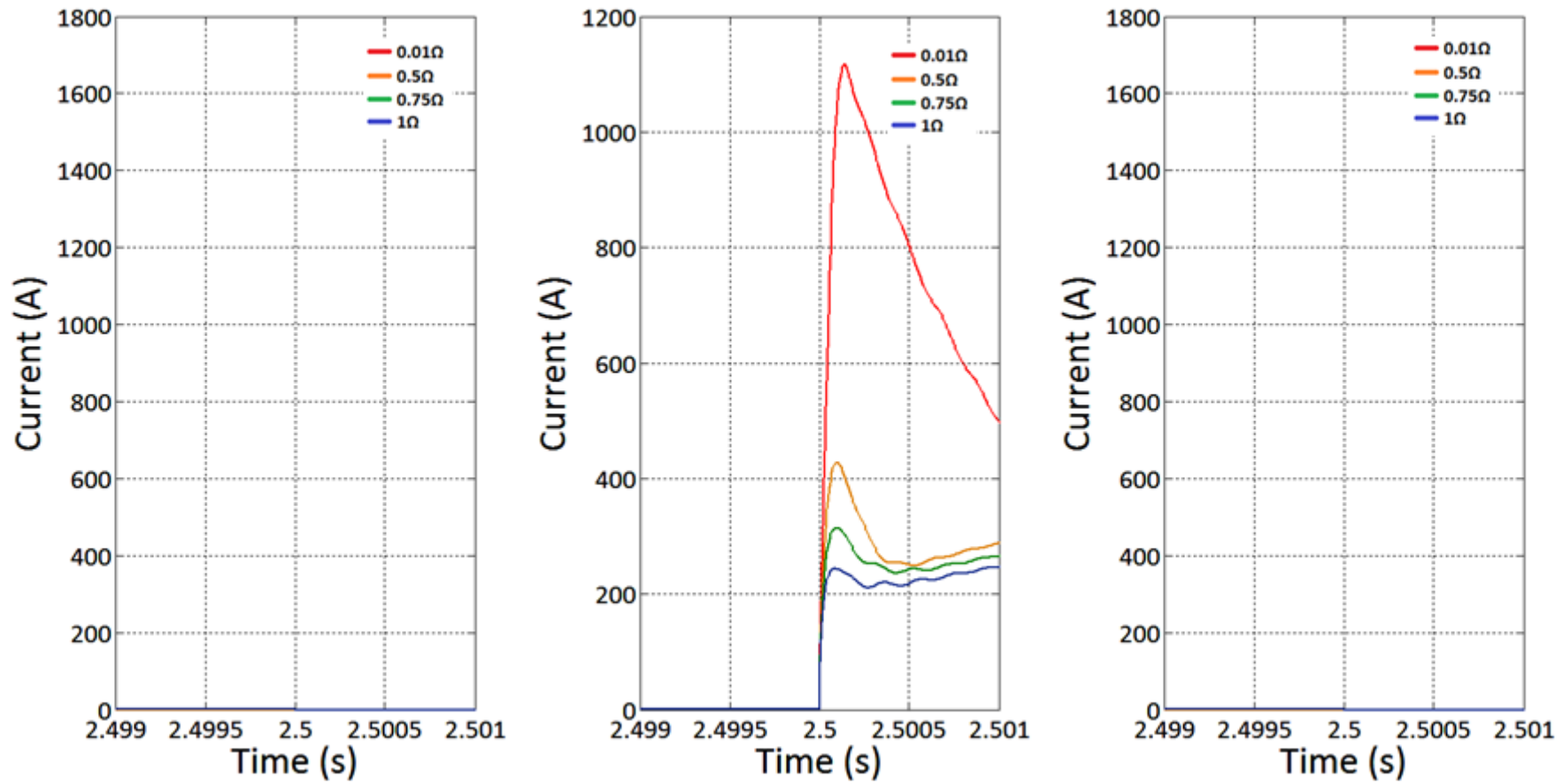
Figure 6.5: Differential current around Bus 2 for 0.01Ω, 0.5Ω, 0.75Ω and 1Ω faults at locations F1, F2 and F3 on network configuration 2

6.3.1 Initial rate-of-change of current

The second method for rapid fault detection and discrimination exploits the proportional relationship between the voltage across a capacitor, the initial rate-of-change of current as it discharges into a fault, and the line inductance, L. Consider the representative RLC circuit diagram shown in Figure 6.6.
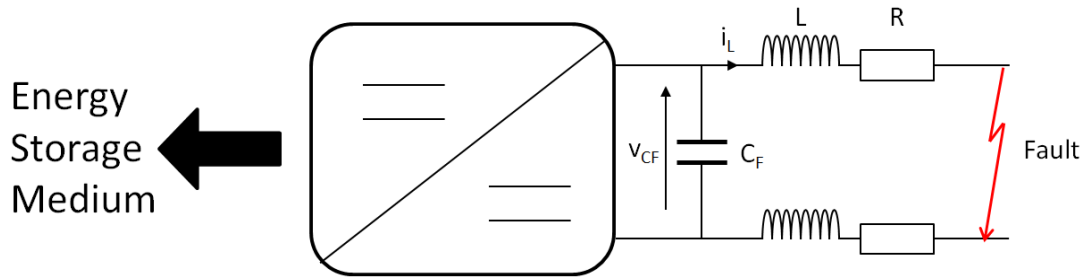
Figure 6.6: Representative RLC circuit of a faulted circuit with respect to the ESS converter interface

In the event of a fault, the voltage at the point of fault will decrease rapidly creating a potential difference between the capacitor voltage v_{CF} and the voltage across the fault. To balance these voltages, the capacitor will discharge current. Assuming that the fault occurs at $t = 0$, line inductance, L_{meas}, can be approximated by the equation [24]

$$L_{meas} = \frac{v_{CF}(0) - i_L(0)(R + R_F)}{\frac{di_L(t \to 0)}{dt}}, \tag{6.1}$$

where $v_{CF}(0)$ is the voltage across the discharging capacitor at the time of fault, R is the line resistance and R_F is the fault resistance. Assuming inductance per meter of the power system cables is known (in H/m), and assuming that the cable

resistance R is negligible (due to the relatively low line resistance of a physically compact power system), as $R_F \rightarrow 0$, the measurement of the initial $\frac{di_L(t \rightarrow 0)}{dt}$ will enable the distance to the fault from the point of current measurement to be approximated [24]. The sensitivity and impact of high-impedance faults on this detection method is addressed later in this section. The capacitor voltage, $v_{CF}(0)$, at the time of fault can be assumed to be the nominal voltage of the system when performing this calculation. Computation of the rate-of-change of current can be made over a discrete sampling time period, δt, where

$$\frac{\delta i}{\delta t} = \frac{i(t + \delta t) - i(t)}{\delta t}.$$

(6.2)

Due to the very rapid rise time of the current in the event of a fault, accurately measuring the initial rate-of-change of current requires a relatively small sampling time in the order of micro-seconds. Use of a sampling time that is greater than the rise time of the discharging capacitor will result in an inaccurate $\delta i/\delta t$ measurement, where the rising edge of the current profile may not be captured. In addition to the high frequency analogue-to-digital conversion of current samples, the extensive computational overhead associated with processing these samples to accurately compute $\delta i/\delta t$ is substantially greater than conventional current measurement techniques.

This method of measuring $\delta i/\delta t$ is applied to the filter capacitor of the ESS converter integrated within the reference DC power system model, using a δt sampling time of 10µs. Figures 6.7 and 6.8 show the computed profiles of $\delta i/\delta t$ for 0.01Ω, 0.5Ω, 0.75Ω and 1Ω faults at locations F_1, F_2 and F_3 for configuration 1 and 2 respectively. The magnitudes of the initial $\delta i/\delta t$ measurements at $t = 0$ are also presented in Table 6.1.

Table 6.1: Initial $\delta i/\delta t$ measurements for F1, F2 and F3 faults at $t = 0$

Fault location	Fault impedance (Ω)	Configuration 1 initial $\delta i/\delta t$ (A/s)	Configuration 2 initial $\delta i/\delta t$ (A/s)
F1	0.01	21,000,000	9,600,000
	0.5	13,000,000	6,800,000
	0.75	11,000,000	6,000,000
	1	9,000,000	5,200,000
F2	0.01	6,700,000	21,000,000
	0.5	5,500,000	15,000,000
	0.75	5,000,000	14,000,000
	1	4,600,000	12,500,000
F3	0.01	5,800,000	11,400,000
	0.5	4,100,000	9,200,000
	0.75	3,800,000	8,400,000
	1	3,500,000	7,800,000

Note that the magnitudes of the initial $\delta i/\delta t$ measurements for each fault location decrease as a function of increasing fault impedance. This is due to a non-negligible voltage developing across the fault resistance, R_F. However, for the fault resistances simulated at each fault location, the range of $\delta i/\delta t$ magnitudes measured, although wide, are still relatively distinctive.

For example, from Figure 6.7 it is clear that the magnitude of the initial $\delta i/\delta t$ for all evaluated F_1 faults is greater than that of F_2 and F_3 faults, when the ESS is integrated to bus B_1. An initial $\delta i/\delta t$ measurement of 9,000,000 − 21,000,000A/s is obtained for F_1 faults between 1Ω − 0.01Ω in comparison to 4,600,000 − 6,700,000A/s and 3,500,000 − 5,800,000A/s for F_2 and F_3 faults respectively. Therefore, if a $\delta i/\delta t$ greater than 3x10^{6} A/s is measured, corresponding to a threshold marginally lower than the $\delta i/\delta t$ measurement for a 1Ω fault at F_3, it can be assumed that a fault is detected on the network. Furthermore, discrimination of the fault location may be achieved if the $\delta i/\delta t$ measurement is compared to a second threshold of 8,000,000A/s. Note that the initial $\delta i/\delta t$ measured for 0.01Ω short-circuit faults at F_2 and F_3 do not exceed this upper threshold. If this upper threshold is exceeded, the fault can be safely assumed to be a close-up fault (i.e. F_1). Otherwise, the fault is

considered to be located downstream with respect to the ESS. These minimum thresholds are depicted in Figure 6.7.

Similarly, when the ESS is on bus B_2, the initial $\delta i/\delta t$ measurements for all F_2 faults are greater than all F_1 and F_3 faults, as shown in Figure 6.8. 1Ω - 0.01Ω faults at location F2 result in a $\delta i/\delta t$ of 12,500,000 – 21,000,000A/s, whereas F_1 and F_3 faults produce a $\delta i/\delta t$ of 5,200,000 – 9,600,000A/s and 7,800,000 – 11,400,000A/s respectively. To determine if there is a fault on the network, a $\delta i/\delta t$ measurement greater than minimum threshold of 4,000,000A/s can be applied, whilst exceeding a second threshold of 12,000,000A/s can discriminate the location of the fault as being at F_2 (i.e. close-up) in this network configuration.

This method of calculating $\delta i/\delta t$ also removes the intrinsic drawback associated with derivative measurements, i.e. sensitivity to noise. Assuming the presence of significant harmonics on the system which may propagate throughout the network due to the likely integration of switching converters and harmonic loads, this method will be immune to such interference due to the relatively small numerator term in the equation under non transient conditions. In the event of more significant transients of greater magnitude, such as a fault on the network, the numerator term of equation 6.2, $i(t + \delta t) - i(t)$ will be intrinsically greater (by an order of 1,000,000). Similarly, measurement noise may prove to be a potential hindrance to accurately measuring the initial $\delta i/\delta t$. Any electromagnetic interference (EMI) impacting the measurement sensor and its corresponding means of feedback to the computation device may significantly impact the measurement of $\delta i/\delta t$. This may produce false trip/threshold conditions. A possible solution to this would be to use reliable and EMI resistant instrumentation and communications infrastructure such as optical based SCADA systems.

Another potential drawback associated with using this method (not necessarily for ESS control, but for other applications such as fast acting protection/fault detection) is the potential sensitivity to load transients. If the activation or switch on of a load, regardless of its impedance, were to occur in the same manner as a fault condition

(i.e. passive turn on of a load with no control over inrush) then a false alarm (or notification) signal of there being a fault on the network may occur. However, modern SSPC technology can accommodate for potential false trip conditions by controlling inrush by means of applying a ramped voltage output from the device gate driver [141], significantly increasing the response time of the respective load transient.
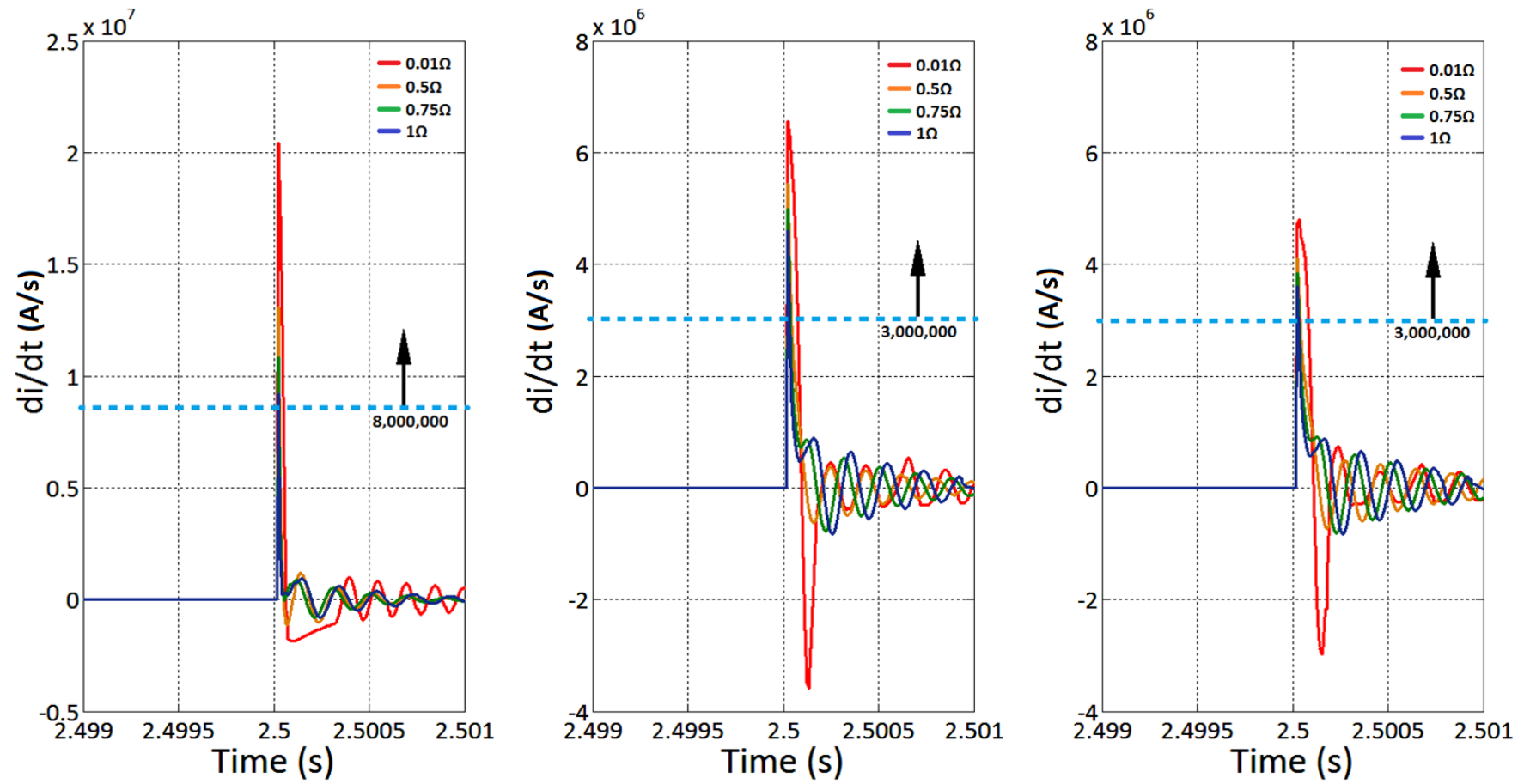
Figure 6.7: di/dt measurements for F1, F2 and F3 faults for configuration 1
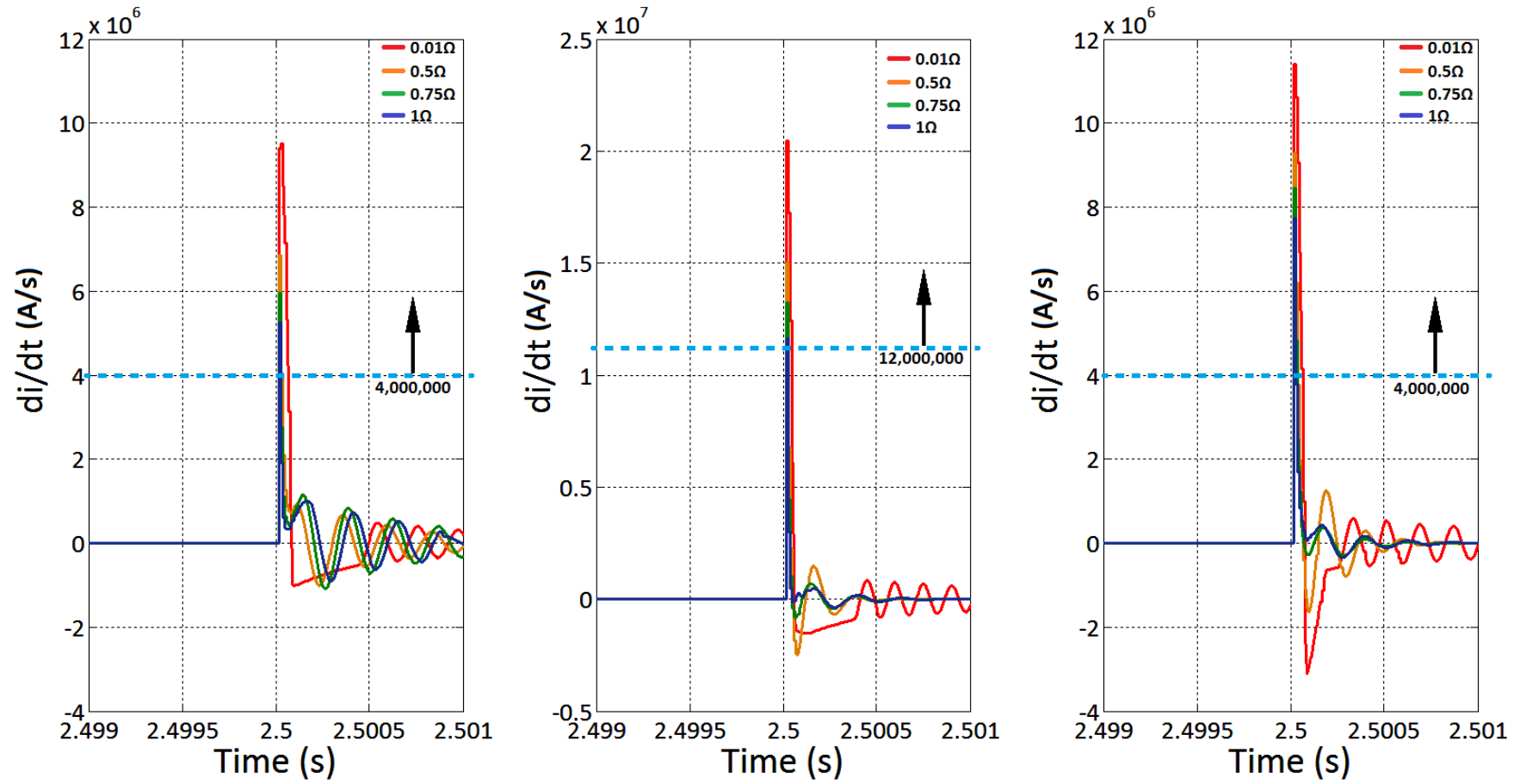
Figure 6.8: di/dt measurements for F1, F2 and F3 faults for configuration 2

6.4 Implementation and evaluation of ESS FMC

This section first describes the implementation of ESS FMC, specifcally using the initial $\delta i/\delta t$ discrimination method. The operation of the inherent backup protection functionality offered by ESS FMC is also demonstrated. Second, the performance of the protection system is evaluated using this method and is compared to the baseline and alternative protection systems proposed in Chapter 5.

6.4.1 FMC algorithm

The FMC algorithm continuously measures $\delta i/\delta t$ using equation 6.2. This measurement is then compared to two distinct and predetermined thresholds that are specific to the configuration of the network. A flow diagram describing the implementation of ESS FMC algorithm is illustrated in Figure 6.9.

If the $\delta i/\delta t$ measurement is greater than the lower and upper thresholds, then the ESS is commanded to initiate function 1 and immediately rampdown the ESS current output. For example, an F_1 fault in configuration 1 up to an impedance of 1Ω will result in an initial $\delta i/\delta t$ measurement greater than the lower threshold of 3,000,000A/s and greater than the upper threshold of 8,000,000A/s as indicated in Figure 6.7. This condition is indicative of a close-up fault condition. Similarly, a close-up F_2 fault in configuration 2 up to 1Ω will result in a $\delta i/\delta t$ measurement greater than the lower threshold of 4,000,000A/s and upper threshold of 12,000,000A/s.

If the lower $\delta i/\delta t$ threshold is breached but upper threshold is not, then the ESS is commanded to initiate function 2 of the ESS FMC. This condition is indicative of a downstream fault condition. F_2 and F_3 fault in network configuration 1 and F_1 and F_3 faults in network configuration 2, up to 1Ω, will trigger this function. This function commands the ESS to continue suppling maximum fault current for a

predetermined period of time. This time may be selected based on the expected time of operation of downstream protection. If the fault is cleared within this timescale, which is determined by the recovery of the voltage to nominal levels, then normal operation of the ESS will continue. If the voltage does not recover within this period, then the ESS is commanded to ramp down. This scenario may occur in the event that downstream protection fails to operate. Accordingly, this enables ESS FMC to deliver inherent backup functionality.

In the event that the measurement of $\delta i/\delta t$ is less than the lower threshold, then the normal operation of the ESS continues.
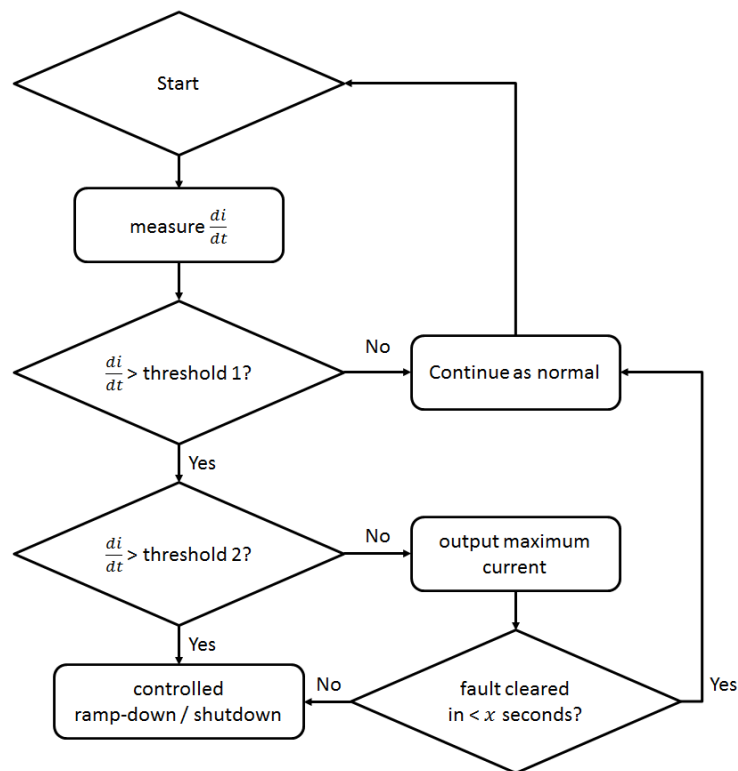
Figure 6.9: Fault mode control algorithm

6.4.2 Performance of ESS FMC

The FMC algorithm was implemented in Simulink and applied to the ESS controller within the reference DC power system model. The unmodified baseline protection system described in Chapter 5 was also utilised. The performance of this protection system was evaluated with the ESS FMC implemented in both configurations of the network in comparison to the default configuration. Results are shown in Table 6.2.

Table 6.2: Performance of protection using ESS FMC

Fault location	Fault impedance (Ω)	Default configuration		Configuration 1		Configuration 2	
		tripped device	trip time (ms)	tripped device	trip time (ms)	tripped device	trip time (ms)
F1	0.5	P1	8	P1	8	P2 then P1	8.3
	0.75	P1	8.2	P1	8.2	P2 then P1	9.3
	1	P1	8.3	P1	8.3	P2 then P1	13.2
F2	0.5	P2	6.1	P2	1.8	P2	6.1
	0.75	P2	6.6	P2	2.1	P2	6.6
	1	P2	7	P2	2.6	P2	7
F3	0.5	P3	3.5	P3	1	P3	1
	0.75	P3	3.9	P3	1.3	P3	1.2
	1	P3	4.3	P3	1.5	P3	1.5

From Table 6.2, it is clear that the protection blinding effects caused by the ESS for close-up faults can be eliminated with the use of ESS FMC. The ability for F_1 faults in configuration 1 and F_2 faults in configuration 2 to be reliably discriminated using the $\delta i/\delta t$ measurement, triggering the rapid ramp-down the ESS output yields equivalent trip-time performance to the baseline protection system. At the same time, it enables the ESS to accelerate the performance of P_2 and P_3 for downstream faults. Similar results are obtained for configuration 2 of the network.

However, trip-time performance for close-up faults can be further improved with the use of inter-tripping between the ESS and P_1 for configuration 1 and P_2 for configuration 2. In configuration 1 of the network, inter-tripping when the

shutdown/ramp-down function of the ESS FMC is triggered with protection device P_1 improves its trip-time performance to match that of the differential scheme evaluated in Chapter 5 for a fault at F_1. Again for configuration 2, inter-tripping the ramp-down function of the ESS FMS with protection device P_2 yields similar results to the differential scheme. These results are shown in Table 6.3.

Table 6.3: Performance of protection using ESS FMC with inter-tripping

Fault location	Fault impedance (Ω)	Default configuration		Configuration 1		Configuration 2	
		tripped device	trip time (ms)	tripped device	trip time (ms)	tripped device	trip time (ms)
	0.5	P1	8	P1	0.1	P2 then P1	8.3
F1	0.75	P1	8.2	P1	0.1	P2 then P1	9.3
	1	P1	8.3	P1	0.1	P2 then P1	13.2
	0.5	P2	6.1	P2	1.8	P2	0.1
F2	0.75	P2	6.6	P2	2.1	P2	0.1
	1	P2	7	P2	2.6	P2	0.1
	0.5	P3	3.5	P3	1	P3	1
F3	0.75	P3	3.9	P3	1.3	P3	1.2
	1	P3	4.3	P3	1.5	P3	1.5

It is clear from the simulation results of the reference DC power system presented in Tables 6.2 and 6.3 that the application of ESS FMC improves the performance of the baseline protection system. Although this type of control will add cost and complexity to the design of the ESS controller and converter interface, it will enable conventional time-graded network protection to function optimally, delivering baseline equivalent performance for close-up faults. In addition, it enables the operation of downstream protection devices to be accelerated for downstream faults.

With the additional functionality of inter-tripping between appropriate breaker devices in conjunction with the ramp-down trigger of ESS FMC, the performance of the baseline protection system can be further improved to match that of the best performing existing solution (differential protection) evaluated in Chapter 5. It is therefore evident that ESS FMC meets both protection system design criteria set in

Chapter 5, whereby the adverse impact of ESS integration is minimised and the overall performance of the system is enhance by enabling a more effective use of the ESS during and post fault conditions.

6.4.3 Inherent backup protection functionality of ESS FMC

The inherent backup protection functionality associated with ESS FMC is demonstrated in this section. Given that the initial $\delta i/\delta t$ measurement of the filter capacitor associated with the ESS converter interface enables downstream faults to be discriminated, the automatic ramp down of ESS current output after a predetermined period of time, together with the inter-tripping functionality with specific network protection devices, enables backup protection functionality to be achieved in the event that downstream devices fail to isolate faulted sections of the network.

6.4.3.1 Configuration 1

To demonstrate this inherent backup protection functionality, the time-constrained threshold associated with the restoration of voltage after fault clearance is set to 5ms for configuration 1 of the network for ramping down ESS output. This threshold corresponds to a moderately greater time than the worst case downstream protection operation time of P_2 when the ESS is operational (1Ω fault at F_2). Simulations of downstream faults (F_2 and F_3) are repeated but with protection device P_2 permanently closed and then with P_2 and P_3 permanently closed, emulating failure-to-open conditions. The respective results are presented in Tables 6.4 and 6.5.

Table 6.4: Performance of protection using ESS FMC with P_2 failure

Fault location	Fault impedance (Ω)	Default configuration		Configuration 1	
		tripped device	trip time (ms)	tripped device	trip time (ms)
F2	0.5	P2	6.1	P1	5
	0.75	P2	6.6	P1	5
	1	P2	7	P1	5
F3	0.5	P3	3.5	P3	1
	0.75	P3	3.9	P3	1.3
	1	P3	4.3	P3	1.5

Table 6.5: Performance of protection using ESS FMC with P_2 and P_3 failures

Fault location	Fault impedance (Ω)	Default configuration		Configuration 1	
		tripped device	trip time (ms)	tripped device	trip time (ms)
F2	0.5	P2	6.1	P1	5
	0.75	P2	6.6	P1	5
	1	P2	7	P1	5
F3	0.5	P3	3.5	P1	5
	0.75	P3	3.9	P1	5
	1	P3	4.3	P1	5

These results show that the time-retracted current output of the ESS enabled by ESS FMC in conjunction with inter-tripping with protection device P_1 prevents a network fault from being present on the network for greater than 5ms, even if downstream protection fails to operate.

6.4.3.2 Configuration 2

For configuration 2, the backup protection time-constrained threshold is set to 7ms for ramping down ESS output. This threshold is reflective of a moderately greater time required for tripping protection device P_2 for a 1Ω fault at F_1, as indicated in Figure 5.5 (b) in Chapter 5. Table 6.6 presents the backup protection results for downstream faults for network configuration 2 assuming a P_3 failure, whilst Table 6.7 presents the results assuming P_2 and P_3 failures.

Table 6.6: Performance of protection using ESS FMC with P_3 failure

Fault location	Fault impedance (Ω)	Default configuration		Configuration 2	
		tripped device	trip time (ms)	tripped device	trip time (ms)
	0.5	P1	8	P2 then P1	8.3
F1	0.75	P1	8.2	P2 then P1	9.3
	1	P1	8.3	P2 then P1	13.2
	0.5	P3	3.5	P2	7
F3	0.75	P3	3.9	P2	7
	1	P3	4.3	P2	7

Table 6.7: Performance of protection using ESS FMC with P_2 and P_3 failures

Fault location	Fault impedance (Ω)	Default configuration		Configuration 2	
		tripped device	trip time (ms)	tripped device	trip time (ms)
	0.5	P1	8	P1	8.4
F1	0.75	P1	8.2	P1	9.5
	1	P1	8.3	P1	13.5
	0.5	P3	3.5	P1	8.5
F3	0.75	P3	3.9	P1	9.8
	1	P3	4.3	P1	13.9

The trip-times of protection device P_2 shown in Table 6.6 (operated as a result of the inter-tripping with the ESS FMC ramp-down function) for the faults thrown at location F_3 are all 7ms. This is evident that the backup protection functionality enabled by ESS FMC is operational and minimises prolonged fault exposure.

However, in the event that protection device P_2 and P_3 are malfunctioning and are permanently closed, the worst case backup trip-time of P_1 is 13.5ms for a 1Ω fault at F_1 and 13.9ms at F_3. This performance is only moderately slower than the expected performance when all network protection devices are fully operational.

6.5 Conclusion

The proposed ESS fault mode control has been demonstrated through modelling and simulation to deliver equivalent protection performance utilising the existing baseline protection system to that of the best performing alternative protection approach (differential protection) for the reference DC power system model. In addition, the inherent backup protection functionality of this method makes it a viable solution to alleviate the adverse effects of integrating a high-power ESS into a compact DC power system whilst improving its safety. The primary advantage of this method over differential protection is that it does not require the use of a network wide high-bandwidth communications system to function. However, the $\delta i/\delta t$ discrimination method utilised is sensitive to fault impedance, which may limit its use for very high-impedance faults. Within the case studies presented in this chapter, faults up to 1Ω were discriminated. Physically larger power systems with greater line impedance or networks with high-impedance grounding systems may not allow for this discrimination method to be accurately used. In these cases, differential based methods may be a more viable alternative.

Chapter 7

Conclusions and further work

7.1 Summary

This thesis has presented a number of contributions to knowledge. Through simulation and experimental validation, it has been demonstrated that a high-power high-bandwidth ESS, by design, can contribute significant levels of current to a fault as it attempts to sustain the network voltage. This behaviour inadvertently reduces the fault current contribution from the primary source of power on the network, reducing the effectiveness of associated protection devices (protection blinding). Several key DC power system design and operation parameters that impact on the ESS fault response have been quantified and a new critical fault impedance term, beyond which protection blinding can be expected to occur, was introduced. This work is presented in Chapter 4 of this thesis and has been published in reference [27].

Enhancements to typical compact DC power system protection schemes which more effectively account for the presence of ESS were proposed and evaluated. Differential protection schemes were shown to eliminate protection blinding whilst offering the greatest flexibility in increasing protection speed and fault discrimination, and maximising ESS availability. Adaptive protection schemes were shown to be a reliable backup option where a consistent protection system response can be obtained despite the potentially intermittent nature of the ESS fault current contribution. This work is presented in Chapter 5 of this thesis.

Finally, a novel control strategy that actively modifies the fault response of the ESS to facilitate the use of conventional overcurrent schemes was proposed, demonstrated and evaluated. This solution minimises the adverse effects of the ESS

response during faults whilst enabling a more effective use of the ESS during and post faults, delivering comparable protection system performance to that of the differential protection solution. This solution also provides inherent backup protection. This work is presented in Chapter 6 of this thesis

7.2 Conclusions

The basis of the work presented in this thesis and the contributions to knowledge that it provides will enable systems integrators to establish the most suitable protection solution when considering the integration of high-power energy storage in existing and new build power system applications. In particular, the trade-offs of modifying existing protection systems within established platforms may not be feasible due to the significant certification costs. For example, incorporation of protection devices that allow for trip settings to be adapted to accommodate for network configuration changes, such as the potential for the ESS to be taken offline during system operation, intrinsically adds significant complexity to the dynamics of the system under both normal and abnormal operating conditions. Accordingly, the fundamental operating states of the power system will change. Such major changes in the functional behaviour of established power systems are likely to warrant the requirement of re-certification to ensure safety standards are upheld and that failure of such safety critical subsystems will not ultimately lead to the catastrophic failure of the entire system. Indeed, the integration of an ESS into an existing system in itself may result in the requirement to reclassify and re-certify the host power system. However, this may not be the case if the ESS has little impact on the performance of the primary generation under fault conditions. In these cases, moderately degraded protection performance may be tolerated if the ESS is sufficiently low rated or if the likelihood of high-impedance fault conditions is rare.

For retrofit applications where a sufficiently high-power ESS is to be integrated, the systems integrator has the tools presented in this thesis to evaluate the potential

impact on the existing network wide protection system performance. If the costs associated with the implementation and certification of the proposed ESS fault mode control is sufficiently lower than the additional weight, cost and complexity of incorporating a high-bandwidth communications based protection system for the desired application then this option should certainly be explored.

Alternatively, for new build applications where the ESS fault response will likely impact on the fault response of primary sources on the network, then the use of a dedicated differential unit based protection system is a viable option. Indeed, differential protection is a well-established protection method that has been widely implemented within aircraft power systems for protecting critical sections of AC distribution systems, and therefore offers a useful precedent in its introduction for protecting DC systems. Although research and development of high-speed differential protection for DC power systems is still ongoing due to the challenges associated with DC current sensing and measurement technology, as well as high-bandwidth communication systems, its functional operating states do not change as a function of power system configuration. Accordingly, certification of such protection systems for aircraft applications may prove to be more achievable than other solutions. This is due to the maturity and reliability of differential protection systems.

7.3 Recommendation of Future Work

Looking forward, a number of work streams are recommended to progress this research. The first work stream involves the development of a comprehensive protection framework for system integrators to assist in the selection of appropriate protection schemes and converter-level protection functions when considering the integration of a high-power, high-bandwidth ESS within a compact DC power system.

This work will require structuring the protection schemes evaluated in this thesis into a system-wide protection framework which guides the system integrator through a series questions regarding the system's features, its architecture and key network parameters. This will establish the system's protection requirements. By defining protection system operational constraints such as the desired maximum fault impedance sensitivity, minimum speed requirements and selectivity options, the optimal primary, secondary and further backup protection schemes may be established. This framework, together with any additional constraints such as weight, complexity and cost, will help the system integrator to make a more informed decision in the implementation of a protection strategy when considering the integration of a high-power ESS into a compact DC network.

The second area for exploration relates to design of a robust ESS control system that ensures stability of its operation under all operating conditions when operating in parallel to a primary conversion system. The conceptual controller design used in the case studies performed in this thesis assumed ideal network operating conditions prior to fault application. Under these conditions, the steady-state network voltage was assumed to be settled to precisely to the desired nominal level (270V). However, both the ESS converter controller and the primary generation converter controller were operating to regulate the same network parameter – the system voltage. In practice, the measurement of the actual system voltage may have an off-set from the reference voltage set point within the ESS controller. Any minor deviation from this set point for the system modelled in this thesis will result in the ESS being commanded to absorb or deliver energy to the network. Therefore, it is recommended that more robust control system designs are explored in future such as dead zone controllers and more robust droop control mechanisms when researching the dynamics of interacting controllers.

The third recommended area of future research is to conceptually analyse the dynamics of power systems that incorporate high-power ESS from an energy flow perspective. Analysis of the use of all sources of energy on an aircraft system is a

wide area of research that may enable energy optimisation, minimisation of fuel consumption and reduction in the rating of energy resources on future aircraft platforms. With the incorporation of high-power energy storage on these future systems, another dimension to this energy flow optimisation problem is introduced. Research in this area may offer opportunities to explore novel uses of high-power energy storage in innovative ways that will enhance their overall performance of these platforms.

The final recommended work stream involves the hardware implementation of fault mode control on a prototype high-power ESS to validate its operational benefits over more complex, system wide protection approaches. In order to implement fault mode control, a high-power, high-bandwidth, bi-directional DC-DC converter interface for a supercapacitor ESS must be developed that offers galvanic isolation, current limiting capability and rapid shut-down functionality. One example converter topology that offers this functionality is the dual active bridge converter and has been discussed in the thesis.

The detection mechanisms that enable fault location to be discriminated, such as current differential zones or the use of *di/dt* trip thresholds, must also be fully evaluated before integration with the ESS converter to trigger fault mode control. One particularly challenging aspect of the *di/dt* discrimination method that requires investigation is its dependability when discriminating against high-impedance close-up faults. For instance, these particular fault types may look like distant faults, triggering the wrong FMC behaviour. However, failsafe modes of operation (such as supplying limited fault current for a reduced time period) may be incorporated to overcome these issues.

The operation of fault mode control must override any normal operating mode of the converter and perform the function of either continuing the supply of current into faults that will accelerate downstream fault detection, or rapidly disengaging the ESS in the event of close-up faults to ensure protection blinding does not occur.

The complexity, cost, ease of certification and achievable performance of this protection function must then be evaluated and traded-off against the performance and drawbacks of more sophisticated protection schemes.

Progression of the research in all these streams of work will contribute to the safe integration of high-power energy storage systems within future compact DC power system applications.

Bibliography

[1]   X. Roboam, B. Sareni, and A. Andrade, "More Electricity in the Air: Toward Optimized Electrical Networks Embedded in More-Electrical Aircraft," *IEEE Industrial Electronics Magazine*, vol. 6, no. 4, pp. 6–17, 2012.

[2]   H. Abu-Rub, M. Malinowski, K. Al-Haddad, "Power Electronics for More Electric Aircraft," *Power Electronics for Renewable Energy Systems, Transportation and Industrial Applications*, Wiley-IEEE Press, 2014.

[3]   P. Athalye, D. Maksimovic, and R. Erickson, "High-Performance Front-End Converter for Avionics Applications," *IEEE Transaction on Aerospace Electronic Systems*, vol. 39, no. 2, pp. 462–470, 2003.

[4]   S. L. Arevalo, P. Zanchetta, P. W. Wheeler, A. Trentin, and L. Empringham, "Control and Implementation of a Matrix-Converter-Based AC Ground Power-Supply Unit for Aircraft Servicing," *IEEE Transactions on Industrial Electronics*, vol. 57, no. 6. pp. 2076–2084, 2010.

[5]   J. Sun, M. Chen, and K. J. Karimi, "Aircraft Power System Harmonics Involving Single-Phase PFC Converters," *IEEE Transactions on Aerospace and Electronic Systems*, vol. 44, no. 1. pp. 217–226, 2008.

[6]   K. Emadi, M. Ehsani, A. Emadi, and M. Ehsani, "Aircraft Power Systems: Technology, State of the Art, and Future Trends," *IEEE Transaction on Aerospace Electronic Systems Magazine*, vol. 15, no. 1, pp. 28–32, 2000.

[7]   R. T. Naayagi, A. J. Forsyth, and R. Shuttleworth, "High-Power Bidirectional DC–DC Converter for Aerospace Applications," *IEEE Transactions on Power Electronics*, vol. 27, no. 11, pp. 4366–4379, 2012.

[8]   M. A. Maldonado, N. M. Shah, K. J. Cleek, and G. J. Korba, "Power Management and Distribution System for a More-Electric Aircraft (MADMEL): Program Status," *IEEE Transactions on Aerospace Electronic Systems Magazine*, vol. 14, no. 12, pp. 3–8, 1999.

[9]   D. Izquierdo, R. Azcona, F. J. López Del Cerro, C. Fernández, and B. Delicado, "Electrical Power Distribution System (HV270DC), for Application in More Electric Aircraft," *Conference Proceedings of IEEE Applications of Power Electronics Conference Exposition*, no. 1, pp. 1300–1305, 2010.

[10]   K. Rajashekara, "Converging Technologies for Electric / Hybrid Vehicles and More Electric Aircraft Systems," *SAE Technical Paper*, vol. 2016, 2012.

[11]   L. B. Buss, "'Electric Airplane' Environmental Control Systems Energy Requirements," *IEEE Transactions on Aerospace and Electronic Systems*, vol. 20, no. 3. pp. 250–256, 1984.

[12]   B. Sarlioglu and C. T. Morris, "More Electric Aircraft: Review, Challenges, and Opportunities for Commercial Transport Aircraft," *IEEE Transactions on Transportation Electrification*, vol. 1, no. 1. pp. 54–64, 2015.

[13]   M. J. Provost, "The More Electric Aero-Engine: A General Overview from an Engine Manufacturer," *International Conference Power Electronics Machines and Drives*, vol. 2002, pp. 246–251, 2002.

[14]   M. T. E. Heinrich, F. Kelch, P. Magne, and A. Emadi, "Regenerative Braking Capability Analysis of an Electric Taxiing System for a Single Aisle Midsize Aircraft," *IEEE Transactions on Transportation Electrification*, vol. 1, no. 3. pp. 298–307, 2015.

[15]   J. Chen, M. Weiszer, P. Stewart, and M. Shabani, "Toward a More Realistic, Cost-Effective, and Greener Ground Movement Through Active Routing. Part I: Optimal Speed Profile Generation," *IEEE Transactions on Intelligent Transportation Systems*, vol. 17, no. 5. pp. 1196–1209, 2016.

[16]   C. M. Ananda, "General Aviation Aircraft Avionics: Integration & system tests," *IEEE Aerospace and Electronic Systems Magazine*, vol. 24, no. 5. pp. 19–25, 2009.

[17]   M. Sinnett, "787 No-Bleed Systems: Saving Fuel and Enhancing Operational Efficiencies," *Boeing Aero Magazine Quarter 4*, pp. 6–11, 2007.

[18]   M. Tooley and D. Wyatt, "Aircraft Electrical and Electronic Systems: Principles, Maintenance and Operation," Butterworth-Heinemann, 2008.

[19]   A. S. Gohardani, G. Doulgeris, and R. Singh, "Challenges of future aircraft propulsion: A review of distributed propulsion technology and its potential application for the all electric commercial aircraft," *Progress in Aerospace Science*, vol. 47, no. 5, pp. 369–391, 2011.

[20]   P. Wheeler and S. Bozhko, "The More Electric Aircraft: Technology and challenges.," *IEEE Electrification Magazine*, vol. 2, no. 4. pp. 6–12, 2014.

[21]   J. S. Cloyd, "Status of the United States Air Force's More Electric Aircraft Initiative," *IEEE Aerospace and Electronic Systems Magazine*, vol. 13, no. 4. pp. 17–22, 1998.

[22]   M. Hirst, A. Mcloughlin, P. J. Norman, and S. J. Galloway, "Demonstrating the More Electric Engine: A Step Towards the Power Optimised Aircraft," *IET Electric Power Applications*, vol. 5, no. 1. pp. 3–13, 2011.

[23]   J. A. Rosero, J. A. Ortega, E. Aldabas, and L. Romeral, "Moving Towards a More Electric Aircraft," *IEEE Aerospace and Electronic Systems Magazine*, vol. 22, no. 3. pp. 3–9, 2007.

[24]   S. Fletcher, "Protection of Physically Compact Multiterminal DC Power Systems," Thesis, University of Strathclyde, 2013.

[25] D. D. Rastler, "Electricity Energy Storage Technology Options: A White Paper Primer on Applications, Costs and Benefits," *Electric Power Research Institute*, p. 170, 2010.

[26] F. Coffele, A. Dyśko, C. Booth, and G. Burt, "Quantitative Analysis of Network Protection Blinding for Systems Incorporating Distributed Generation," *IET Generation Transmission Distribution*, vol. 6, no. 12, pp. 1218–1224, 2012.

[27] P. Rakhra, P. J. Norman, S. D. A. Fletcher, S. J. Galloway, and G. M. Burt, "Evaluation of the Impact of High-Bandwidth Energy-Storage Systems on DC Protection," *IEEE Transactions on Power Delivery*, vol. 31, no. 2, pp. 586–595, 2016.

[28] A. Baker, S. Dutton, and D. Kelly, "Composite Materials for Aircraft Structures, Amaerican Institure of Aeronautics and Astronautics," American Institute of Aeronautics and Astronautics, 2nd edition, 2004.

[29] R. F. Gibson, "A Review of Recent Research on Mechanics of Multifunctional Composite Materials and Structures," *Composite Structures*, vol. 92, no. 12. pp. 2793–2810, 2010.

[30] D. M. Bushnell, "Aircraft Drag Reduction - A Review," in *Proceedings of the Institution of Mechanical Engineers, Part G: Journal of Aerospace Engineering*, vol. 217, no. 1, pp. 1–18, 2003.

[31] A. A. Cusher and A. Gopalarathnam, "Drag Reduction on Aircraft Configurations with Adaptive Lifting Surfaces," *Aerospace Science Technology*, vol. 34, no. 1, pp. 35–44, 2014.

[32] N. Nguyen and J. Urnes Sr, "Aeroelastic modeling of elastically shaped aircraft concept via wing shaping control for drag reduction," *AIAA Atmospheric Flight Mechanics Conference*, no. 650, 2012.

[33] A. M. Stoll, J. Bevirt, M. D. Moore, W. J. Fredericks, and N. K. Borer, "Drag Reduction Through Distributed Electric Propulsion," in *14th AIAA Aviation Technology, Integration, and Operations Conference*, no. 6, pp. 1–10, 2014.

[34] O. Rodionova, M. Sbihi, D. Delahaye, and M. Mongeau, "North Atlantic Aircraft Trajectory Optimization," *IEEE Transactions on Intelligent Transportation Systems*, vol. 15, no. 5. pp. 2202–2212, 2014.

[35] W. H. Ip, D. Wang, and V. Cho, "Aircraft Ground Service Scheduling Problems and Their Genetic Algorithm With Hybrid Assignment and Sequence Encoding Scheme," *IEEE Systems Journal*, vol. 7, no. 4. pp. 649–657, 2013.

[36] J. Montoya, S. Rathinam, and Z. Wood, "Multiobjective Departure Runway Scheduling Using Dynamic Programming," *IEEE Transactions on Intelligent Transportation Systems*, vol. 15, no. 1. pp. 399–413, 2014.

[37] G. Clare and A. G. Richards, "Optimization of Taxiway Routing and Runway Scheduling," *IEEE Transactions on Intelligent Transportation Systems*, vol. 12, no. 4. pp. 1000–1013, 2011.

[38] Y. Eun, I. Hwang, and H. Bang, "Optimal Arrival Flight Sequencing and Scheduling Using Discrete Airborne Delays," *IEEE Transactions on Intelligent Transportation Systems*, vol. 11, no. 2. pp. 359–373, 2010.

[39] W. Pearson, "The More Electric/All Electric Aircraft - A Military Fast Jet Perspective," *IEE Colloquium on All Electric Aircraft*, pp. 1-7, 1998.

[40] T. Tyler, "International Air Transport Association Technology Roadmap," International Air Transport Association, 4th edition, 2013.

[41] I. Moir and A. Seabridge, "Aircraft Systems: Mechanical, Electrical, and Avionics Subsystems Integration," Wiley, 3rd edition, 2008.

[42] I. Moir and A. Seabridge, "Design and Development of Aircraft Systems," Wiley, 2nd edition, 2012.

[43] E. Ganev, "Selecting the Best Electric Machines for Electrical Power-Generation Systems: High-performance solutions for aerospace More electric architectures.," *IEEE Electrification Magazine*, vol. 2, no. 4. pp. 13–22, 2014.

[44] P. H. Mellor, S. G. Burrow, T. Sawata, and M. Holme, "A Wide-Speed-Range Hybrid Variable-Reluctance/Permanent-Magnet Generator for Future Embedded Aircraft Generation Systems," *IEEE Transactions on Industry Applications*, vol. 41, no. 2. pp. 551–556, 2005.

[45] W. U. N. Fernando, M. Barnes, and O. Marjanovic, "Direct Drive Permanent Magnet Generator Fed AC-DC Active Rectification and Control for More-Electric Aircraft Engines," *IET Electric Power Applications*, vol. 5, no. 1. pp. 14–27, 2011.

[46] Z. Xu, D. Zhang, F. Wang, and D. Boroyevich, "A Unified Control for the Combined Permanent Magnet Generator and Active Rectifier System," *IEEE Transactions on Power Electronics*, vol. 29, no. 10. pp. 5644–5656, 2014.

[47] A. Mitcham and J. Cullen, "Permanent Magnet Generator Options for the More Electric Aircraft," *International Conference Power Electronics Machines and Drives*, no. 487, pp. 241–245, 2002.

[48] R. Burgos, G. Chen, F. Wang, D. Boroyevich, W. G. Odendaal, and J. D. Van Wyk, "Reliability-Oriented Design of Three-Phase Power Converters for Aircraft Applications," *IEEE Transactions on Aerospace and Electronic Systems*, vol. 48, no. 2. pp. 1249–1263, 2012.

[49] M. Villani, M. Tursini, G. Fabri, and L. Castellini, "High Reliability Permanent Magnet Brushless Motor Drive for Aircraft Application," *IEEE Transactions on Industrial Electronics*, vol. 59, no. 5. pp. 2073–2081, 2012.

[50] C. Gerada and K. J. Bradley, "Integrated PM Machine Design for an Aircraft EMA," *IEEE Transactions on Industrial Electronics*, vol. 55, no. 9. pp. 3300–3306, 2008.

[51] A. Trentin, P. Zanchetta, P. Wheeler, and J. Clare, "Power Conversion for a Novel AC/DC Aircraft Electrical Distribution System," *IET Electrical Systems in Transportation*, vol. 4, no. 2. pp. 29–37, 2014.

[52] T. Yang, S. Bozhko, and G. Asher, "Active Front-End Rectifier Modelling using Dynamic Phasors for More-Electric Aircraft Applications," *IET Electrical Systems in Transportation*, vol. 5, no. 2. pp. 77–87, 2015.

[53] M. Hartmann, "Ultra-Compact and Ultra-Efficient Three-Phase PWM Rectifier Systems for More Electric Aircraft," Thesis, ETH Zürich, 2011.

[54] B. J. Arnet and L. P. Haines, "High Power DC-to-DC Converter for Supercapacitors," *IEEE Conference International Electronics Machines Drives*, pp. 985–990, 2001.

[55] T. Kostakis, P. J. Norman, S. J. Galloway, and G. M. Burt, "Demonstration of Fast-Acting Protection as a Key Enabler for More-Electric Aircraft Interconnected Architectures," *IET Electrical Systems in Transportation*, vol. 7, no. 2. pp. 170–178, 2016.

[56] J. Chang and A. Wang, "New VF-power System Architecture and Evaluation for Future Aircraft," *IEEE Transactions on Aerospace Electronic Systems*, vol. 42, no. 2, pp. 527–539, 2006.

[57] H. Zhang, F. Mollet, C. Saudemont, and B. Robyns, "Experimental Validation of Energy Storage System Management Strategies for a Local DC Distribution System of More Electric Aircraft," *IEEE Transactions on Industrial Electronics*, vol. 57, no. 12, pp. 3905–3916, 2010.

[58] M. Farhadi and O. Mohammed, "Energy Storage Technologies for High Power Applications," *IEEE Transactions on Industry Applications*, vol. 52, no. 3, pp. 1953–1961, 2015.

[59]   D. Wu, R. Todd, and A. J. Forsyth, "Adaptive Rate-Limit Control for Energy
       Storage Systems," *IEEE Transactions on Industrial Electronics*, vol. 62, no. 7,
       pp. 4231–4240, Jul. 2015.

[60]   X. Roboam, O. Langlois, H. Piquet, B. Morin, and C. Turpin, "Hybrid Power
       Generation System for Aircraft Electrical Emergency Network," *IET Electronic
       Systems in Transportation*, vol. 1, no. 6, p. 148, 2011.

[61]   N. Doerry, J. Amy, and C. Krolick, "History and the Status of Electric Ship
       Propulsion, Integrated Power Systems, and Future Trends in the U.S. Navy,"
       Proceedings of the IEEE, vol. 103, no. 12, pp. 2243–2251, 2015.

[62]   J. M. Crider and S. D. Sudhoff, "Reducing Impact of Pulsed Power Loads on
       Microgrid Power Systems," *IEEE Transactions on Smart Grid*, vol. 1, no. 3, pp.
       270–277, Dec. 2010.

[63]   P. Magne, B. Nahid-Mobarakeh, and S. Pierfederici, "Active Stabilization of
       DC Microgrids Without Remote Sensors for More Electric Aircraft," *IEEE
       Transactions on Industry Applications*, vol. 49, no. 5. pp. 2352–2360, 2013.

[64]   K. N. Areerak, S. V Bozhko, G. M. Asher, L. De Lillo, and D. W. P. Thomas,
       "Stability Study for a Hybrid AC-DC More-Electric Aircraft Power System,"
       IEEE Transactions on Aerospace and Electronic Systems, vol. 48, no. 1. pp.
       329–347, 2012.

[65]   L. Herrera, W. Zhang, and J. Wang, "Stability Analysis and Controller Design of
       DC Microgrids With Constant Power Loads," *IEEE Transactions on Smart Grid*,
       vol. 8, no. 2, pp. 881–888, 2015.

[66]   B. J. Baliga, "The Future of Power Semiconductor Device Technology,"
       Proceedings of the IEEE, vol. 89, no. 6. pp. 822–832, 2001.

[67]   J. Biela, U. Badstuebner, and J. W. Kolar, "Impact of Power Density
       Maximization on Efficiency of DC-DC Converter Systems," *IEEE Transactions
       on Power Electronics*, vol. 24, no. 1. pp. 288–300, 2009.

[68] H. Zhang, L. M. Tolbert, and B. Ozpineci, "Impact of SiC Devices on Hybrid Electric and Plug-In Hybrid Electric Vehicles," *IEEE Transactions on Industry Applications*, vol. 47, no. 2. pp. 912–921, 2011.

[69] F. Wang, Z. Zhang, T. Ericsen, R. Raju, R. Burgos, and D. Boroyevich, "Advances in Power Conversion and Drives for Shipboard Systems," *Proceedings of the IEEE*, vol. 103, no. 12, pp. 2285–2311, 2015.

[70] D. R. Trainer and C. R. Whitley, "Electric Actuation - Power Quality Management of Aerospace Flight Control Systems," *IET International Conference Power Electronics Machines and Drives*, no. 487, pp. 229–234, 2002.

[71] S. D. A. Fletcher, P. J. Norman, S. J. Galloway, and G. M. Burt, "Determination of Protection System Requirements for DC Unmanned Aerial Vehicle Electrical Power Networks for Enhanced Capability and Survivability," *IET Electrical Systems in Transportation*, vol. 1, no. 4, p. 137, 2011.

[72] C. G. Hodge and D. J. Mattick, "The Electric Warship II," *Transactions of the IMarE Evening Paper,* vol. 109, no.2, pp. 127-144, 1996.

[73] C. G. Hodge and D. J. Mattick, "The Electric Warship I," *Transactions on IMarE*, vol. 108, no. 2, pp. 109–125, 1995.

[74] J. I. Hanania, "A Study of Some Features of AC and DC Electric Power Systems for a Space Station," NASA, pp. 223–228, 1983.

[75] K. George, "DC Power Production, Delivery and Utilization: An EPRI White Paper," Electrical Power Research Institue, *Available h ttp//www. epri. org [Accessed 25.05.17]*, 2006.

[76] T. Kaipia, P. Salonen, J. Lassila, and J. Partanen, "Possibilities of the Low Voltage DC Distribution Systems," in *Proceedings of the NORDAC 2006 Conference, Stockholm*, 2006.

[77] B. H. Chowdhury and S. Rahman, "A Review of Recent Advances in Economic Dispatch," *IEEE Transactions on Power Systems*, vol. 5, no. 4. pp. 1248–1259, 1990.

[78] M. E. Baran and N. R. Mahajan, "DC Distribution for Industrial Systems: Opportunities and Challenges," *IEEE Transactions on Industry Applications*, vol. 39, no. 6. pp. 1596–1601, 2003.

[79] S. A. Long, D. R. Trainer, and J. Chivite, "Ultra-compact Intelligent Electrical Networks," in *1st SEAS DTC Technical Conference*, pp. 201–208, 2006.

[80] P. J. Norman, S. J. Galloway, G. M. Burt, D. R. Trainer, and M. Hirst, "Transient Analysis of the More-Electric Engine Electrical Power Distribution Network," *IET International Conference Power Electronics Machines and Drives*, pp. 681–685, 2008.

[81] J. G. Ciezki and R. W. Ashton, "Selection and Stability Issues Associated with a Navy Shipboard DC Zonal Electric Distribution System," *IEEE Transactions on Power Delivery*, vol. 15, no. 2, pp. 665–669, 2000.

[82] F. Gao, S. Bozhko, G. Asher, P. Wheeler, and C. Patel, "An Improved Voltage Compensation Approach in a Droop-Controlled DC Power System for the More Electric Aircraft," *IEEE Transactions on Power Electronics*, vol. 31, no. 10. pp. 7369–7383, 2016.

[83] D. Salomonsson, L. Soder, and A. Sannino, "Protection of Low-Voltage DC Microgrids," *IEEE Transactions on Power Delivery*, vol. 24, no. 3, pp. 1045–1053, 2009.

[84] D. Izquierdo, A. Barrado, C. Raga, M. Sanz, and A. L´Azaro, "Protection Devices for Aircraft Electrical Power Distribution Systems: State of the Art," *IEEE Transactions on Aerospace Electronic Systems*, vol. 47, no. 3, pp. 1538–1550, 2011.

[85]   R. Schmerda, R. Cuzner, R. Clark, D. Nowak, and S. Bunzel, "Shipboard Solid-State Protection: Overview and Applications," *IEEE Electrification Magazine*, vol. 1, no. 1, pp. 32–39, 2013.

[86]   "787 Batteries and Advanced Airplanes," Boeing Website, Available: http://787updates.newairplane.com/787-Electrical-Systems/Batteries-and-Advanced-Airplanes, *[Accessed 25.05.17]*, 2013.

[87]   J. Hale, "Boeing 787 from the Ground Up," *AERO Magazine*, pp. 17–23, 2006.

[88]   F. A. Inthamoussou, J. Pegueroles-Queralt, and F. D. Bianchi, "Control of a Supercapacitor Energy Storage System for Microgrid Applications," *IEEE Transactions on Energy Conversion,* vol. 28, no. 3. pp. 690–697, 2013.

[89]   L. Xu and D. Chen, "Control and Operation of a DC microgrid with Variable Generation and Energy Storage," *IEEE Transactions on Power Delivery*, vol. 26, no. 4, pp. 2513–2522, 2011.

[90]   S. Vazquez, S. M. Lukic, E. Galvan, L. G. Franquelo, and J. M. Carrasco, "Energy Storage Systems for Transport and Grid Applications," *IEEE Transactions on Industrial Electronics*, vol. 57, no. 12, pp. 3881–3895, 2010.

[91]   S. Samineni, B. K. Johnson, H. L. Hess, and J. D. Law, "Modeling and Analysis of a Flywheel Energy Storage System for Voltage Sag Correction," *IEEE Transactions on Industrial Applications*, vol. 42, no. 1, pp. 42–52, 2006.

[92]   B. Zahedi and L. E. Norum, "Modelling and Simulation of All-Electric Ships With Low-Voltage DC Hybrid Power Systems," *IEEE Transactions on Power Electronics*, vol. 28, no. 10. pp. 4525–4537, 2013.

[93]   P. Rakhra, P. Norman, S. Fletcher, S. Galloway, and G. Burt, "A Holistic Approach towards Optimizing Energy Storage Response during Network Faulted Conditions within an Aircraft Electrical Power System," *SAE International Journal of Aerospace*, vol. 5, no. 2, pp. 548–556, 2012.

[94]   A. Khaligh, "Battery, Ultracapacitor, Fuel Cell, and Hybrid Energy Storage Systems for Electric, Hybrid Electric, Fuel Cell, and Plug-In Hybrid Electric Vehicles: State of the Art," *IEEE Transactions on Vehicular Technololgy*, vol. 59, no. 6, pp. 2806–2814, 2010.

[95]   P. F. Ribeiro, B. K. Johnson, M. L. Crow, A. Arsoy, and Y. Liu, "Energy Storage Systems for Advanced Power Applications," *Proceedings IEEE*, vol. 89, no. 12, pp. 1744–1756, 2001.

[96]   R. T. Naayagi and A. J. Forsyth, "Bidirectional DC-DC Converter for Aircraft Electric Energy Storage Systems," *5th IET International Conference Power Electronics Machines and Drives*, pp. 1-6, 2010.

[97]   S. M. Lukic, J. Cao, R. C. Bansal, F. Rodriguez, A. Emadi, "Energy Storage Systems for Automotive Applications," *IEEE Transactions on Industrial Electronics*, vol. 55, no. 6, pp. 2258–2267, 2008.

[98]   M. H. Ali, B. Wu, and R. A. Dougal, "An Overview of SMES Applications in Power and Energy Systems," *IEEE Transaction on Sustainable Energy*, vol. 1, no. 1, pp. 38–47, 2010.

[99]   I. J. Cohen, D. A. Wetz, J. M. Heinzel, and Q. Dong, "Design and Characterization of an Actively Controlled Hybrid Energy Storage Module for High-Rate Directed Energy Applications," *IEEE Transactions on Plasma Science*, vol. 43, no. 5. pp. 1427–1433, 2015.

[100]   P. Thounthong, S. Raël, and B. Davat, "Analysis of Supercapacitor as Second Source Based on Fuel Cell Power Generation," *IEEE Transactions on Energy Conversion*, vol. 24, no. 1, pp. 247–255, 2009.

[101]   J. Leuchter, P. Bauer, and V. Stekly, "Battery-Supercapacitors Mixed as Electrical Power Buffers," *International Conference Power Electronics Machines and Drives,* pp. 1–6, 2010.

[102] H. Liu, Z. Wang, S. Qiao, and Y. Liu, "Improvement of Engine Cold Start Capability Using Supercapacitor and Lead-Acid Battery Hybrid," *Conference Proceedings IEEE Applied Power Electronics Conference Exposition*, pp. 668–675, 2008.

[103] R. Todd and A. J. Forsyth, "HIL Emulation of All-Electric UAV Power Systems," *2009 IEEE Energy Conversion Congress Exposition,* pp. 411–416, 2009.

[104] R. Todd and A. J. Forsyth, "DC-Bus Power Quality for Aircraft Power Systems During Generator Fault Conditions," *IET Electrical Systems in Transportation*, vol. 1, no. 3. pp. 126–135, 2011.

[105] K. Zach, H. Auer, and G. Lettner, "Facilitating Energy Storage to Allow High Penetration of Intermittent Renewable Energy," *StoRE Project Deliverable*, pp. 49, 2012.

[106] G. Watch, "Electrochemical Energy Storage: A Mission to the USA," Department of Trade and Industry Report, 2004.

[107] Special Working Group on Electrical Energy Storage, "Electrical Energy Storage: White Paper," International Electrotechnical Commission, p. 78, 2011.

[108] B. Zakeri and S. Syri, "Electrical Energy Storage Systems: A Comparative Life Cycle Cost Analysis," *Renewable Sustainable Energy Review*, vol. 42, pp. 569–596, 2015.

[109] D. Manz, R. Piwko, and N. Miller, "Look Before You Leap: The Role of Energy Storage in the Grid," *IEEE Power and Energy Magazine*, vol. 10, no. 4. pp. 75–84, 2012.

[110] H. Zhang, F. Mollet, S. Breban, S. Chrisophe, B. Robyns, and R. Meuret, "Hybrid Storage and Dissipation Systems Based Power Management Strategies in a Local Dc Power Distribution System of More Electric Aircraft," *International Congress Aeronautic Science*, no. 7, pp. 1–8, 2010.

[111] H. Chen and A. Khaligh, "Hybrid Energy Storage System for Unmanned Aerial Vehicle (UAV)," *36th Annual Conference IEEE Industrial Electronics Society*, pp. 2851–2856, 2010.

[112] V. A. Boicea, "Energy Storage Technologies: The Past and the Present," *Proceedings of the IEEE*, vol. 102, no. 11. pp. 1777–1794, 2014.

[113] X. Luo, J. Wang, M. Dooner, and J. Clarke, "Overview of Current Development in Electrical Energy Storage Technologies and the Application Potential in Power System Operation," *Applied Energy*, vol. 137, pp. 511–536, 2015.

[114] M. S. Whittingham, "History, Evolution, and Future Status of Energy Storage," *Proceedings of the IEEE*, vol. 100, Special Centennial Issue, pp. 1518–1534, 2012.

[115] M. A. Fetcenko, S. R. Ovshinsky, B. Reichman, K. Young, C. Fierro, J. Koch, A. Zallen, W. Mays, and T. Ouchi, "Recent Advances in NiMH Battery Technology," *Journal of Power Sources*, vol. 165, no. 2, pp. 544–551, 2007.

[116] C. S. Hearn, M. C. Lewis, S. B. Pratap, R. E. Hebner, F. M. Uriarte, D. Chen, and R. G. Longoria, "Utilization of Optimal Control Law to Size Grid-Level Flywheel Energy Storage," *IEEE Transactions on Sustainable Energy*, vol. 4, no. 3, pp. 611–618, 2013.

[117] A. Jaafar, C. R. Akli, B. Sareni, X. Roboam, and A. Jeunesse, "Sizing and Energy Management of a Hybrid Locomotive Based on Flywheel and Accumulators," *IEEE Transactions on Vehicular Technology*, vol. 58, no. 8. pp. 3947–3958, 2009.

[118] J. D. Boyes and N. H. Clark, "Technologies for Energy Storage: Flywheels and Superconducting Magnetic Energy Storage," *2000 Power Engineering Society Summer Meeting*, vol. 3, no. 1, pp. 1548–1550, 2000.

186

[119] Y. Cheng, "Assessments of Energy Capacity and Energy Losses of Supercapacitors in Fast Charging-Discharging Cycles," *IEEE Transactions on Energy Conversion*, vol. 25, no. 1, pp. 253–261, 2010.

[120] N. Kularatna, J. Fernando, and A. Pandey, "Surge Endurance Capability Testing of Supercapacitor Families," *Proceedings Industrial Electronics Conference*, no. 1, pp. 1858–1863, 2010.

[121] A. Chu and P. Braatz, "Comparison of Commercial Supercapacitors and High-Power Lithium-Ion Batteries for Power-Assist Applications in Hybrid Electric Vehicles," *Journal of Power Sources*, vol. 112, no. 1, pp. 236–246, 2002.

[122] R. L. Spyker, "Classical Equivalent Circuit Parameters for a Double-Layer Capacitor," *IEEE Transactions on Aerospace Electronic Systems*, vol. 36, no. 3, pp. 829–836, 2000.

[123] P. Thounthong, S. Rael, and B. Davat, "Control Strategy of Fuel Cell and Supercapacitors Association for a Distributed Generation System," *IEEE Transactions on Industrial Electronics*, vol. 54, no. 6. pp. 3225–3233, 2007.

[124] K. Rajashekara, "Parallel Between More Electric Aircraft and Electric/Hybrid Vehicle Power Conversion Technologies," *IEEE Electrification Magazine*, vol. 2, no. 2. pp. 50–60, 2014.

[125] A. Lücken, J. Brombach, and D. Schulz, "Design and Protection of a High Voltage DC Onboard Grid with Integrated Fuel Cell System on More Electric Aircraft," *International Conference Electrical Systems for Aircraft, Railway, Ship Propulsion,* pp. 1–6, 2010.

[126] N. Lapeña-Rey, J. Mosquera, E. Bataller, and F. Ortí, "First Fuel-Cell Manned Aircraft," *Journal of Aircraft.*, vol. 47, no. 6, pp. 1825–1835, 2010.

[127] "Solar Impulse 2: Batteries," Solar Impulse Website, Available: http://www.solarimpulse.com/infocard-Batteries, *[Accessed 25.05.17],* 2016

[128] M. Williamson, "Air Power the Rise of Electric Aircraft," *Engineering & Technology*, vol. 9, no. 10. pp. 77–79, 2014.

[129] G. Romeo, F. Borello, and E. Cestino, "Design of Inter-City Transport Aircraft Powered by Fuel Cell & Flight Test of Zero Emission 2-Seater Aircraft," *Electrical Systems for Aircraft, Railway and Ship Propulsion,* pp. 1–7, 2012.

[130] Y. Zhai, Y. Dou, D. Zhao, P. F. Fulvio, R. T. Mayes, and S. Dai, "Carbon Materials for Chemical Capacitive Energy Storage," *Advanced Materials*, vol. 23, no. 42, pp. 4828–4850, Nov. 2011.

[131] C. Xu, B. Xu, Y. Gu, Z. Xiong, J. Sun, and X. S. Zhao, "Graphene-Based Electrodes for Electrochemical Energy Storage," *Energy Environment Science*, vol. 6, no. 5, pp. 1388–1414, 2013.

[132] Q. Liu, M. H. Nayfeh, and S.-T. Yau, "Supercapacitor Electrodes Based on Polyaniline–Silicon Nanoparticle Composite," *Journal of Power Sources,* vol. 195, no.12, pp. 3956–3959, 2010.

[133] F. Markoulidis, C. Lei, and C. Lekakou, "Fabrication of High-Performance Supercapacitors Based on Transversely Oriented Carbon Nanotubes," *Applied Physics A*, vol. 111, no. 1, pp. 227–236, 2013.

[134] E. Chemali, M. Peindl, P. Malysz, and A. Emadi, "Electrochemical and Electrostatic Energy Storage and Management Systems for Electric Drive Vehicles: State-of-the-Art Review and Future Trends," *IEEE Journal of Emerging and Selected Topics in Power Electronics*, vol. 4, no. 3, pp. 1117-1134, 2016.

[135] T. Dragicevic, H. Pandzic, D. Skrlec, I. Kuzle, J. M. Guerrero, and D. S. Kirschen, "Capacity Optimization of Renewable Energy Sources and Battery Storage in an Autonomous Telecommunication Facility," *IEEE Transactions on Sustainable Energy*, vol. 5, no. 4. pp. 1367–1378, 2014.

[136] E. Ribeiro, A. J. M. Cardoso, and C. Boccaletti, "Fuel Cell-Supercapacitor System for Telecommunications," *5th IET International Conference on Power Electronics, Machines and Drives,* pp. 1–6, 2010.

[137] Department of Defense Interface Standard, "MIL-STD-704F Aircraft Electric Power Characteristics," 2004.

[138] A. Eid, H. El-Kishky, M. Abdel-Salam, and T. El-Mohandes, "Power Quality Investigations of VSCF Aircraft Electric Power Systems," *Annual Proceedings Southeast Symposium on Systems Theory*, vol. 25, no. 1, pp. 171–176, 2010.

[139] X. Lu and R. Silva, "The Modular Design of an Aircraft Power Distribution System," *SAE Technical Paper*, 2010.

[140] A. Yazdani and R. Iravani, "Voltage-Sourced Converters in Power Systems: Modeling, Control, and Applications," Wiley-IEEE Press, 2010.

[141] D. Izquierdo, A. Barrado, C. Fernandez, M. Sanz, and P. Zumel, "Behavioral Model for a Solid-State Power Controller," *IEEE Transactions on Aerospace Electronic Systems Magazine*, vol. 28, no. 12, pp. 4–11, 2013.

[142] R. Todd, F. Bryan, A. J. Forsyth, C. Gan, and J. Bossard, "Effects of Electrical Power Off-Take on Finite Inertia Mechanical Systems," *2011 IEEE Energy Conversion Congress and Exposition*. pp. 1476–1482, 2011.

[143] V. Bolborici, F. P. Dawson, and K. K. Lian, "Hybrid Energy Storage Systems: Connecting Batteries in Parallel with Ultracapacitors for Higher Power Density," *IEEE Industry Applications Magazine*, vol. 20, no. 4. pp. 31–40, 2014.

[144] G. Xu, L. Xu, D. Morrow, and D. Chen, "Coordinated DC Voltage Control of Wind Turbine With Embedded Energy Storage System," *IEEE Transactions on Energy Conversion*, vol. 27, no. 4, pp. 1036–1045, 2012.

[145] D. W. Swett and J. G. Blanche, "Flywheel Charging Module for Energy Storage Used in Electromagnetic Aircraft Launch System," *IEEE Transactions on Magnetics*, vol. 41, no. 1. pp. 525–528, 2005.

[146] A. J. Forsyth and R. Todd, "DC-Bus Power Quality for UAV Systems During Generator Fault Conditions," in *5th IET International Conference on Power Electronics, Machines and Drives*, pp. 354–354, 2010.

[147] J. Zumberge, J. Wolff, K. Mccarthy, T. O. Connell, E. Walters, G. Russell, and C. Lucas, "Integrated Aircraft Electrical Power System Modeling and Simulation Analysis," *SAE Technical Paper*, 2010.

[148] J. M. Guerrero, L. G. De Vicuna, and J. Uceda, "Uninterruptible Power Supply Systems Provide Protection," *IEEE Industrial Electronics Magazine*, vol. 1, no. 1. pp. 28–38, 2007.

[149] B. Roberts and J. McDowall, "Commercial Successes in Power Storage," *IEEE Power and Energy Magazine*, vol. 3, no. 2. pp. 24–30, 2005.

[150] R. S. Weissbach, G. G. Karady, and R. G. Farmer, "A Combined Uninterruptible Power Supply and Dynamic Voltage Compensator Using a Flywheel Energy Storage System," *IEEE Transactions on Power Delivery*, vol. 16, no. 2. pp. 265–270, 2001.

[151] K. Rajashekara, J. Grieve, and D. Daggett, "Hybrid Fuel Cell Power in Aircraft," *IEEE Industry Applications Magazine*, vol. 14, no. 4. pp. 54–60, 2008.

[152] Air Accidents Investigation Branch, "Aircraft Accident Report 2/2009 - Boeing 777-222, N786UA, 26 February 2007 Air Accidents Investigation Branch report," Available: https://www.gov.uk/aaib-reports/n786ua-2-2009-26-february-2007, *[Accessed 25.05.17]*, 2007

[153] United States Air Force AAIB, "Aircraft Accident Investigation, F-22, T/N 00-4013, Tyndall Air Force Base, Florida, 15 November 2012," 2012.

[154] G. G. Gutierrez, D. M. Romero, M. R. Cabello, E. Pascual-Gil, L. D. Angulo, D. G. Gomez, and S. G. Garcia, "On the Design of Aircraft Electrical Structure Networks," *IEEE Transactions on Electromagnetic Compatibility*, vol. 58, no. 2. pp. 401–408, 2016.

[155] Alstom Grid, "Network Protection & Automation Guide," *Alstom Grid*, 2011.

[156] North American Electric Reliability Corporation, "Protection System Reliability Redundancy of Protection System Elements NERC System Protection and Control Task Force," 2008.

[157] "IEEE Standard for Trip Systems for Low-Voltage (1000 V and below) AC and General Purpose (1500 V and below) DC Power Circuit Breakers," *IEEE STD C37.17-2012 (Revision of ANSI C37.17-1997)*. pp. 1–27, 2012.

[158] "IEEE Standard for Low-Voltage AC Power Circuit Breakers Used in Enclosures," *IEEE STD C37.13-2008*. pp. 1–29, 2009.

[159] "IEEE Standard Requirements for Instrument Transformers," *IEEE STD C57.13-2016 (Revision of IEEE STD C57.13-2008)*. pp. 1–96, 2016.

[160] J. R. Brauer, "Hall Effect and Magnetoresistive Sensors," *Magnetic Actuators and Sensors*, Wiley-IEEE Press, p. 400, 2014.

[161] K. Bohnert, P. Gabus, J. Nehring, and H. Brandle, "Temperature and Vibration Insensitive Fiber-Optic Current Sensor," *Journal of Lightwave Technology*, vol. 20, no. 2. pp. 267–276, 2002.

[162] A. Patel and M. Ferdowsi, "Current Sensing for Automotive Electronics: A Survey," *IEEE Transactions on Vehicular Technology*, vol. 58, no. 8. pp. 4108–4119, 2009.

[163] M. E. El-Hawary, "System Protection," *Electrical Power Systems: Design and Analysis*, Wiley-IEEE Press, pp. 541–623, 1995.

[164] Sensata Technologies, "Klixon Precision Products Aircraft Circuit Breakers," Sensata Website, Available: http://www.sensata.com/download/klixon-circuit-breaker-aircraft-catalog.pdf, *[Accessed 25.05.17]*, 2017

[165] E-T-A, "E-T-A Remote Control Circuit Breaker 4930 (RCCB) Data sheet," E-T-A Website, Available: https://www.e-t-a.com/products/circuit_protection_devices/high_performance_circuit_breakers/p/4930/ *[Accessed 25.05.17]*, 2017

[166] Leach International Corporation, "Leach International - Solutions for Power Switching and Control Capabilities Overview Datasheet," Available: https://www.esterline.com/Portals/3/Literature/Custom%20Equipment%20Relay%20Boxes%20and%20Assemblies.pdf, *[Accessed 25.05.17]*, 2003.

[167] A. A. Sallam and O. P. Malik, "Protection of Electric Distribution Systems," *Electric Distribution Systems*. Wiley-IEEE Press, pp. 163–235, 2011.

[168] Air Accidents Investigation Branch, "Airbus A319-131, G-EUPZ, 15 March 2009 Air Accidents Investigation Branch report," Available: https://www.gov.uk/aaib-reports/airbus-a319-131-g-eupz-15-march-2009, *[Accessed 25.05.17]*, 2009.

[169] C. Furse and R. Haupt, "Down to the wire [aircraft wiring]," *IEEE Spectrum*, vol. 38, no. 2. pp. 34–39, 2001.

[170] Safran Labinal Power Systems, "Safran Labinal Power Systems Circuit Breaker Data Sheet," Available: https://www.safran-electrical-power.com/electricalcomponentscatalog/pdf/3-TF300-1E_Circuit_Breaker_Catalog.pdf, *[Accessed 25.05.17]*, 2015.

[171] R. Grassetti, R. Ottoboni, M. Rossi, and S. Toscani, "Low Cost Arc Fault Detection in Aerospace Applications," *IEEE Instrumentation & Measurement Magazine*, vol. 16, no. 5. pp. 37–42, 2013.

[172] M. Faifer, R. Ottoboni, M. Rossi, S. Toscani, and R. Grassetti, "A Method for the Detection of Series Arc Faults in DC Aircraft Power Networks," *2013 IEEE International Instrumentation and Measurement Technology Conference,* pp. 778–783, 2013.

[173] P. Smith, C. Furse, and J. Gunther, "Analysis of Spread Spectrum Time Domain Reflectometry for Wire Fault Location," *IEEE Sensors Journal*, vol. 5, no. 6. pp. 1469–1478, 2005.

[174] X. Yao, L. Herrera, S. Ji, K. Zou, and J. Wang, "Characteristic Study and Time-Domain Discrete- Wavelet-Transform Based Hybrid Detection of Series DC Arc Faults," *IEEE Transactions on Power Electronics*, vol. 29, no. 6. pp. 3103–3115, 2014.

[175] H. Zhang, T. Chen, and W. Li, "Arc Fault Signatures Detection on Aircraft Wiring System," *2006 6th World Congress on Intelligent Control and Automation*, vol. 2. pp. 5548–5552, 2006.

[176] A. Yaramasu, Y. Cao, G. Liu, and B. Wu, "Aircraft Electric System Intermittent Arc Fault Detection and Location," *IEEE Transactions on Aerospace and Electronic Systems*, vol. 51, no. 1. pp. 40–51, 2015.

[177] Q. Zhou, M. Sumner, and D. Thomas, "Fault Location for Aircraft Distribution Systems Using Harmonic Impedance Estimation," *IET Electrical Systems in Transportation*, vol. 2, no. 3. pp. 119–129, 2012.

[178] Q. Zhou, M. Sumner, and D. Thomas, "Mathematical Analysis of the Equivalent Impedance at the Harmonic Frequency for the Proposed Aircraft Power System," *IET Electrical Systems in Transportation*, vol. 3, no. 4. pp. 87–101, 2013.

[179] E. Christopher, M. Sumner, D. W. P. Thomas, X. Wang, and F. de Wildt, "Fault Location in a Zonal DC Marine Power System Using Active Impedance Estimation," *IEEE Transactions on Industry Applications*, vol. 49, no. 2. pp. 860–865, 2013.

[180] K. Jia, T. Bi, B. Liu, E. Christopher, D. W. P. Thomas, and M. Sumner, "Marine Power Distribution System Fault Location Using a Portable Injection Unit," *IEEE Transactions on Power Delivery*, vol. 30, no. 2. pp. 818–826, 2015.

[181] S. D. A. Fletcher, P. J. Norman, S. J. Galloway, P. Crolla, and G. M. Burt, "Optimizing the Roles of Unit and Non-unit Protection Methods Within DC Microgrids," *IEEE Transactions on Smart Grid,* vol. 3, no. 4. pp. 2079–2087, 2012.

[182] P. Cairoli, I. Kondratiev, and R. A. Dougal, "Coordinated Control of the Bus Tie Switches and Power Supply Converters for Fault Protection in DC Microgrids," *IEEE Transactions on Power Electronics*, vol. 28, no. 4. pp. 2037–2047, 2013.

[183] A. A. Elserougi, A. S. Abdel-Khalik, A. M. Massoud, and S. Ahmed, "A New Protection Scheme for HVDC Converters Against DC-Side Faults With Current Suppression Capability," *IEEE Transactions on Power Delivery*, vol. 29, no. 4, pp. 1569–1577, 2014.

[184] P. Cairoli and R. A. Dougal, "New Horizons in DC Shipboard Power Systems: New Fault Protection Strategies are Essential to the Adoption of DC Power Systems," *IEEE Electrification Magazine*, vol. 1, no. 2, pp. 38–45, 2013.

[185] X. Li, Q. Song, W. Liu, H. Rao, S. Xu, and L. Li, "Protection of Nonpermanent Faults on DC Overhead Lines in MMC-Based HVDC Systems," *IEEE Transactions on Power Delivery*, vol. 28, no. 1, pp. 483–490, 2013.

[186] J. Yang, J. E. Fletcher, and J. O'Reilly, "Multiterminal DC Wind Farm Collection Grid Internal Fault Analysis and Protection Design," *IEEE Transactions on Power Delivery*, vol. 25, no. 4, pp. 2308–2318, 2010.

[187] J.D. Park, J. Candelaria, L. Ma, and K. Dunn, "DC Ring-Bus Microgrid Fault Protection and Identification of Fault Location," *IEEE Transactions on Power Delivery*, vol. 28, no. 4, pp. 2574–2584, 2013.

[188] N. R. Mahajan, "System Protection for Power Electronic Building Block Based DC Distribution Systems," Thesis, North Carolina State University, 2004.

[189] K. Jia, M. Sumner, E. Christopher, T. Bi, and D. Thomas, "Advanced DC Zonal Marine Power System Protection," *IET Generation Transmission and Distribution*, vol. 8, no. 2, pp. 301–309, 2014.

[190] D. Jovcic, M. Taherbaneh, J.P. Taisne, and S. Nguefeu, "Offshore DC Grids as an Interconnection of Radial Systems: Protection and Control Aspects," *IEEE Transactions on Smart Grid*, vol. 6, no. 2, pp. 903–910, 2015.

[191] F. M. Uriarte, A. L. Gattozzi, J. D. Herbst, H. B. Estes, T. J. Hotz, A. Kwasinski, and R. E. Hebner, "A DC Arc Model for Series Faults in Low Voltage Microgrids," *IEEE Transactions on Smart Grid*, vol. 3, no. 4, pp. 2063–2070, 2012.

[192] D. R. Doan, "Arc Flash Calculations for Exposures to DC Systems," *IEEE Transactions on Industry Applications,* vol. 46, no. 6, pp. 2299–2302, 2010.

[193] Data Device Corporation, "Solid-State Power Controller Datasheet," Available: http://www.ddc-web.com/, *[Accessed 25.05.17]*, 2017.

[194] A. Shipley, "Power Controller System." US Patent US9118177B2, 2015.

[195] Z. Liu, R. Fuller, and W. Pearson, "SSPC Technologies for Aircraft High Voltage DC Power Distribution Applications," *SAE Technical Paper*, 2012.

[196] Z. R. Ivanović, E. M. Adžić, M. S. Vekić, S. U. Grabić, N. L. Čelanović, and V. A. Katić, "HIL Evaluation of Power Flow Control Strategies for Energy Storage Connected to Smart Grid Under Unbalanced Conditions," *IEEE Transactions on Power Electronics*, vol. 27, no. 11, pp. 4699–4710, 2012.

[197] L. Corradini, P. Mattavelli, E. Tedeschi, and D. Trevisan, "High-Bandwidth Multisampled Digitally Controlled DC–DC Converters Using Ripple Compensation," *IEEE Transactions on Industrial Electronics*, vol. 55, no. 4, pp. 1501–1508, 2008.

[198] R. Li, T. O'Brien, J. Lee, and J. Beecroft, "A Unified Small Signal Analysis of DC-DC Converters with Average Current Mode Control," *IEEE Energy Conversion Congress and Exposition,* pp. 647–654, 2009.

[199] A. T. Elsayed, T. A. Youssef, and O. A. Mohammed, "Modelling and Control of a Low-Speed Flywheel Driving System for Pulsed-Load Mitigation in DC Distribution Networks," *IEEE Transactions on Industry Applications*, vol. 52, no. 4, pp. 3378–3387, 2016.

[200] B. M. Huhman, J. M. Neri, and D. A. Wetz, "Application of a Compact Electrochemical Energy Storage to Pulsed Power Systems," *IEEE Transactions on Dielectrics and Electrical Insulation*, vol. 20, no. 4, pp. 1299–1303, 2013.

[201] M. E. Baran and N. R. Mahajan, "Overcurrent Protection on Voltage-Source-Converter-Based Multiterminal DC Distribution Systems," *IEEE Transactions on Power Delivery*, vol. 22, no. 1, pp. 406–412, 2007.

[202] Z. Wang, X. Shi, Y. Xue, L. M. Tolbert, F. Wang, and B. J. Blalock, "Design and Performance Evaluation of Overcurrent Protection Schemes for Silicon Carbide (SiC) Power MOSFETs," *IEEE Transactions on Industrial Electronics*, vol. 61, no. 10. pp. 5570–5581, 2014.

[203] H. Matsuo, F. Kurokawa, and M. Asano, "Overcurrent limiting characteristics of the DC-DC converter with a new digital current-injected control circuit," *IEEE Transactions on Power Electronics*, vol. 13, no. 4. pp. 645–650, 1998.

[204] A. D. Crane, "Power distribution systems." US Patent US20130200691A1, 2010.

[205] J. Shen, S. Dusmez, and A. Khaligh, "Optimization of Sizing and Battery Cycle Life in Battery/Ultracapacitor Hybrid Energy Storage Systems for Electric Vehicle Applications," *IEEE Transactions on Industrial Informatics*, vol. 10, no. 4. pp. 2112–2121, 2014.

[206] M. Ammar and G. Joós, "A Short-Term Energy Storage System for Voltage Quality Improvement in Distributed Wind Power," *IEEE Transactions on Energy Conversion*, vol. 29, no. 4. pp. 997–1007, 2014.

[207] T. Nam, J. W. Shim, and K. Hur, "The Beneficial Role of SMES Coil in DC Lines as an Energy Buffer for Integrating Large Scale Wind Power," *IEEE Transactions on Applied Superconductivity*, vol. 22, no. 3, p. 1-8, 2012.

[208] D. Somayajula and M. L. Crow, "An Integrated Dynamic Voltage Restorer-Ultracapacitor Design for Improving Power Quality of the Distribution Grid," *IEEE Transactions on Sustainable Energy*, vol. 6, no. 2. pp. 616–624, 2015.

[209] Won-Sik Moon, Jong-Nam Won, Jae-Sun Huh, and Jae-Chul Kim, "A Study on the Application of a Superconducting Fault Current Limiter for Energy Storage Protection in a Power Distribution System," *IEEE Transaction on Applied Superconductivity*, vol. 23, no. 3, Jun. 2013.

[210] H. V Padullaparti, P. Chirapongsananurak, M. E. Hernandez, and S. Santoso, "Analytical Approach to Estimate Feeder Accommodation Limits Based on Protection Criteria," *IEEE Access*, vol. 4. pp. 4066–4081, 2016.

[211] "IEEE Standard Definitions for Power Switchgear," *IEEE Std C37.100-1992*. p.1, 1992.

[212] S. Recoskie, A. Fahim, W. Gueaieb, and E. Lanteigne, "Hybrid Power Plant Design for a Long-Range Dirigible UAV," *IEEE/ASME Transactions on Mechatronics*, vol. 19, no. 2. pp. 606–614, 2014.

[213] S. D. A. Fletcher, P. Norman, S. Galloway, P. Rakhra, G. Burt, and V. Lowe, "Modeling and Simulation Enabled UAV Electrical Power System Design," *SAE International Journal of Aerospace*, vol. 4, no. 2, pp. 1074–1083, 2011.

[214] H. Chen and A. Khaligh, "Hybrid Energy Storage System for Unmanned Aerial Vehicle (UAV)," *I36th Annual Conference on IEEE Industrial Electronics Society*, pp. 2851–2856, 2010.

[215] R. Loh, Y. Bian, and T. Roe, "UAVs in Civil Airspace: Safety Requirements," *IEEE Aerospace and Electronic Systems Magazine*, vol. 24, no. 1. pp. 5–17, 2009.

[216] Mathworks, "MATLAB & SIMULINK: version (R2015b)," Power Systems Modelling Software, 2015.

[217] "Aircraft Electrical Power Systems Modeling and Simulation Definitions." *SAE International Standard SAE AIR 6326*, 2015.

[218] I. Jadric, D. Borojevic, and M. Jadric, "Modeling and Control of a Synchronous Generator with an Active DC Load," *IEEE Transactions on Power Electronics*, vol. 15, no. 2. pp. 303–311, 2000.

[219] P. J. Norman, "Methods for the Efficient and Accurate Simulation of Marine and Aerospace Electrical Power Networks," Thesis, University of Strathclyde, 2009.

[220] W. Lin and D. Jovcic, "LCL and L-VSC Converters With DC Fault Current-Limiting Property and Minimal Power Losses," *IEEE Transactions on Power Delivery*, vol. 29, no. 5. pp. 2359–2368, 2014.

[221] W. A. Atkey, A. T. Bernier, M. D. Bowman, T. A. Campbell, J. M. Cruse, C. J. Fiterman, C. S. Meis, C. Ng, F. Nozari, and E. Zielinski, "Electric-Based Secondary Power System Architectures for Aircraft." US7950606B2, 2011.

[222] R. A. Huggins, "Energy Storage: Fundamentals, Materials and Applications." Springer International Publishing, 2015.

[223] T. Takagi, Y. Yamakoshi, M. Yamaura, R. Kondow, and T. Matsushima, "Development of a New Type Fault Locator Using the One-Terminal Voltage and Current Data," *IEEE Transactions on Power Apparatus and Systems*, vol. 101, no. 8. pp. 2892–2898, 1982.

[225] D. W. P. Thomas, C. Christopoulos, Y. Tang, P. Gale, and J. Stokoe, "Single Ended Travelling Wave Fault Location Scheme Based on Wavelet Analysis," *8th IEEE International Conference on Developments in Power System Protection*, vol. 1, pp. 196–199, 2004.

[226] S. D. A. Fletcher, P. J. Norman, K. Fong, S. J. Galloway, and G. M. Burt, "High-Speed Differential Protection for Smart DC Distribution Systems," *IEEE Transactions on Smart Grid*, vol. 5, no. 5. pp. 2610–2617, 2014.

[227] J. E. Hill, S. D. A. Fletcher, P. J. Norman, and S. J. Galloway, "Protection System for an Electrical Power Network." US Patent US8842401B2, 2014.